Self-Assembling Peptides as Potential Carriers for the Delivery of the Hydrophobic Anticancer Agent Ellipticine

by

Shan-Yu Fung

A thesis
presented to the University of Waterloo
in fulfillment of the
thesis requirement for the degree of
Doctor of Philosophy
in
Chemical Engineering

Waterloo, Ontario, Canada, 2008

AUTHOR'S DECLARATION

I hereby declare that I am the sole author of this thesis. This is a true copy of the thesis, including any required final revisions, as accepted by my examiners.

I understand that my thesis may be made electronically available to the public.

Abstract

Self-assembling peptides have emerged as new nanobiomaterials in the areas of nanoscience and biomedical engineering. In this category are self-assembling, ionic-complementary peptides, which contain a repeating charge distribution and alternating hydrophobic and hydrophilic residues in the amino acid sequence, leading to a unique combination of amphiphilicity and ionic complementarity. These peptides can self-assemble into stable nanostructures or macroscopic membranes that can withstand conditions of high temperature, extreme pH, many digesting enzymes and denaturation agents. Moreover, they exhibit good biocompatibility with various cultured mammalian cells, and do not have detectable immune responses when introduced into animals. These properties make them ideal materials for tissue scaffolding, regenerative medicine and drug delivery.

This thesis focuses on the utilization of self-assembling peptides for hydrophobic anticancer drug delivery. The hydrophobic anticancer agent ellipticine was selected as a model drug. The studies include: (i) characterization of the photophysical properties of ellipticine in different environments; (ii) study of the formation of peptide-ellipticine complexes and the release kinetics; (iii) investigation of the cellular toxicity of the complexes and ellipticine uptake; (iv) study of the peptide sequence effect on the complex formation and *in vitro* delivery.

Prior to applying ellipticine to the peptide-based delivery system, the fundamental studies on the effect of solution conditions, especially solvent polarity and hydrogen bonding, on the fluorescence of ellipticine were carried out. Ultraviolet (UV) absorption and fluorescence emission of ellipticine were found to be solvent/environment dependent. The absorption and emission maxima shifted to higher wavelengths (red shift) with increased solvent polarity. Large Stokes' shifts were due to intramolecular charge transfer (ICT), which was enabled by large solvent polarity and hydrogen bonding of ellipticine with the solvents. The photophysical response of ellipticine to

changes in solvent polarity and hydrogen bond formation could be used to infer the location of ellipticine in a heterogeneous medium, such as liposomes and cultured cells.

EAK16-II, a model self-assembling peptide, was found to be able to stabilize ellipticine in aqueous solution. The equilibration time required to form peptide-ellipticine complex suspensions was found to be peptide concentration-dependent and related to the peptide critical aggregation concentration (CAC, ~0.1 mg/mL). With different combinations of EAK16-II and ellipticine concentrations, two molecular states (protonated or crystalline) of ellipticine could be obtained in the complexes. The release kinetics of ellipticine from the complex into egg phosphatidylcholine (EPC) vesicles (cell membrane mimics) was also affected by the peptide concentration used in the drug formulation. A higher peptide concentration resulted in a faster transfer rate, in relation to the size of the resulting complexes. Subsequent cellular studies on two cancer cell lines, A549 and MCF-7, showed that the complexes with protonated ellipticine were more effective against both cell lines, but their dilutions were not very stable. In addition, it was found that ellipticine uptake in both cell lines was very fast and through direct membrane permeation.

Three peptides, EAK16-II, EAK16-IV and EFK16-II, either having a different charge distribution (EAK16-II vs. EAK16-IV) or hydrophobicity (EAK16-II vs. EFK16-II), were tested for the complexation and *in vitro* delivery of ellipticine. It was found that EAK16-II and EAK16-IV were able to stabilize protonated or crystalline ellipticine depending on the peptide concentration; EFK16-II, on the other hand, could stabilize neutral ellipticine molecules and ellipticine (micro)crystals. The viability results showed that the charge distribution of the peptides seemed not to affect the complex formation and its therapeutic efficacy *in vitro*; however, the increase in hydrophobicity of the peptides significantly altered the states of stabilized ellipticine and increased the stability of the complexes. This work provides essential information for peptide sequence design in the development of self-assembling peptide-based delivery of hydrophobic anticancer drugs.

Acknowledgements

I would like to express my great thanks to my supervisor, Dr. Pu Chen, who has provided me unlimited support, valuable advisory and critical guidance during my PhD study at the University of Waterloo. His guidance helped me through difficulties in the research and encouraged me in pursuing advanced research in nano-bioengineering. In addition, he assisted me to build up the ability required to become a creative, open minded, thoughtful and independent researcher. I also very much appreciate his providing me with such a great chance to continue to work in this cutting-edge and innovative research field after my Master studies with him.

My next acknowledgements go to the following individuals who have contributed to the experiments, discussions and/or suggestions on my PhD research projects. Professor Jean Duhamel in the Department of Chemistry has elaborated the photophysical methods (fluorescence and UV absorption) for the characterization of molecular interactions and provided great collaboration on the pilot studies using a hydrophobic model compound as the delivery cargo; one of his current PhD student, Christine Keyes-Baig, carried out many experiments and trials during our early collaboration. Professor Mingyao Liu and Dr. Bing Han at the University of Toronto have collaborated with us on the *in vivo* studies, which is still on going. We have frequent joint-meetings and tele-conferences to exchange ideas and discuss results on the cellular and animal delivery. Dr. Bing Han also helped the initial setup and training on cell culture experiments at Waterloo. Professor Liu's previous and current graduate students, Peter Tang and Roli Bawa, conducted cellular uptake experiments and *in vivo* delivery. My colleague, Dr. Hong Yang, helped conduct experiments for the characterization of peptide assemblies and perform early dynamic light scattering (DLS) experiments. Professor Mario Gauthier and his student, Jason Dockendorff, gave advice on DLS experiments and provided training using their DLS instrument and the viscometer in the Department of Chemistry. Professors Mark

Pritzker and William A. Anderson as my committee members involved in project discussions and gave advice for my research.

I also want to extend my special thanks to our current and previous group members as well as visiting scholars: Dr. Hong Yang, Dr. Yooseong Hong, Dr. Hyuk Sang Park, Dr. Elias Biswas, Michelle Zhou, Parisa Sadatmousavi, Francis Wang, Dr. H. Adikane, Bobby Dhadwar, Andrew Prpch, Maggie Law, Nasim Hyder, Yuebiao Sheng and others for their helpful suggestions, advice and any support during my study at Waterloo. Howard Siu, Christine Keyes-Baig and other students in Professor Duhamel's group are very appreciated for their help on time-resolved fluorescence measurements and other instruments. Thank to all staff members in the Department of Chemical Engineering for their help during my PhD studies.

During my PhD study, I also received great help from undergraduate research assistants working in our group: Jeremy, Priya, Diane, Krista, Renee, Brandon, Navneet, Amy, Andrea, Afsheen, Cheryl, Lex, Sonja, Ted, Edi and Anterjot. Their efforts are acknowledged.

Lastly, and also most importantly, I would like to thank my lovely, and the greatest wife, Hong, for her endless love, unlimited support and enormous encouragement when I encountered difficulties, felt depressed and lost strength. Also, I thank my families and Hong's for their non-stopping support. Without them, none of my achievements would be possible.

This thesis, a product of my PhD study, is dedicated to all of them, especially to my wife.

Table of Contents

List of Figures

List of Tables

Nomenclatures

Acronym	Full name
ACN	Acetonitrile
ADSA-P	Axisymmetric drop shape analysis-profile
AFM	Atomic force microscopy
ANS	1-anilinonaphthalene-8-sulfonic acid
BuOH	Butanol
CAC	Critical aggregation concentration
CD	Circular Dichroism
CHex	Cyclohexane
CMC	Critical micelle concentration
CPT	Camptothecin
DDS	Drug delivery system
Diox	1,4-dioxane
DIVEMA	Poly(divinylether-co-maleic anhydride)
DLS	Dynamic light scattering
DMEM	Dulbecco's modified eagle medium
DMF	Dimethylformamide
DMSO	Dimethyl sulfoxide
Dox	Doxorubicin
EAce	Ethyl acetate
EDTA	Ethylenediaminetetraacetic acid
EPC	Egg phosphatidylcholine
EPR	Enhanced permeability retention
EPT	Ellipticine
EtOH	Ethanol
FACS	Fluorescence-activated cell sorting
FBS	Fetal bovine serum
Hex	Hexane
HOPG	Highly ordered pyrolytic graphite

HPMA	Poly(N-[2-hydroxypropyl]-methacrylamide)
ICT	Intramolecular charge transfer
IGF	Insulin-like growth factor
*i*PrOH	*iso*-propanol
LHRH	Luteinizing hormone-releasing hormone
LUV	Large unilamellar vesicle
MDR	Multidrug resistance
MeOH	Methanol
MLV	Multi-lamellar vesicle
MPS	Mononuclear phagocytic system
MTT	3-(4,5-Dimethylthiazol-2-yl)-2,5-diphenyltetrazolium bromide
Mw	Molecular weight
PBS	Phosphate buffer saline
PC	Phosphatidylcholine
PCL	Polycaprolactone
PDGF	Platelet-derived growth factor
PE	Phosphatidylethanolamine
PEG	Polyethylene glycol
PEO	Poly(ethylene oxide)
PFA	Paraformaldehyde
PG	Poly(L-glutamic acid)
PK	Pharmacokinetics
PPO	Poly(propylene oxide)
RES	Reticuloendothelial system
SDS	Sodium dodecyl sulfate
SEDDS	Self-emulsifying drug delivery system
SEM	Scanning electron microscopy
SMA	Poly(styrene-co-maleic anhydride)
SUV	Small unilamellar vesicle
*t*AmOH	*tert*-amyl alcohol
TEM	Transmission electron microscopy
THF	Tetrahydrofuran

Tol	Toluene
Tris	Tris(hydroxymethyl)methylamine
TSCPC	Time-correlated single photon counting
UV	Ultraviolet
VIP	Vasoactive intestinal peptide

Chapter 1
Introduction

1.1 Overview

Cancer is the second most common cause of death in the developed countries after heart disease, causing over 70,000 fatalities each year in Canada.[1] It is a type of genetic disease, resulting from the mutation of genes in a normal cell and causing it to malfunction, especially in cell growth and recognition with the adjacent cells.[2,3] Such a malfunction leads to uncontrollable cell growth and cell metastasis. Since cancerous cells originate from the normal cells in the body, they are barely "seen" by our immune systems in early stages, leading to challenges for early cancer diagnoses. This immune "invisibility" of the cancerous cells in combination with their uncontrollable growth and metastasis makes cancer one of the most difficult diseases to fight.

By far, there have been three major types of cancer treatments practically used in clinics: surgery, radiotherapy and chemotherapy.[3] Surgery and radiotherapy are local treatments to remove or sterilize defined solid tumor masses. They often prove successful for locally confined, primary solid tumors. Chemotherapy, on the other hand, is a systemic therapy to kill tumor cells throughout the body, which is especially useful for metastatic tumors. It is also applied as the adjuvant treatment after surgery or radiotherapy. Other cancer treatments have been emerging from a better understanding of the cellular and molecular biology of cancer.[2,4] They include adoptive immunotherapy, cancer vaccine, gene therapy, antisense and RNAi therapy, hormone and growth factor antagonists, antiangiogenesis therapy, inhibitors for cell cycle and cancer-promoting proteins.[2,4-12] Although some of these new strategies have shown promise in preclinical tests, they still have a long way toward clinical applications. Nevertheless, at present, about 50% of cancer patients

can be cured, with chemotherapy contributing to cures in 10-15% of the patients. This indicates that the chemical control of neoplasia plays an important role in cancer treatment and the development of advanced chemotherapy will benefit more cancer patients.

However, two main obstacles exist in the conventional cancer chemotherapy. One is the severe side effects of the cytotoxic chemicals; the other is the development of drug resistance.[13] The harmful side effects can result in patient non-compliance and cause damage to healthy tissues/organs (especially fast replicating tissues including the bone marrow and the gastrointestinal tract mucosa), which in turn greatly limits the applicable dosage.[8,13-15] This is because most chemotherapeutic agents lack specificity in reaching tumor tissue; such poor specificity at the cellular level also significantly reduces the therapeutic efficacy. The "cellular" drug resistance arises from a defence mechanism of cancer cells in response to the chemotherapeutic agents, known as the multidrug resistance (MDR) phenotype, which involves active efflux of a broad range of cytotoxic drug molecules out of the cytoplasm by membrane-bound transporters.[4,13] In addition, massive solid tumors can create various drug permeation barriers (comparing to non-aggregating cancer cells), leading to a relatively low intratumoral drug concentration in solid tumors, referred as "non-cellular" drug resistance. These limitations may be overcome with delivery devices, e.g., nanocarriers, capable of passive or active targeting.[8,15-19] The nanocarriers are small enough (< 200 nm) to extravasate out of tumor microvasculature and accumulate in the tumor interstitium, known as the enhanced permeability and retention (EPR) effect.[15,20] They can also be linked to targeting molecules that can recognize and bind specifically to cancer cells. This further improves the delivery efficacy and significantly reduces undesired side effects.

Many delivery devices have been developed to improve solubility, transport, safety, targeting and efficacy of chemotherapeutic agents. These delivery constructs include liposomes,[21,22] polymeric and surfactant micelles,[23-26] nanoparticles,[13,15,27-29] polymeric vesicles,[30,31] microemulsions,[32]

micro/nano-encapsulation,[33] emulsification,[34] cyclodextrans,[35] dendrimers[36] and carbon nanotubes.[37] The basic principle of these delivery vehicles for chemotherapeutics is to provide an enclosed, protective, hydrophobic interior that can molecularly solubilize hydrophobic anticancer drugs, and circulate in the blood steam. They can be made to achieve controlled release, active targeting and/or passive targeting (EPR) delivery by appropriate material design, post surface modification and control of the vehicle size. Although they all have achieved varying degrees of success in delivering chemotherapeutics, some challenges still remain in their biocompatibility, biostability and toxicity of the vehicles after degradation.[38,39]

In addition to polymers, lipids, surfactants and some inorganic materials, self-assembling peptides have drawn much attention in drug delivery due to their desirable chemical/physical properties and biological functionalities. First, the peptides can be easily engineered to form a variety of stable nanostructures such as fibers,[40,41] rod,[42] tubes,[43] nanovesicles[44] and globules,[45,46] which can be readily used as delivery constructs. Second, the peptide sequence can be designed to incorporate natural binding motifs to inorganic materials,[41,47,48] oligonucleotides (e.g., antisenses),[49,50] siRNA and hydrophobic compounds.[51] Third, they can possess the natural propensities for cell penetration and targeting.[52,53] Fourth, some peptide sequences possess therapeutic effects.[54,55] With such features, self-assembling peptides have great potential as delivery constructs for nanomedicines.[56-58]

In this research, a special class of ionic-complementary, self-assembling peptides is used to explore the capability of such peptides in stabilizing hydrophobic anticancer drugs in aqueous solution and delivering them *in vitro*. This sets up the basis to develop self-assembling peptide-mediated delivery of cancer chemotherapeutics *in vitro*. The selection of this particular class of self-assembling peptides is based on the following reasons. First, these peptides have a simple sequence and unique structure for the study and possible control of peptide assembly.[59] In the case of EAK16-II, as an example, the peptide contains 16 amino acids in sequence, but is made of only three different

amino acids: glutamic acid (E), lysine (K) and alanine (A). These three amino acids are arranged in a special manner with hydrophobic (A) and hydrophilic residues (K or E) alternating in the sequence, rendering the peptide amphiphilic. In addition, the charged amino acid residues of EAK16-II alternate in a regular fashion ($--++--++$), resulting in ionic complementarity.[60,61] Second, most of these peptides have been found to form stable, β-sheet-rich nanostructures in aqueous solution.[60-62] In a β-sheet arrangement, all hydrophilic residues of the peptide are arranged on one side and the hydrophobic residues are on the other side. This unusual amphiphilic property allows the peptide to interact with both hydrophilic and hydrophobic (drug) molecules. Third, the unique molecular structure of EAK16-II enables various interactions (hydrogen bonding, electrostatic and hydrophobic interactions) to stabilize the assembled nanoconstructs, which can withstand extreme pHs, high temperature, many digestion enzymes and denaturation agents.[61,62] Fourth, these peptides have non-detectable immune response when introduced into animals, indicating good biocompatibility.[61,63,64] Fifth, fundamental aspects of peptide self-assembly have been explored by our research group for several years. Previous studies have shown that many factors such as peptide sequence[45,46] and concentration,[40,65] salt type and concentration,[41,65,66] solution pH,[45] surfaces[67,68] and mechanical force[69] affect the self-assembled micro-/nanostructures of these peptides and their derivatives. These fundamental studies provide essential information for physicochemical control over peptide self-assembly and nanostructure. The combination of the simple structure, unique properties, good (bio)stability and biocompatibility, as well as our previous knowledge of these peptides make them ideal candidates as delivery vehicles for hydrophobic anticancer drug. In fact, such a potential for hydrophobic anticancer drug delivery was first explored by our group and elaborated in this study.

A hydrophobic compound, pyrene, was first used to demonstrate the capability of self-assembling peptides in delivering hydrophobic cargos in the early studies.[51,56] Following the success in pyrene delivery, a hydrophobic anticancer agent, ellipticine, was applied for developing self-

assembling peptide-based delivery system here for the following reasons: first, the photophysical properties of ellipticine enable us to monitor the interaction of ellipticine with the peptide and locate it in different micro-environments;[70] its characteristic fluorescence can be used to monitor cellular uptake, by fluorescence imaging and fluorescence-activated cell sorting (FACS) techniques. Second, ellipticine is extreme hydrophobic with a low water solubility of ~0.62 μM at neutral pH,[71] comparable to that of the model hydrophobic compound pyrene.[72] Third, its great anticancer activity makes ellipticine one of the promising candidates in cancer chemotherapy.[73] Fourth, the discovery of severe side effects of ellipticine derivatives during early clinical trials suggests that a novel delivery system is required.[73,74]

This research project focuses on the complexation and *in vitro* delivery of the hydrophobic anticancer drug ellipticine using self-assembling, ionic-complementary peptides. In order to apply fluorescence techniques to investigate the complexation of ellipticine with the peptides, the release kinetics of ellipticine from the complexes, and cellular uptake of ellipticine, the photophysical properties of ellipticine in different environments were systematically studied. The self-assembling peptide EAK16-II was first used to stabilize ellipticine in aqueous solution. The kinetics of complex formation, molecular states of stabilized ellipticine and its release into a cell membrane mimic were investigated, and related to the peptide and ellipticine concentrations. The peptide-ellipticine complexes with certain combinations of peptide and ellipticine concentrations were further tested on their cellular toxicity and uptake into two cancer cell lines (A549 and MCF-7) to obtain the *in vitro* therapeutic effect. This information will be critical to the next phase of *in vivo* studies. In addition to EAK16-II, other two self-assembling peptides were used here to gain information of peptide sequence effects on the formation of peptide-ellipticine complexes and their anticancer activity *in vitro*. Based on the results reported in this work, strategies could be developed to design appropriate self-assembling peptides to construct functional nanocarriers for advanced cancer chemotherapy.

1.2 Research Objectives

The goal of this research is to develop self-assembling peptide-mediated delivery of hydrophobic anticancer drugs. To achieve this goal, the hydrophobic anticancer agent ellipticine is selected as the delivery cargo to test the principles of complexation with self-assembling peptides, release kinetics and the anticancer activity *in vitro*. The specific objectives of this thesis are listed in the following:

1. Characterization of the photophysical properties of ellipticine in different solution environments; these properties provide essential information for studying the complexation, release and possibly cellular delivery, using fluorescence and/or UV absorption techniques.

2. Study of the complex formation of ellipticine with a model self-assembling peptide, EAK16-II, and the release kinetics of ellipticine from the resulting complexes.

3. Evaluation of the therapeutic efficacy of the complexes *in vitro* with two cancer cell lines, non-small cell lung cancer cell A549 and breast cancer cell MCF-7.

4. Investigation of the peptide sequence effect on the complex formation and its anticancer activity *in vitro*; the results will aid to the peptide design in the development of the self-assembling peptide-mediated delivery.

1.3 Outline of the Thesis

This thesis consists of seven chapters. The scope of each chapter is listed as follows:

Chapter 1 gives an overview of the thesis, including a brief introduction to cancer chemotherapy, hydrophobic drug delivery systems, self-assembling peptides and their potential applications in drug delivery. The objectives and the scope of the thesis are also given in this chapter.

Chapter 2 provides a review of delivery systems for hydrophobic anticancer drugs, the hydrophobic anticancer agent ellipticine and its delivery methods. The properties of self-assembling peptides and their recent developments in drug delivery are also reviewed.

Chapter 3 presents a thorough investigation of the photophysical properties of ellipticine in different solvent environments. Of particular interest is the solvent-dependent fluorescence of ellipticine for the characterization of complexation with peptides and its release.

Chapter 4 deals with the complex formation of ellipticine with a self-assembling peptide, EAK16-II, and the release kinetics of ellipticine from the complexes. The concentration effect of both the peptide and ellipticine on complexation and release is investigated.

Chapter 5 reports the anticancer activity of the peptide-ellipticine complexes *in vitro* and the cellular uptake of ellipticine. The importance of the peptide-to-ellipticine ratio (by mass) to the efficacy of *in vitro* delivery is also described.

Chapter 6 investigates the peptide sequence effect on the complex formation of ellipticine and the cellular toxicity of the complexes. The effects of charge distribution and hydrophobicity of three different self-assembling peptides are studied.

Chapter 7 presents the conclusions of studies in the thesis, contributions of this research and recommendations for future work.

Chapter 2
Literature Review

2.1 Current Advances in Hydrophobic Anticancer Drug Delivery

Nearly 40% of new drug candidates discovered today are hydrophobic compounds, possessing poor water solubility.[75-77] These hydrophobic, potent compounds are often involved in various essential clinical treatments, especially in cancer chemotherapy. Unfortunately, their solubility problem in aqueous solution limits their clinical use since this prevents them from dissolving in the bloodstream, circulating in the host body and reaching their intended targets.[76,78] In addition, the clinical dosage cannot be reached due to the poor drug solubility. For cytotoxic drugs, administration of bare drugs can cause serious side effects; other common problems associated with free drugs include fast drug degradation, unfavourable pharmacokinetics and poor biodistribution.[79] Therefore, drug delivery systems, capable of solubilizing and carrying a hydrophobic drug to the intended targets, are being avidly studied and developed to supply additional therapies and new chemotherapeutics for clinical use.[14,39,79] Some examples of problems that can be ameliorated by using a drug delivery system are listed in Table 2.1.

Many delivery systems for hydrophobic anticancer drugs have been developed. They can be briefly categorized into five classes: polymeric conjugates, (micro)emulsions, micellar systems, liposomes and nanoparticles.[80-82] The primary goal of these systems is to improve the solubility of the hydrophobic entities so that they can be properly administered and circulated in the body. The optimal goal is to achieve targeted delivery, a concept of the "magic bullet" proposed by Ehrlich in the early 20th century, through either active or passive mechanisms as the ideal cancer

chemotherapy.[80,83] The advances in each class of the hydrophobic drug delivery systems are briefly reviewed in the following sections.

Table 2.1 Non-ideal properties of drugs and their therapeutic implications.[79]

Problem	Implication	Effect of DDS
Poor solubility	A convenient pharmaceutical format is difficult to achieve, as hydrophobic drugs may precipitate in aqueous media. Toxicities are associated with the use of excipients such as Cremphor® EL (the solubilizer for paclitaxel in Taxol).	DDS such as lipid micelles or liposomes provide both hydrophilic and hydrophobic environments, enhancing drug solubility.
Tissue damage on extravasation	Inadvertent extravasation of cytotoxic drugs leads to tissue damage, e.g., tissue necrosis with free doxorubicin.	Regulated drug release from the DDS can reduce or eliminate tissue damage on accidental extravasation.
Rapid breakdown of the drug *in vivo*	Loss of activity of the drug follows administration, e.g., loss of activity of camptothecins at physiological pH.	DDS protects the drug from premature degradation and functions as a sustained release system. Lower doses of drug are required.
Unfavorable pharmacokinetics	Drug is cleared too rapidly, by the kidney, for example, requiring high doses or continuous infusion.	DDS can substantially alter the PK of the drug and reduce clearance. Rapid renal clearance of small molecules is avoided.
Poor biodistribution	Drugs that have widespread distribution in the body can affect normal tissues, resulting in dose-limiting side effects, such as the cardiac toxicity of doxorubicin.	The particulate nature of DDS lowers the volume of distribution and helps to reduce side effects in sensitive, nontarget tissues.
Lack of selectivity for target tissues	Distribution of the drug to normal tissues leads to side effects that restrict the amount of drug that can be administered. Low concentrations of drugs in target tissues will result in suboptimal therapeutic effects.	DDS can increase drug concentrations in diseased tissues such as tumors by the EPR effect. Ligand-mediated targeting of the DDS can further improve drug specificity.

DDS: drug delivery system; EPR: enhanced permeability and retention; PK: pharmacokinetics

2.1.1 Polymeric Conjugates

Polymeric conjugated systems have been widely used for the delivery of anticancer drugs. This concept was first clearly presented by Ringsdorf in 1975.[84] The drug is covalently linked to a hydrophilic polymeric carrier to enhance the drug solubility in aqueous solution. In addition, the linkage of small hydrophobic molecules with a macromolecule can alter the pathway of cellular uptake. It has been found that the soluble macromolecular conjugates preferentially enter cells via endocytosis, which can significantly reduce the unspecific uptake by healthy tissue through direct cell membrane permeation.[85] Such a mode of entry can bypass some of the common mechanisms of multidrug resistance (e.g., cell membrane efflux pumps).[86] Three endocytosis mechanisms can occur for the soluble macromolecules: i) fluid-phase endocytosis, ii) adsorptive endocytosis, and iii) receptor-mediated endocytosis. By introducing cell recognition moieties to the conjugates, receptor-mediated endocytosis can be achieved, consequently affecting the biodistribution, also known as active targeting.[15] Even without such cell-specific targeting moieties, the polymeric conjugates are found to preferentially localize in the tumor tissue due to the EPR effect.[84,85] These advantages make the polymeric conjugates attractive in anticancer drug delivery.

The materials used to conjugate anticancer drugs can be broadly divided into synthetic and natural systems. The synthetic polymers are nonimmunogenic, but many of them are not biodegradable. These include poly(N-[2-hydroxypropyl]-methacrylamide) (HPMA), poly(styrene-co-maleic anhydride) (SMA), poly(divinylether-co-maleic anhydride) (DIVEMA) and poly(ethylene glycol) (PEG).[80,84] Natural biodegradable materials used for conjugation are poly(L-glutamic acid) (PG), some proteins, dextran and chitoson.[80,85] The anticancer drugs Doxorubicin, Paclitaxel and Camptothecin can be successfully delivered using HPMA copolymer, PG and PEG conjugates; some of them are currently undergoing clinical trials as listed in Table 2.2.

Table 2.2 Polymer-drug conjugates in clinical trials.[84]

Polymer	Polymer-Drug Conjugate	Phase of Clinical Trials
HPMA	HPMA-Doxorubicin (PK1)	II
	HPMA-Doxorubicin-Galactosamine (PK2)	I/II
	HPMA-Paclitaxel (PNU166945)	I
	HPMA-Camptothecin (PNU16648, MAG-CPT)	I
	HPMA-*cis*-Platinate (AP5280)	I/II
PG	PG-Paclitaxel (CT-2103, XYOTAX)	III
	PG-Camptothecin (CT-2106)	I
PEG	PEG-Camptothecin (PEG-CPT)	II

An important issue for polymeric-conjugate delivery systems is the proper release of the drug, which depends on the carrier-drug linkage. The ideal linkage should be broken only when the conjugates are internalized by the cells inside the endosomes or lysosomes.[84] However, the commonly used pH-sensitive linkers, such as ester bonds, *cis*-aconityl spacers and hydroazone linkages, can also be hydrolyzed in the blood stream. Also, the degradation of disulfide bonds is relatively nonspecific in the blood stream and on the cell membranes. Such nonspecific release of the free drug results in the development of side effects. To overcome this obstacle, special linkers that are stable in the circulation and can be specifically cleaved in the lysosome are used. Amide bonds, usually from a short peptide spacer, perform this function. One example is the glycylphenylalanylleucylglycyl (GFLG) linker, which is susceptible to lysosomal cathepsin B (a cysteine protease), while remaining stable in the blood stream.[87]

In addition to the passive targeting of the conjugates, active targeting can be achieved by linking a targeting moiety to enhance the specificity of internalization.[15,88] This is especially useful for spreading tumors, metastases, and types of cancer that do not form solid tumors. The targeting moieties are usually antibodies, vitamins or analogs, and proteins/peptides. Recently, a PEG-

camptothecin conjugate system was developed to incorporate a targeting moiety/penetration enhancer using a synthetic analogue of luteinizing hormone-releasing hormone (LHRH) peptide.[89] In addition, a synthetic analogue of BCL2 homology 3 domain (BH3) peptide was introduced as a suppressor of cellular antiapoptotic defense. Such a combination of active targeting and inhibition of cellular antiapoptotic defense significantly enhances the antitumor activity compared to the individual components applied separately. Although the conjugated system has shown great promise in advanced cancer chemotherapy, the synthesis of a multicomponent conjugate involves a series of chemical reactions and purifications, which in turn greatly complicate the manufacturing processes.

2.1.2 (Micro)emulsions

(Micro)emulsions are stable mixtures of oil, water and surfactants, frequently in combination with a cosurfactant. Such systems are useful for drug delivery due to their ease of preparation, capability of solubilizing large amounts of hydrophobic drugs and sustained release of the drugs. Although microemulsions and emulsions are usually treated as similar drug delivery systems, they are, in fact, fundamentally different.[82] Microemulsions are thermodynamically stable systems but emulsions are merely kinetically stable, i.e., emulsions will eventually undergo phase separation. Accordingly, microemulsions form spontaneously without the application of external work; the preparation of emulsions, on the other hand, requires energy and usually involves the use of high-pressure homogenization. A distinguishable difference between the two systems is the size of the droplets and their visual appearance: microemulsions contain small droplets (typical 10-100 nm) and are transparent while emulsions consist of relatively large droplets (typically 0.1-10 μm) and look milky. Nevertheless, both systems can form various oil-in-water (o/w), water-in-oil (w/o) or bicontinuous microstructures depending on the properties of surfactants and the water-oil composition.

Although (micro)emulsions have great ability to solubilize diverse drug molecules ranging from hydrophilic proteins/peptides to hydrophobic drugs, their use in parenteral delivery (including anticancer drug delivery) has been much less explored and is very challenging. This is often related to the instability of the (micro)emulsions upon dilution after intravenous administration. Also, the toxicity and biodegradability issues greatly limit the selection of surfactants and cosurfactants in this administration route.[90] Thus, searching for pharmaceutically acceptable excipients becomes important in order to apply (micro)emulsions to anticancer drug delivery. Examples include naturally occurring lecithins and glycerides, some non-ionic surfactants (e.g., polyoxyethylene sorbitan monooleate Tween 80 and polyoxyethylene sorbitan monolaurate Tween 20) and sugar surfactants (e.g., alkyl glucosides).[90] In general, (micro)emulsions are often explored as the delivery systems for topical and oral administration.[82,90,91]

Self-emulsifying drug delivery systems (SEDDS), which are very closely related to (micro)emulsions, have recently drawn much attention for oral delivery of hydrophobic drugs.[91] The system contrains an isotropic mixture of oils, surfactants, or alternatively, one or more hydrophilic solvents and cosolvents/surfactants. When the mixture is diluted in aqueous media, it automatically forms a fine o/w emulsion or microemulsion. Such systems are expected to improve the rate and extent of drug absorption. SEDDS has been applied to the oral delivery of paclitaxel and shown to be promising compared to the comercial formulation.[92] This may provide an alternative administration route for anticancer drug delivery.

2.1.3 Micellar Systems

Micelle-based carriers have been attracting many scientists in academia and the pharmaceutical industry. They provide a set of unique features in drug formulation and targeting for water insoluble drugs. Micelles, in general, are formed via molecular self-assembly of amphiphiles having a

core/shell structure when their concentration is above a threshold level referred to as the "critical micelle concentration" (CMC). Below the CMC, amphiphilic molecules exist as unimers. The hydrophobic core serves as a reservoir for solubilizing the hydrophobic drugs, while the corona provides hydrophilicity to the system so the micelles can be delivered in aqueous solution. The sequestration of anticancer drugs in the inner core can protect them from degradation, lower the cytotoxicity to the healthy tissues during circulation, and reverse MDR.[26] Micelles may also increase the systemic half-life of drugs and passively enhance their accumulation at the tumor site via the EPR effect.[26,83]

Micelles can be subdivided into two different groups according to the molecular weight of the materials: low-molecular-weight surfactant micelles and polymeric micelles. The pharmaceutically acceptable surfactant micelles (or FDA approved) for parenteral administration are poly(ethylene oxide) [PEO]-based amphiphiles. The most common commercial surfactants for anticancer drug delivery are polyethoxylated castor oil (Cremophor® EL), PEO 660 12-hydroxystearate (Solutol® HS15) and polysorbates (PEO-based sorbitan fatty ester, Tween®).[83] They have been used in (micro)emulsions as well (see Section 2.1.2). Cremophor® EL has been used to solubilize several anticancer drugs. One famous example is paclitaxel, which has been clinically used as Taxol® in cancer chemotherapy for many years.[35] Unfortunately, many of these surfactant micelles have major drawbacks due to their *in vivo* toxicity and biocompatibility. For instance, Cremophor® EL can extract plasticizers from the infusion bags and tubing sets, causing severe hepatotoxicity.[93] In addition, it has been associated with acute hypersensitivity reactions, including dyspnea, rash, chest pain, tachycardia, hypotension, angioedima and generalized urticaria;[94] it is also found to be neurotoxic and nephrotoxic.[35] Furthermore, surfactant micelles are not very stable upon dilution due to their relatively high CMC and low core viscosity. All these problems hinder their use in advanced cancer chemotherapy.

Polymeric micelles, on the other hand, offer several advantages over surfactant micelles in delivering hydrophobic anticancer drugs. First, they often have a low CMC, resulting in a higher stability upon dilution.[26,77] Second, the hydrophobic core can be tailored for different drugs. Third, the hydrated outer shell can offer effective steric protection and minimize uptake by phagocytes. Fourth, the circulation time can be increased as well as the biodistribution. However, the long term toxicity still remains an unsolved issue although considerable preliminary data suggest that some polymeric micelles are biocompatible. Biodegradability of the polymeric micelles would be another issue to consider.

Most polymeric micelles used for anticancer drug delivery are made of amphiphilic block or graft copolymers.[26,95] The block copolymers consist of hydrophilic (A) and hydrophobic (B) blocks arranged in an AB di-block or ABA tri-block sequence. The graft copolymers are usually synthesized by grafting hydrophobic blocks onto a hydrophilic backbone. The hydrophilic block is usually non-biodegradable poly(ethylene oxide) (PEO, similar to poly(ethylene glycol) PEG), whereas the hydrophobic blocks could be poly(propylene oxide) (PPO), poly(D,L-lactide) (PDLLA), poly(L-amino acid), poly(ester) and phospholipid.[25,76,77,83,96,97] They all have certain degrees of success in delivering anticancer drugs *in vitro* and/or *in vivo*.[77,80,83] Recently, a multifunctional micellar system capable of cell targeting and distribution imaging was developed to deliver the anticancer drug doxorubicin *in vitro*.[98] The system was made of a graft copolymer, a diblock copolymer and two functionalized diblock copolymers into a multifunctional micelle by carefully designing each component in the mixture (Figure 2.1). This indicates that functionalized polymeric micelles may hold great promise in future cancer chemotherapy.

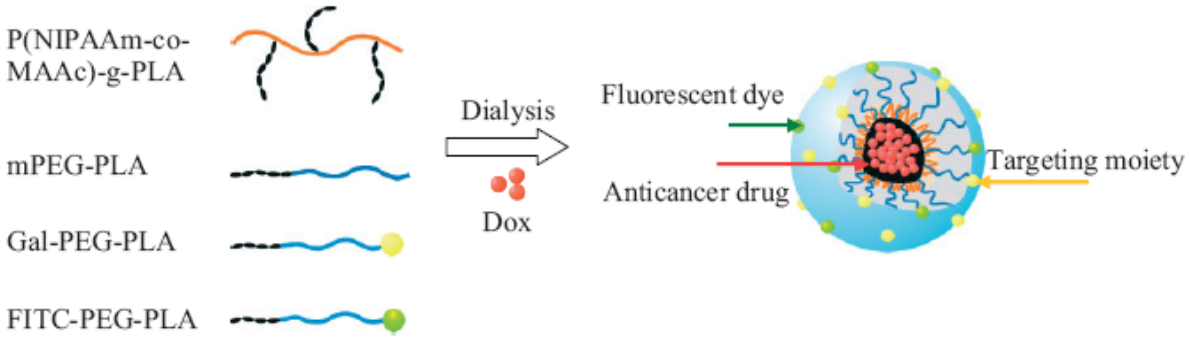

Figure 2.1 Schematic representation of multifunctional micelle structure made of a graft copolymer, a diblock copolymer and two functionalized diblock copolymers. Dox: doxorubicin; P(NIPAAm-co-MAAc)-g-PLA: poly(N-isopropyl acrylamide-co-methacryl acid)-g-poly(D,L-lactide); mPEG-PLA: methoxy poly(ethylene glycol)-b-poly(D,L-lactide); Gal-PEG-PLA: galactosamine-PEG-PLA; FITC-PEG-PLA: fluorescein isothiocyanate-PEG-PLA.[98]

2.1.4 Liposomes

Among many drug carrier systems, liposomes represent a mature technology for gene and anticancer drug delivery.[21,80] They are phospholipid vesicles composed of a bilayered lipid membrane, made from natural lipids such as phosphatidylcholine (PC), phosphatidylglycerol and cholesterol. These vesicles can carry hydrophilic drugs inside the core of the liposome (aqueous compartment) and hydrophobic drugs in the bilayered membrane. Depending on the preparation method (usually sonication or filtration) and the nature of the lipids, the size of liposomes ranges from 0.05 to 5.0 μm in diameter.[80,99] There are three major types of liposomes: multi-lamellar vesicles (MLV, > 0.1 μm), small unilamellar vesicles (SUV, < 0.1 μm) and large unilamellar vesicles (LUV, > 0.1 μm). MLV and LUV can carry both hydrophobic and hydrophilic cargos while SUV is not suitable for hydrophilic drugs due to low encapsulation efficiency (~1%). By virtue of their biodegradable and

nontoxic nature, liposomes can be safely administered without severe side effects. However, conventional liposomes through parenteral administration are recognized as foreign particles and are taken up by the mononuclear phagocytic system (MPS or the reticuloendothelial system RES).[80,99] This leads to fast clearance of liposomes from the blood circulation and limits the use of liposomal delivery to the tumors in liver, spleen and the bone marrow. Another obstacle of conventional liposomes is the fast leakage of drugs. This can be overcome by introducing cholesterol or using certain lipids (e.g., distearoylphosphatidylcholine, DSPC) to increase the phase-transition temperature.[99] A combination of cholesterol and DSPC, in fact, were used to construct the first comercial liposomal vehicle (DaunoXome®) to deliver daunorubicin.

A significant advance in liposomal delivery is the development of long-circulating liposomal carriers by coating the outer shell with PEG.[22,99,100] Other synthetic polymers that can serve the same purpose include poly(acrylamide) and poly(N-vinyl pyrrolidine).[80] Another important factor to extend the blood circulation and enhance the EPR effect is the size of the liposomes;[101] small-sized liposomes tend to have longer circulation time and avoid mononuclear phagocyte system (MPS) uptake. The optimal liposome size for longer blood circulation and higher tumor accumulation ranges from 50 to 200 nm.[101] The pegylated liposome carrier leads to another clinical delivery method for doxorubicin (Doxil®).[102]

Other advances in liposomal delivery include the incorporation of active cell targeting and design of pH/temperature-sensitive liposome vehicles. To achieve active targeting, the targeting moieties (e.g., antibodies, peptides and folates) are coupled to an anchor inserted into the bilayer or to the distal end of the PEG grafted to the liposome surface.[22,100,103] The pH-sensitive liposomes are composed of a mixture of phosphatidyl ethanolamine (PE) with an acidic phospholipid.[104] At pH < 6.5, PE becomes protonated and undergoes a transition from the bilayer phase to a hexagonal phase, resulting in the destabilization of the liposomes to release the drugs. Such a mechanism is especially

useful for delivering hydrophilic molecules. Similarly, the induction of a rapid release of liposomal content can be achieved using temperature-sensitive liposomes made of lipids with a phase transition temperature of around 40°C.[100] The transition can be triggered by local heating or hyperthermia. The triggered release of anticancer drugs from liposomes can also overcome the cancer-associated MDR.[105]

2.1.5 Nanoparticles

Due to the fast developing field of nanotechnology over the past decade, novel nanoparticles have been produced and benefited modern cancer chemotherapy and diagnosis.[18,19,38,106] Nanoparticles are broadly defined as being submicronic (< 1 μm) colloidal systems.[80,107] They may be classified as either nanospheres, where the drug is dispersed throughout the system, or nanocapsules, where the drug is entrapped in a cavity surrounded by a shell. According to this definition, most polymeric micelles and liposome vesicles can be regarded as nanoparticles, which have been reviewed in the previous sections. Other nano-particulated delivery systems include ceramic nanoparticles, chitosan nanoparticles, solid lipid nanoparticles (SLN), dendrimers and magnetic nanoparticles.[13,38,80,108,109] Each system has its advantages towards anticancer drug delivery. For example, the iron oxide magnetic nanoparticles coated with oleic acid and Pluronic polymers can deliver doxorubicin while simultaneously allowing magnetic targeting and/or imaging.[110] Dendrimers, as another example, are nanospheres with unique structural features, well-defined size according to the generation and controlled surface functionalities.[109] They can carry diverse molecules via hydrophobic interaction, ionic attraction and hydrogen bonding.

The major attempt of using nanoparticles for cancer chemotherapy is to achieve targeted delivery – the “magic bullet”. Strategies involve passive and active targeting. Although some of these concepts have been mentioned in the previous sections, an overview is given hereafter.

Passive targeting is based on the unique properties of most tumor microenvironments: (i) leaky tumor vasculature, which is more highly permeable to macromolecules than normal tissue; (ii) a dysfunctional lymphatic drainage system, which results in enhanced fluid retention in the tumor interstitial space.[15,111] These characteristics lead to 100 times higher accumulation of nanoparticles in tumor tissue than in normal tissue (Figure 2.2). This phenomenon of tumor-specific deposition is known as enhanced permeability and retention (EPR). The extent of nanoparticle extravasation depends on the size of open interendothelial gap junctions and trans-endothelial channels. The cutoff size has been reported to be 380-780 nm.[107] In general, particles with diameters less than 200 nm and a molecular weight above 40 kDa are the most effective for extravasating tumor microvasculature.[15,111] This approach has been widely applied to long-circulating delivery systems for cancer chemotherapy.

Different from passive targeting, active targeting is achieved by the incorporation of targeting molecules, which can recognize specific cancer cells and deliver the particles to the targets efficiently.[15-17] This approach can minimize the harmful side effects on healthy tissues while maximize the therapeutic efficacy. The targeting molecules include monoclonal antibodies (mAb), nucleic acid ligands (aptamers), peptides, folic acids (folates) and nanobodies.[15] Monoclonal antibodies are the first and still the preferred class of targeting molecules. However, the use of mAb still has many challenges and limitations such as the large size, complicated conjugation procedures and high cost to manufacture compared to the drug cargos. Nanobodies are the fragments of antibodies and could be good alternatives. An attractive and promising alternative to antibodies are peptides due to their small size, low immunogenecity, higher stability and ease of manufacture.[112] Examples are cyclic RGD peptide (Cilengitide®), cell-surface hormone receptors (LHRH receptors and somatostatin receptors) and tumor vasculature antigens.[15] The possibility of peptides in targeted delivery of anticancer drugs opens an avenue for peptide-mediated cancer chemotherapy.

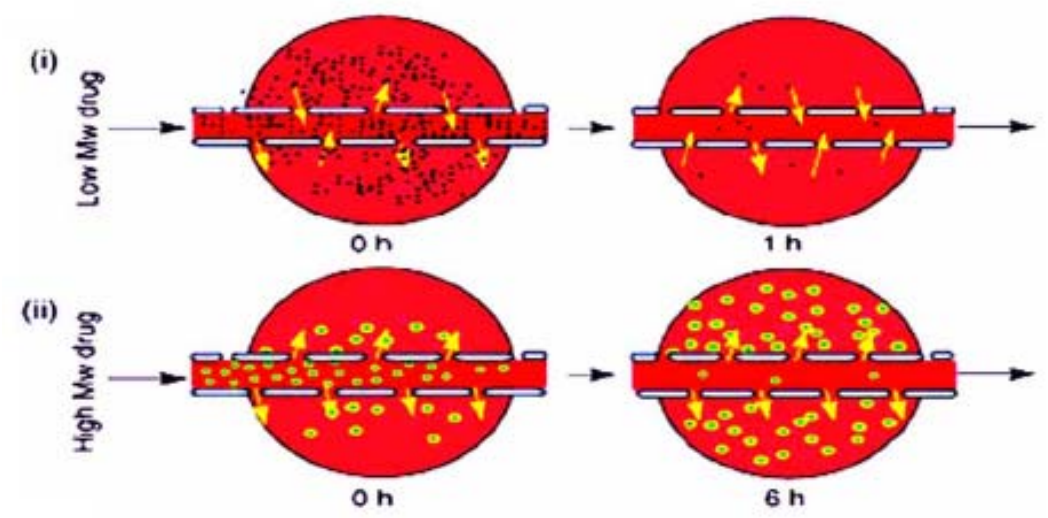

Figure 2.2 Diagrammatic representation of the enhanced permeability and retention effect. Low molecular-weight (Mw) drugs (black spots) can diffuse freely in and out of the tumor blood vessels because of their small size; hence, the effective concentration of the drug in the tumor diminishes after 1 h when the drug concentration in plasma becomes low (i). The high Mw drug (green circles) cannot diffuse back into the blood stream because of its large size. Thus, there is progressive accumulation of macromolecular drug in the tumor tissues with time by the enhanced permeability and retention (EPR) effect (ii). [111]

2.2 Self-Assembling Ionic-Complementary Peptides

In the past decade, short peptide sequences have attracted much attention for their use and design to construct functional nano/microstructures for various applications in nanoscience, surface engineering and biomedical technology.[60,113-117] These peptides share a common feature of self-association in aqueous solution. They are either portions of natural proteins or derived by *de novo* biomolecular design. Short fragments of natural proteins, such as β-amyloid peptides and prion peptides, have been

found to self-assemble into fibril structures in various environments.[118-120] On the other hand, synthetic peptides can be easily engineered to self-assemble into functional supramolecules, by taking advantage of the intrinsic properties of amino acids.[41,121-123] The combination of various molecular interactions existing in the amino acids, including hydrogen bonding, ionic interaction and hydrophobic interaction, governs the self-assembly behavior.

Among many self-assembling peptides is a special class of ionic-complementary peptides. These peptides have emerged as promising nanobiomaterials for many biomedical applications.[59,60] They are originally derived from a short segment (EAK16-II) of a Z-DNA binding protein in yeast by Zhang *et al.*[61,124] These peptides contain a unique amphiphilic molecular structure and can self-assemble into β-sheet-rich nanofibers and macroscopic membranes.[61] With relatively good biocompatibility and biodegradability, such peptides have been used as scaffolds for tissue engineering and 3-D cell cultures, novel materials for regenerative medicine, and nanocarriers for therapeutic agents.[58,60,125,126] Detailed information of their physical and biochemical properties, self-assembly process and factors influencing the assembly, and their potential applications in drug delivery will be reviewed in the following sections.

2.2.1 Molecular Structure and Physical/Biochemical Properties

Molecular structure

Self-assembling ionic-complementary peptides are characterized by an alternating arrangement of negatively and positively charged residues. In order to have ionic complementarity, the distribution of the charges should follow certain patterns. There are three types of charge distributions that are simplest and most widely studied. They are type I ($-+$ or $+-$), type II ($--++$ or $++--$) and type IV ($----++++$ or $++++----$). Such ordered charge distribution could result in

unique electrostatic interactions, which promote molecular self-assembly in addition to the more usual hydrogen bonding and hydrophobic interaction, and stabilize the assembled nanostructures.

Another feature of self-assembling ionic-complementary peptides is a special arrangement of hydrophobic and hydrophilic amino acid residues alternating in sequence. This leads to a "side-to-side" amphiphilic structure, for a β-strand peptide, where hydrophobic residues are on one side of the peptide backbone and hydrophilic ones are on the other side. Such a structure is different from the "head-to-tail" one of a surfactant.[82] As a result, the molecular self-assembly of these peptides is different from the micelle formation of surfactants.

Table 2.3 lists the family of a special class of self-assembling ionic-complementary peptides that have been studied since 1993.[60-62] The first peptide of its kind is EAK16-II, a 16-amino-acid peptide segment originating from a Z-DNA binding protein.[61,124] Its derivatives, such as EAK16-I and EAK16-IV, have different charge distributions of type I and IV, respectively, from type II. Their molecular structures are shown in Figure 2.3. It has been found that most peptides in this family can self-assemble into β-sheet-rich fibril structures.[60] The fibril formation of these peptides is believed to result from the combination of three different interactions: hydrogen bonding from the peptide backbone, the electrostatic interaction from the ionic-complementary residues, and the hydrophobic interaction from the hydrophobic side. The molecular structure of EAK16-II forms a basis to construct other similar self-assembling ionic-complementary peptides with different functionalities. An example is RADA16-I that has been designed to enhance the biocompatibility and cell adhesion for tissue scaffoldings.[127]

Table 2.3 The family of self-assembling ionic-complementary peptides[60,128,129]

Name	Sequence (n → c)	Charge Distribution	Type	Structure
KADA8-I	n- KADAKADA -c	+ − + −	I	r.c.
KFE8-I^{T}	n- KFEFKFEF -c	+ − + −	I	β
KFE8-I	n- FKFEFKFE -c	+ − + −	I	β
RADA8-I	n- RADARADA -c	+ − + −	I	r.c.
RAEA8-I	n- RAEARAEA -c	+ − + −	I	r.c.
EFK8-I	n- FEFKFEFK -c	− + − +	I	β
EAKA8-I	n- AEAKAEAK -c	− + − +	I	r.c.
KFE12-I	n- FKFEFKFEFKFE -c	+ − + − + −	I	β
KIE12-I	n- IKIEIKIEIKIE -c	+ − + − + −	I	β
KVE12-I	n- VKVEVKVEVKVE -c	+ − + − + −	I	β
KLD12-I	n- KLDLKLDLKLDL -c	+ − + − + −	I	β
KLE12-I	n- KLELKLELKLEL -c	+ − + − + −	I	β
EFK12-I	n- FEFKFEFKFEFK -c	− + − + − +	I	β
RADA16-I	n- RADARADARADARADA -c	+ − + − + − + −	I	β
RGDA16-I	n- RADARGDARADARGDA -c	+ − + − + − + −	I	r.c.
RAEA16-I	n- RAEARAEARAEARAEA -c	+ − + − + − + −	I	β
KADA16-I	n- KADAKADAKADAKADA -c	+ − + − + − + −	I	β
KFE16-I	n- FKFEFKFEFKFEFKFE -c	+ − + − + − + −	I	β
EAKA16-I	n- AEAKAEAKAEAKAEAK -c	− + − + − + − +	I	β
RAD8-II	n- RARADADA -c	+ + − −	II	r.c.
EAH8-II	n- AEAEAHAH -c	− − + +	II	r.c.
ELK8-II	n- LELELKLK -c	− − + +	II	β.
EAK8-II	n- AEAEAKAK -c	− − + +	II	r.c.
EAK12-a	n- AKAKAEAEAKAK –c	+ + − − + +	II	r.c.
RAD16-II	n- RARADADARARADADA -c	+ + − − + + − −	II	β
EAH16-II	n- AEAEAHAHAEAEAHAH -c	− − + + − − + +	II	β
EFK16-II	n- FEFEFKFKFEFEFKFK -c	− − + + − − + +	II	β

ELK16-II	n- LELELKLKLELELKLK -c	− − + + − − + +	II	β
EAK16-II	n- AEAEAKAKAEAEAKAK -c	− − + + − − + +	II	β
KAE16-IV	n- KAKAKAKAEAEAEAEA-c	+ + + + − − − −	IV	β
RAD16-IV	n- RARARARADADADADA -c	+ + + + − − − −	IV	β
EAK16-IV	n- AEAEAEAEAKAKAKAK -c	− − − − + + + +	IV	β
DAR16-IV	n- ADADADADARARARAR -c	− − − − + + + +	IV	α/β
DAR16-IV^{T}	n- DADADADARARARARA -c	− − − − + + + +	IV	α/β
DAR32-IV	n- (ADADADADARARARAR)$_2$ -c	− − − − + + + +	IV	α/β
EAK12-b	n- AKASAEAEAKAK -c	+ − − + +	N/A	r.c.
EAK12-c	n- AKAEAEAEAKAK -c	+ − − − + +	N/A	r.c.
EAK12-d	n- AEAEAEAEAKAK -c	− − − − + +	IV/II	α/β

Note: β: β-sheet; α: α-helix; r.c.: random coil; N/A not applicable.

(A)

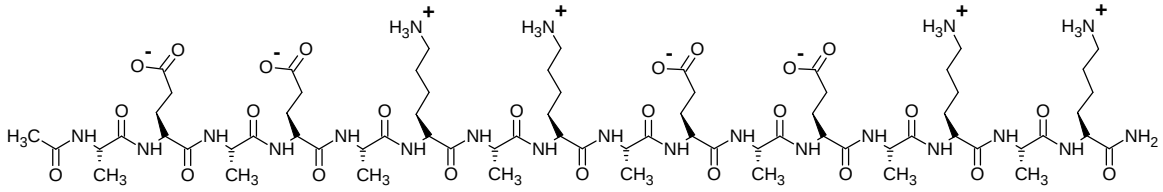

(B)

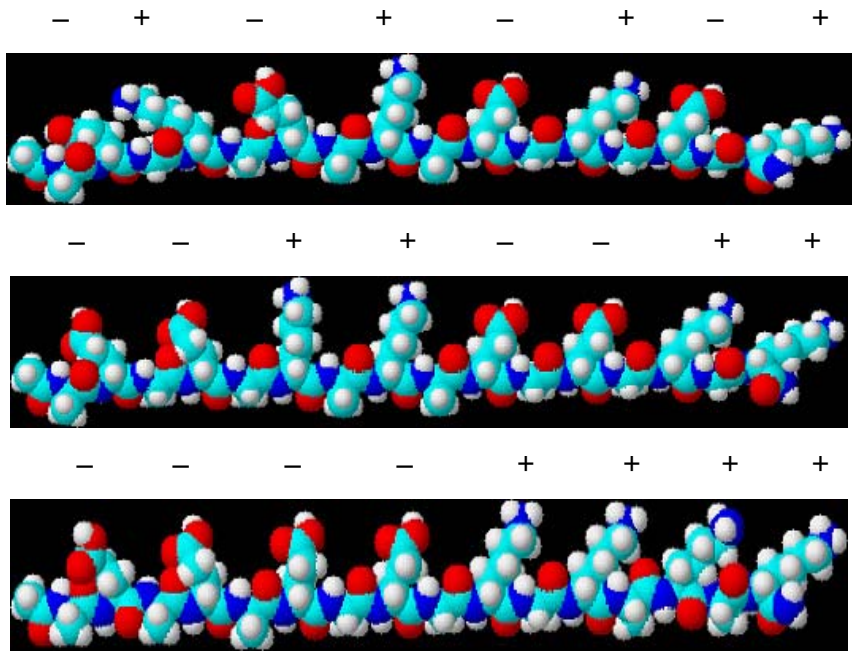

Figure 2.3 (a) Chemical structure of the ionic-complementary peptide EAK16-II. It contains alternating hydrophobic (alanine, A) and hydrophilic (glutamic acid, E and lysine, K) residues, with a type II charge distribution ($--++--++$), where pairs of negatively (E) and positively (K) charged residues alternate. (b) Three-dimensional molecular model of EAK16s. The top, middle and bottom schemes represent the EAK16-I, EAK16-II and EAK16-IV structures, respectively.[129]

Ionic-complementary peptides have several important features. First, their charge distribution can be altered through simple molecular design. For example, the sequence design based on the same

components can generate different charge distributions of type I, II and IV (i.e., EAK16-I, EAK16-II and EAK16-IV). The differences in charge distribution may determine the peptide secondary structure and influence peptide self-assembly. Second, specific peptide chain lengths are required to exhibit ionic complementarity. The length of these peptides varies from eight to thirty-two amino acids in sequence due to the alternating hydrophobic and hydrophilic residues in the peptide sequence (Table 2.3). The minimum number of amino acids required to build type I peptides is four, while the creation of type II and type IV peptides require eight and sixteen amino acids, respectively. The sequence of these short peptides can also be utilized for the design of polypeptides such as poly-EAK.[130] Third, the ionic-complementary peptide family can be easily expanded by using different amino acids. For example, DAR can be derived from EAK by replacing the residues glutamic acid (E) and lysine (K) with aspartic acid (D) and arginine (R), respectively. Similarly, the replacement of the hydrophobic residue alanine (A) of EAK with phenylalanine (F) or leucine (L) will create two other similar peptides EFK and ELK, respectively. Such simple replacement maintains the intrinsic properties of ionic-complementarity and self-assembly. In some cases, it can also strengthen the propensity of the peptides to form the desired supramolecules (e.g., the introduction of more hydrophobic residues can reduce the peptide length required to form a predominant β-sheet structure).

Unusually stable β-sheet formation

An important characteristic of ionic-complementary peptides is the spontaneous formation of unusually stable β-sheets in aqueous solution.[60,62,131] Once the β-sheets are formed, they remain unchanged under a broad range of physicochemical conditions (extreme pH, high temperature and dilution) and are even impervious to denaturing agents.[62] The β-sheet character of EAK16-II exhibits a maximum ellipticity at 218 nm and a minimum ellipticity at 195 nm in the CD spectra, even at the very low peptide concentration of 0.612 μM.[62] In addition, the CD spectra of EAK16-II show that β-

sheets remain stable up to 90 °C, which are much more stable than most proteins (denatured above 65 °C). Also, the β-sheets remain stable at extreme pH (1.5 or 11) since only a small change in the CD spectra at 218 nm can be observed.[62] Unlike normal proteins that denature when the concentration of denaturation agents (e.g., guanidine-HCl and urea) is above 4 M, β-sheet structures of EAK16-II can withstand even 7 M guanidine-HCl and 8 M urea. Such high stability has also been found in 0.1% sodium dodecylsulphate (SDS) solution.

The analysis of the molecular structures and interactions in the self-assembling ionic-complementary peptides may explain the formation of such unusually stable β-sheet structures. The β-sheet formation is mainly caused by the hydrogen bonding between individual peptide backbones, which is evidently found in protein folding and aggregation.[132,133] In addition, charged residues can also interact with each other to stabilize the β-sheets by means of electrostatic intermolecular interactions and hydrogen bonding. Similarly, the hydrophobic interactions from the nonpolar residues also play a role in stabilizing the structure.

Stable and biocompatible supramolecular structure

The self-assembled nano/microstructures of these peptides are also found to be stable under various physiological conditions.[61,62] They have been shown to resist degradation by acidic or basic environments ranging from pH 1.5-11,[61] sodium dodecyl sulfate (SDS)/urea and a number of proteolytic enzymes including trypsin, protease K and pronase.[61,62] In addition, no detectable immune responses are observed when these peptides are injected into rabbits, rats and goats.[61,134] The unusual stability of the peptides in serum, combined with their high resistance to proteolytic digestion, simple composition and apparent lack of cytotoxicity,[61,62,64,134,135] make them attractive for many biomedical applications.

2.2.2 Peptide Self-Assembly and Control

The understanding and precise control of peptide self-assembly is important to regulate the formation of nano/microstructure, formulate peptide-drug complexes, and further control the complex size. There are many internal and external factors that can influence peptide self-assembly. These factors include (a) amino acid sequence, (b) molecular size, (c) peptide concentration, (d) solution pH, (e) ionic strength, (f) solvent, (g) presence of denaturation agents, (h) temperature, (i) time, (j) surface and its property and (k) mechanical force. The effects of amino acid sequence, peptide concentration, pH, the presence of surface and mechanical force on peptide nanostructure formation, which are most relevant to this thesis work, are discussed below.[40,45,65,67-69,128,136]

Effect of amino acid sequence

Peptide sequence serves as an internal factor that tunes peptide self-assembly. The type, number and arrangement of amino acids in the sequence play important roles in determining the secondary structures and self-assembled nanostructures of the peptides. For example, EFK8-I, containing eight amino acids in the sequence, forms β-sheet secondary structure in aqueous solution. However, when phenylalanine (F) is replaced with alanine (A) and maintains the same charge distribution, the resulting peptide EAKA8-I forms random coils instead (Table 2.3). The reason for this phenomenon is still not clear. A possible explanation could be that the steric hindrance of the hydrophobic phenylalanine may help form β-sheets.

In addition to the type of amino acid, the length of the peptide sequence has significant impact on nano/macrostructure formation.[61,62,128,130] EAK16-II (16 amino acids) spontaneously associates to form a macroscopic membrane when dissolved in a salt solution such as phosphate buffer saline (PBS). EAK12 (12 amino acids) can also form membranes, but to a much lesser degree (< 50%). In contrast, EAK8-II (8 amino acids) does not form membranes under the same condition. This might be

due to the fact that peptides with a shorter chain length have fewer ionic-complementary pairs that can assist/stabilize peptide self-assembly.

The difference in charge distribution due to the arrangement of amino acids can alter peptide self-assembly into different nanostructures. For instance, EAK16-I and EAK16-II form fibril-like nanostructures, while EAK16-IV forms globular aggregates at neutral pH (Figure 2.4).[45] Further studies have found that EAK16-IV tends to form β-turn secondary structure via strong intramolecular electrostatic attraction. The assembly of β-turns may result in the formation of globular aggregates. On the other hand, EAK16-II prefers a stretched β-strand, resulting in the formation of linear fibrils. The experimental results are supported by Monte Carlo simulations.[46]

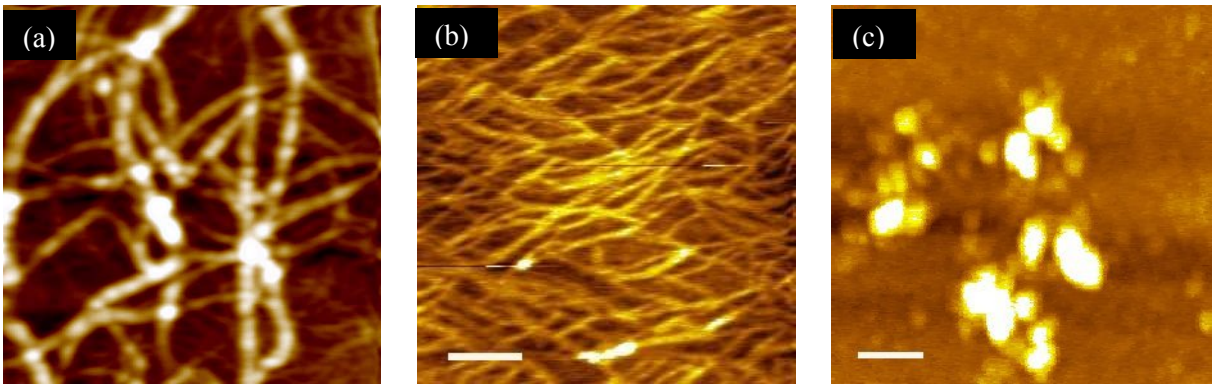

Figure 2.4 AFM images of peptide self-assembled nanostructures from EAK16-I (a), EAK16-II (b) and EAK16-IV (c).[45,65]

Effect of peptide concentration

Another factor that triggers peptide self-assembly and further controls the nanostructure formation is the peptide concentration. For amphiphilic molecules like surfactants, the self-assembly of these

molecules is usually concentration dependent and has a critical concentration that governs the assembly process.[82] As with the micelle formation of surfactants at a concentration above the critical micelle concentration (CMC), self-assembling ionic-complementary peptides are amphiphilic and also have a critical aggregation concentration (CAC). This is expected since the CAC has been reported for many proteins and amphiphilic peptides.[137-141] However, the concentration-dependent self-assembly of most biomolecules follows a nucleation and growth mechanism,[141-145] whereas the CMC represents a threshold concentration above which micellization of surfactants occurs.

The self-assembling ionic-complementary peptide EAK16-II has been found to have a CAC of ~0.1 mg/ml (60 μM) by surface tension measurements.[40] AFM studies of the nanostructure of EAK16-II reveals that nanofiber networks are formed when the peptide concentrations exceed the CAC, while isolated filaments and globules are observed at concentrations below the CAC.[40] In addition, the fibril size and network density are related to the peptide concentration as well. Similarly, EAK16-I has a critical concentration of 0.3 mg/ml (180 μM).[65] Unlike EAK16-II, EAK16-I assembly has been shown from AFM studies to undergo two nanostructure transitions.[65] The first transition from globules to fibril morphology occurs when the peptide concentration is about 0.05 mg/ml (30 μM); the second transition involves dramatic increase in the fibril size as the concentration rises above 0.3 mg/ml (180 μM).

Effect of solution pH

In biological systems, the solution pH is an important environmental factor affecting protein and peptide structures. A pH change will influence the ionic state of the charged residues as well as the net charge of peptides/proteins. This will further affect the self-assembly behavior of the peptide and protein folding/aggregation. Interestingly, the structure of self-assembling ionic-complementary peptides responds to the solution pH differently according to the peptide charge distribution. EAK16-

IV has been found to undergo a nanostructural transition from globular aggregates to fibril-like nanostructures at different solution pH.[45] The globular nanostructures occur at pHs between 6.5 and 7.5, while nanofiber networks appear at pHs beyond this range. In contrast, EAK16-II forms nanofibers throughout the pH range from 4 to 11. These findings suggest that the charge distribution in sequence plays an important role in determining the self-assembled peptide nanostructures. With a type IV charge distribution, strong intramolecular electrostatic attractions occur at neutral pH, which may cause molecular bending and the formation of globular nanostructures. At extreme pHs such as pH 4 and 11, either glutamic acid or lysine residues are neutralized, resulting in weakened intramolecular electrostatic interaction and smaller tendency for the peptide to form a β-turn structure. Thus, nanofiber formation would be predominant.

Effect of surface

Surface/interface plays an important role in many biomolecular processes such as protein aggregation and peptide self-assembly.[146-148] Recently, it has been found that a hydrophilic surface (mica) can assist the assembly of the self-assembling ionic-complementary peptide EAK16-II; the assembly kinetics of the peptide is significantly enhanced on the surface.[68] The surface-assisted peptide assembly follows a nucleation and growth mechanism and involves two steps. First step is the adsorption of nanofibers and fiber clusters (formed in the bulk solution) on the surface to serve as nuclei or seeds. The second step is the fiber elongation from the active ends of the seeds. Nanofibers or fiber clusters that have reached or are close to equilibrium in bulk solution can continually grow on the surface. This surface-induced peptide assembly may provide information to understand and control protein aggregation associated with conformational diseases.[133,149]

Further studies have shown that the adsorption and assembly kinetics of peptide nanofibers on the surface are strongly dependent on the surrounding environment such as solution pH.[68] The amount

of the adsorbed nanofiber "seeds" decreases with increasing solution pH, while the nanofiber growth rate under different solution conditions follows the order: pure water > 1 mM HCl > 1 mM NaOH > 10 mM HCl ≈ 10 mM NaOH ≈ 0. This indicates that solution pH can regulate the adsorption of the "seeds" to the surface as well as the fiber growth rate by affecting the peptide-surface and peptide-peptide interactions, respectively. This provides a way to control peptide assembly and the resulting nanostructures on surfaces (Figure 2.5).

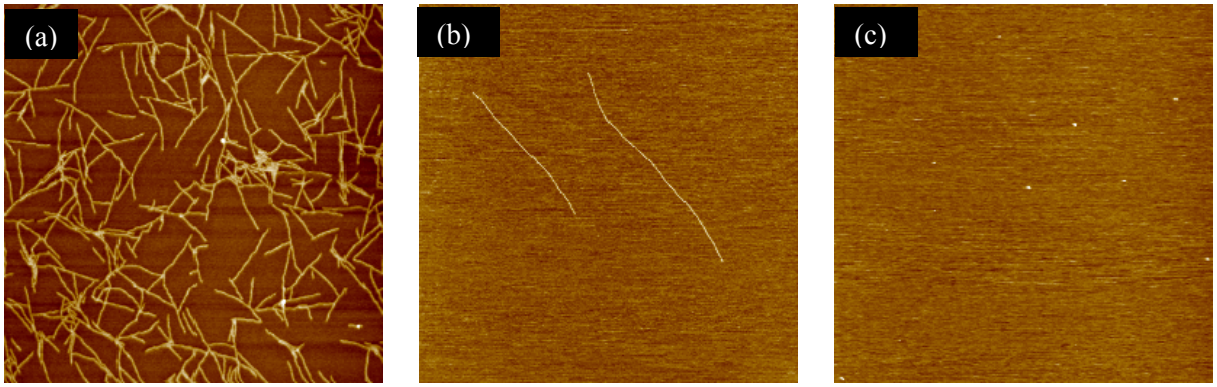

Figure 2.5 AFM images of EAK16-II on mica in various solutions after 30 min: (a) 1 mM HCl; (b) pure water; (c) 1 mM NaOH. Scan area is 2000 nm × 2000 nm.[68]

Surface properties, in some cases, can influence molecular assembly to produce ordered nanostructures.[147,150] It has been found that EAK16-II forms randomly deposited nanofiber networks on the hydrophilic mica surface, whereas well patterned nanostructures on a hydrophobic surface (HOPG) (Figure 2.6).[67] These well-ordered nanofiber patterns on HOPG have preferential orientations at angles of 60° or 120° to each other, resembling the crystallographic structure of the graphite. Similar to EAK16-II assembly on mica, the adsorption of peptide on HOPG surface is also

significantly affected by the solution pH. In acidic environment (e.g., pH ≤ 3), the peptide does not adsorb and assemble on the HOPG surface. However, it can form patterned nanofibers on HOPG in pure water and basic environments. This pH-dependent adsorption of peptides to HOPG is attributed to the changes in peptide hydrophobicity at different pHs.[69]

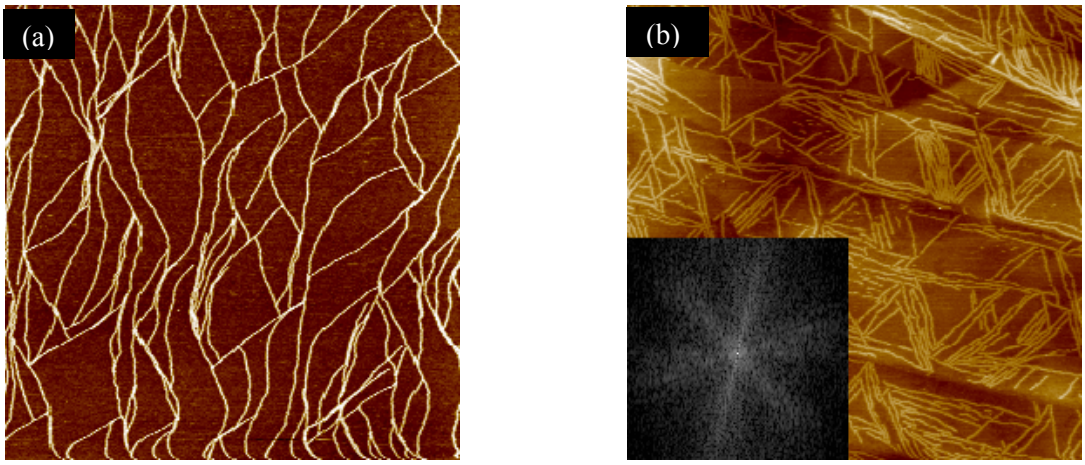

Figure 2.6 AFM images of EAK16-II on mica (a) and on HOPG (b) in various solutions after 30 min. The inset in (b) shows the 2-dimensional Fourier transform of the AFM image and characteristic 6-fold symmetry. Scan areas are 2000 nm × 2000 nm for mica and 1000 nm × 1000 nm for HOPG.[67]

Effect of Mechanical Force

More recently, Yang *et al.*[69] have reported a mechanochemical approach using AFM to control the assembly of EAK16-II over desired regions of a substrate. It has been found that the mechanical force applied by a tapping AFM tip can break the peptide assembled nanostructures. These broken fragments would serve as new nuclei for subsequent assembly to form new nanostructures. The total work applied from a tapping AFM tip to the biomolecules could be manipulated by adjusting the

amplitude of the tip oscillation, the size of the scan area and scan speed. Such an approach could allow one to locally grow nanofibers that densely cover specific regions of the surface (Figure 2.7).

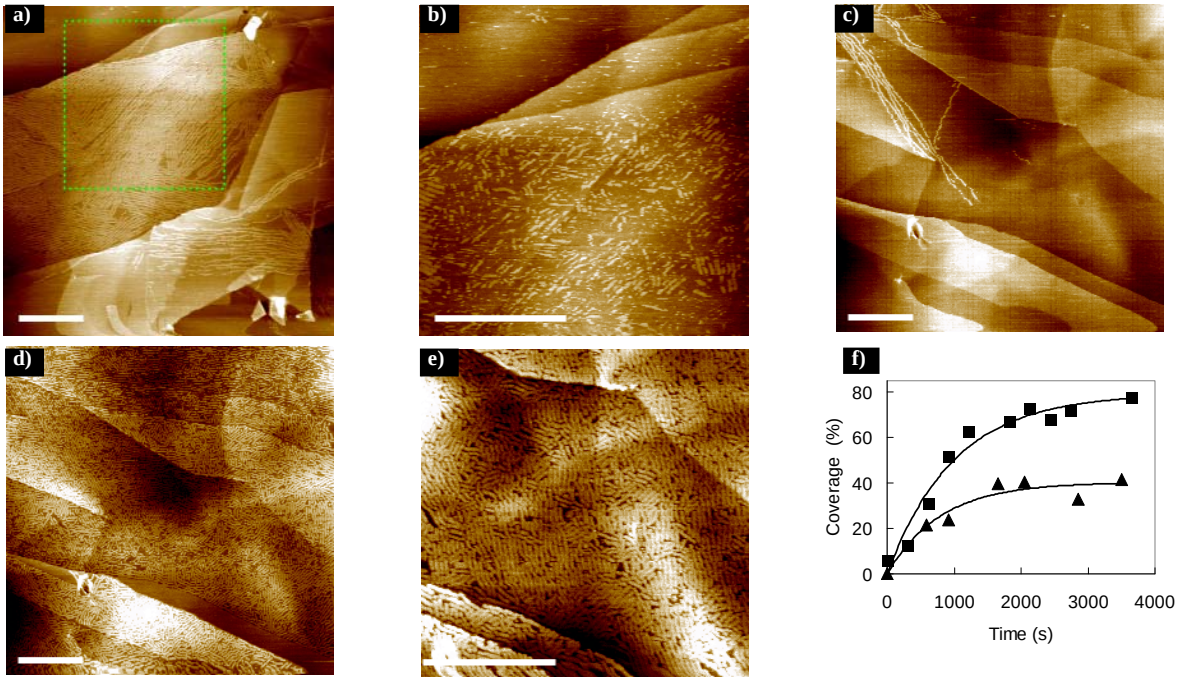

Figure 2.7 AFM images of EAK16-II nanofibers formed on HOPG in pure water (a and b) and 4 μM EAK16-II solution (c and d) under a mechanical force applied by a tapping AFM tip: (a) large-scale 1 × 1 μm^2 scan; (b) 4^{th} zoom-in scan of dotted area in (a); long peptide nanofibers are broken into short nanofiber segments under the mechanical force; (c) 1^{st} and (d) 10^{th} 1 × 1 μm^2 scan of the same location as (c); amount of peptide nanofibers on HOPG increases with the number of repeated scans; (e) zoomed-in scan image after 10^{th} scan reveals many truncated nanofibers formed on HOPG; (f) surface coverage of peptide nanofibers as a function of time; squares represent the coverage at one location with repeated scans and triangles correspond to that at different locations scanned only once. The scale bar corresponds to 200 nm.[69]

The process of breaking peptide assembled nanostructures by an AFM tip also forms the basis for a nanolithography method to pattern the surface. This method requires two steps. The first step is to allow peptides to assemble over the entire surface, forming densely coated peptide assemblies on the surface. The second step is to apply a mechanical force using a tapping AFM tip at desired locations to remove peptide assemblies and expose the surface underneath. This process is done in an environment (e.g., 10 mM HCl solution), where the broken peptides or their assemblies do not re-adsorb to the surface. Such a method can create various patterns with different surface properties at both nano- and microscales.[67,69]

2.2.3 Self-Assembling Peptide Carriers for Drug Delivery

To date, few of the discoveries in molecular therapeutics can truly benefit the treatment and prevention of human disease without effective delivery systems. An ideal delivery system should be able to control pharmacokinetics and pharmacodynamics, avoid non-specific toxicity, have no immunogenicity, possess biorecognition and enhance drug efficacy.[79,151,152] Among many emerging drug carriers, peptides have shown great promise to overcome some major problems in therapeutic delivery, such as safety, efficiency and targeting. The most attractive aspect of peptide-mediated drug delivery is the natural propensities of many peptides for cell penetration and targeting.[112,153,154] Peptide-based delivery systems have shown the potential to deliver therapeutic proteins, bioactive peptides, small molecules and nucleic acids.[57,58,153,154]

Self-assembling ionic-complementary peptides could be a new and promising material as carriers for drug delivery. Their unique amphiphilic structure and ability to self-assemble allow them to encapsulate both hydrophobic chemotherapeutics and hydrophilic gene therapeutics. Moreover, no detectable immune response is observed when these peptides are introduced into animals.[61,64,134] These peptides can spontaneously organize themselves into nano/micro structures that may provide a

protected and stable environment for drug/gene molecules. Another advantage of using peptide-based carriers is the ease of sequence modification and design for cell penetration and targeting. Some examples of using these peptides to deliver protein drugs and hydrophobic compounds are reviewed hereafter.

Protein drug delivery

Self-assembling ionic-complementary peptides have shown success in the local delivery and release of peptide/protein drugs in a controlled manner. A new peptide sequence is designed to incorporate a biotin molecule into a self-assembling peptide motif, RADA16-II. Such a biotinylated RADA16-II has been used to deliver insulin-like growth factor 1(IGF-1) to the myocardium.[58] The biotinylation does not alter the self-assembly property of RADA16-II. Biotin-IGF-1 is then incorporated into the biotinylated RADA16-II by using tetravalent streptavidin to form a "biotin sandwich". This approach allows specific and highly controlled delivery of IGF-1 to local myocardial microenvironments. After injection into the rat myocardium, the biotinylated nanofibers provide sustained IGF-1 delivery for 28 days and increase activation of Akt in the myocardium, indicating an improved cell therapy.

RADA16-II has also been used to locally deliver a platelet-derived growth factor, PDGF-BB, for myocardial protection.[57] PDGF-BB can be directly loaded onto peptide nanofiber matrices via non-specific, weak molecular interactions. The binding capacity of PDGF-BB is found to be 1 ng per microgram of nanofibers. The embedded PDGF-BB within the nanofibers remains biologically active for a prolonged period of 14 days in vivo. Sustained release of PDGF-BB can be achieved using these nanofiber matrices compared with injection of PDGF-BB alone, which will be rapidly eliminated from the blood stream. These results show another successful example of using self-assembling ionic-complementary peptides for the delivery of protein growth factor.

Potential in Hydrophobic Drug Delivery

In addition to delivering protein drugs, self-assembling ionic-complementary peptides have been shown to readily encapsulate hydrophobic materials and increase their solubility in aqueous environments. Recent work using pyrene as a model hydrophobic compound has demonstrated the potential of these peptides for the delivery of hydrophobic anticancer drugs.[51,56] The peptide EAK16-II is found to stabilize hydrophobic pyrene microcrystals in aqueous solution at concentrations up to a ten-thousand fold increase beyond its solubility in water (0.7 μM).[72] Since the encapsulated pyrene is in a crystalline form, more pyrene molecules are encapsulated per peptide, leading to high loading efficiency. The complexation of pyrene with EAK16-II is simply achieved by mixing pyrene crystals with peptide solution while continuously stirring mechanically;[56] peptide monomers and/or small peptide assemblies seem to be more effective at stabilizing pyrene in aqueous solution than mature peptide fibers.

The encapsulated pyrene in the complexes can be released into liposomes (as the cell membrane mimics) in a controlled manner.[51] The complete release has been found to take a few hours, and the release rate is affected by the peptide-to-pyrene ratio during the complexation: the higher the ratio, the slower the release rate (Figure 2.8). This is due to the difference in the density of peptide nanostructures coated on the pyrene microcrystals, as revealed by scanning electron microscopy (SEM). The high peptide-to-pyrene ratio results in solid peptide coatings on the microcrystals, whereas porous coatings occur at low peptide-to-pyrene ratio. This example demonstrates that controllable release of hydrophobic compounds may be achieved by using these self-assembling peptide vehicles. The results also show the possibility of such peptides in the delivery of hydrophobic anticancer agents.

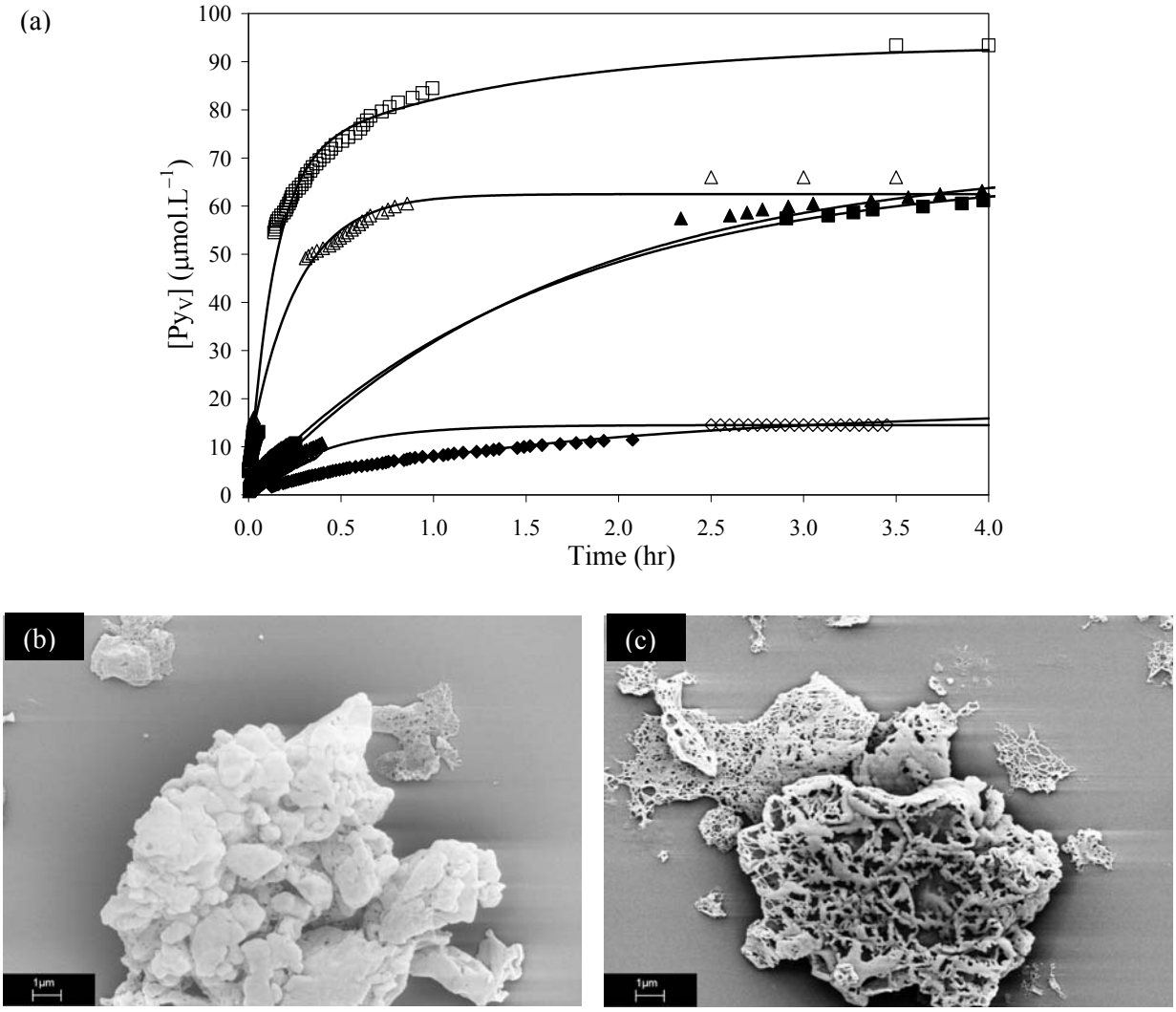

Figure 2.8 (a) The release of molecular pyrene from EAK16-II-pyrene complexes into liposomes. Hollow and solid symbols are for pyrene transfer experiments carried out with 0.1 mg/ml peptide coatings and 0.5 mg/ml peptide coatings, respectively. SEM images of the peptide-pyrene complexes with 0.5 mg/ml (b) and 0.1 mg/ml (c) peptide coatings.[51]

Other novel peptide-based delivery systems have been developed via adopting peptide sequence design for the delivery of either hydrophobic or hydrophilic molecules. One exciting

example is the design of TβP peptide using three functional blocks: a Tat cell penetrating peptide block (Tat_{48-60}, GRKKRRQRRRPPQ), a flexible-linker block (GSGG), and a β-sheet assembly block (KFE12-I) (Figure 2.9).[155] This peptide can self-assemble into stable β-sheet nanoribbons, carrying hydrophobic molecules inside the bilayered ribbons (stabilized by π-π stacking of phenylalanine residues); the cell penetrating motifs allow the nanoribbons to enter the cell and release the cargos into the cytoplasm.

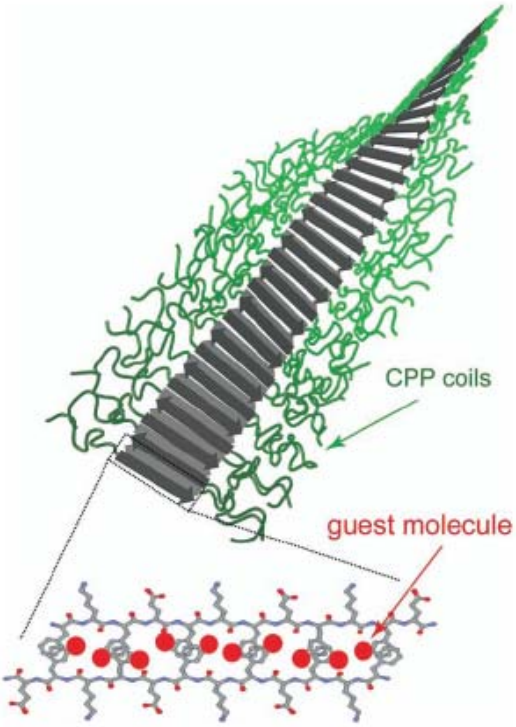

Figure 2.9 Representation of the nanoribbon formed by self-assembly of TβP and encapsulation of hydrophobic guest molecules.[155]

A similar strategy has been applied to design a cell targeting, self-assembling peptide amphiphile to deliver hydrophobic molecules.[156] The peptide amphiphile contains a dioctadecyl moiety as hydrophobic segment, a spacer consisting of a glycine residue and five units of 8-amino-3,6-dioxaoctanoic acid, and a sequence of peptide hormone cholecystokinin, CCK8 (DYMGWMDF), as bioactive hydrophilic peptide. The CCK8 peptide motif possesses dual functions as a biorecognition marker for tumor targeting and the hydrophilic portion of the amphiphile for self-assembly. The nanoconstructs of this peptide amphiphile have been found to be able to encapsulate hydrophobic pyrene and the anticancer drug doxorubicin. All these examples have shown that peptides play an important role in the development of advanced functional drug carriers to achieve effective delivery.

2.3 The Anticancer Agent Ellipticine

Many anticancer agents have been discovered and developed from natural sources[35,157-159] and from a better understanding of molecular genetics and cancer biology.[3,39,160-162] The original strategy of the anticancer drugs was to eradicate the cancer cells. As a result, the conventional anticancer drugs are very cytotoxic. According to their mode of action related to cancer biology, these cytotoxic chemicals can be classified into five categories: antimetabolites, covalent DNA binding drugs, noncovalent DNA binding drugs, inhibitors of chromatin function, and drugs affecting endocrine function.[3] Table 2.4 lists some anticancer drugs in these five categories that have been clinically used. Although these cytotoxic drugs are very effective at killing cancer cells, various side effects can occur during their clinical use. Therefore, novel delivery systems are required to minimize the severe side effects while enhancing the therapeutic efficacy.

Table 2.4 Some anticancer drugs in clinics.[3]

Classes	Mode of Action	Drugs in Clinics
Antimetaboites	Interfere with the production of nucleic acids	*Folate Antagonists*: Methotrexate (MTX, amethopterin); Trimetrexate (TMQ)
		Pyrimidine Antagonists: Fluorouracil (FUra, 5-FU); Fluorodeoxyuridine (FdUrd, 5-FUdR); CB3717; Azacytidine (Aza-C, 5-AC)
		Purine Antagonists: Mercaptopurine (MP, 6-MP); Thioguanine (TG, 6-TG); Tiazofurin; Chlorodeoxyadenosine (CdA); Pentostatin (2'-deoxycoformycin, dCF)
		Sugar-Modified Analogs: Cyhtarabine (ara-C); Fludarabine (F-ara-A)
		Ribonucleotide Reductase Inhibitors: Hydroxyurea (HU)
Covalent DNA-Binding Drugs	DNA cross-linking	*Nitrogen Mustards*: Mechlorethamine (NH_2, nitrogen mustard); Chlorambucil; Melphalan (L-phenylalanine mustard, L-PAM); Cyclophosphaminde; Ifosfamide
		Aziridines: Thiotepa (thio-TEPA); Altretamine (hexamethylmelamine); Mitomycin (mitomycin C)
		Alkane Sulfonates: Busulfan
		Nitrosoureas: Carmustine (BCNU); Lomustine (CCNU); Semustine (methyl-CCNU); Streptozotocin
		Platinum Compounds: Cisplatin (cis-DDP); Carboplatin
		Methylating Agents: Dacarbazine; Procarbazine
Noncovalent DNA-Binding Drugs	DNA intercalating	*Anthracyclines*: Daunorubicin; Doxorubicin; Idarubicin; Mitoxantrone; Dactinomycin; Bleomycin; Plicamycin
Inhibitors of Chromatin Function	Interfere the proteins responsible for the changes of chromosomes	*Topoisomerase Inhibitors*: Etoposide (VP-16); Teniposide (VM-26); Amsacrine (m-AMSA); Camptothecin (CPT-11)
		Microtubule Inhibitors: Vinblastine; Vincristine; Vindesine; Paclitaxel (Taxol)
Drugs Affecting Endocrine Function	Hormone treatment	*Glucocorticoids*: Prednisone; Prednisolone
		Estrogens: Diethylstilbestrol (DES); Ethinyl estradiol
		Antiestrogens: Tamoxifen
		Progestins: Medroxyprogesterone; Megestrol
		Androgens: Fluoxymestrone; Testosterone
		Antiandrogens: Cyproterone acetate; Flutamide
		LHRH (GnRH) Agonists: Goserelin; Leuprolide
		Aromatase Inhibitors: Aminoglutethimide
		Adrenocortical Suppressors: Mitotane (o, p'-DDD)

Among these cytotoxic agents, ellipticine, a natural alkaloid, was isolated from an Australian evergreen tree of the Apocynaceae family in 1959.[73,163] Later, it was found that ellipticine and its derivatives possess anticancer activity against various tumors. One of the ellipticine derivatives, 2-methyl-9-hydroxyellipticinium (NSC 264137, HME) was used in preclinical, phase I and phase II studies in the 1980's.[74,164-166] Unfortunately, it exhibited severe side effects during clinical trials,[73,74,167] and further attempts to develop ellipticine-based anticancer treatment were ceased until new delivery technologies were developed in the late 1990's. The following sections will give a review of ellipticine, including its properties, mode of action in cancer biology and current advances in ellipticine delivery.

2.3.1 Molecular Structure and Physical/Chemical Properties

Ellipticine is a natural alkaloid containing two benzene rings, one pyrrole-like and one pyridine-like ring in the structure with two methyl groups at positions 11 and 5 as shown in Figure 2.10.[73] The planar pyridocarbazole ring system is arc-shaped and appropriately sized for intercalation between the base pairs of DNA; its dimension is similar to the known intercalator proflavin. The molecule is pH sensitive with two protonable ring nitrogens at positions 2 and 6. The pKa of N-6 is less than 1, and that of N-2 is about 6 although it can vary from 4.5 to 7.4 depending on the nature and position of substituents on the ring system.[73,168,169] Generally, both protonated and neutral species can coexist at physiological pH.

According to its molecular structure, the neutral ellipticine is expected to be hydrophobic. The reported water solubility of ellipticine is ~0.6 μM.[71] Such low water solubility makes the delivery of ellipticine in aqueous solution difficult, which limits its clinical applications. The first attempt to increase its water solubility was through chemical modification of N-6 with a methyl group so that the molecule could be protonated.[73,164,167] However, the chemical modification was found to reduce

the anticancer activity of the resulting derivatives.[167,170] Thus, current approaches to solubilize ellipticine would rely on conjugation or delivery vehicles.[71,171,172]

(a)

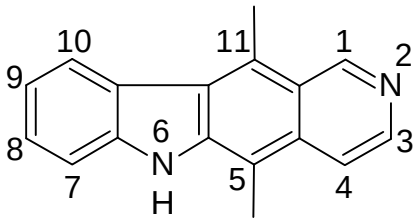

(b)

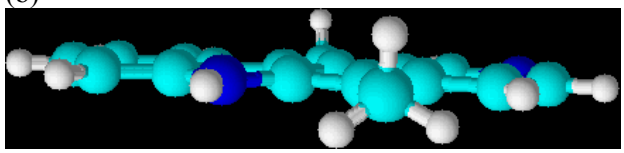

Figure 2.10 (a) Chemical structure of ellipticine; (b) Planar structure of ellipticine. H: white, N: blue, C: canyon.

An attractive feature of ellipticine is its photophysical activity. This allows one to study the interaction of ellipticine with other molecules and its cellular distribution by monitoring the change in absorption and emission spectra of ellipticine. A few scattered studies in the literature have reported the photophysical properties of ellipticine and its derivatives.[73,163,168,173,174] They are summarized hereafter. Ellipticine exhibits several UV absorption bands between 220 and 400 nm, with an extinction coefficient ranging from 3000 to 79000 1/(M·cm).[163] The UV absorption and fluorescence emission is highly dependent on solution pH.[163,168,174] Ellipticine exhibits a maximum of fluorescence at 520 nm in water (excitation at 304 nm), but an emission maximum at ~430 nm in ethanol (excitation at 294 nm), corresponding to protonated and neutral ellipticine, respectively. This solvent-dependent photophysical property could be utilized to characterize the transfer mechanism of ellipticine in a given delivery system. However, a more systemic study on such a property is required.

2.3.2 Mode of Action

The cytotoxicity of ellipticine is believed to be primarily related to two modes of action: (i) intercalation into DNA and (ii) inhibition of DNA topoisomerase II activity.[73,175] The size and planar molecular structure of ellipticine closely resemble those of a purine-pyrimidine complementary base pair, providing favorable conditions for intercalation in DNA. The hydrophobic interaction between the polycyclic aromatic ring of ellipticine and the DNA bases may strengthen the intercalation. In addition, protonation of ellipticine appears to favor its binding to DNA, which in turn causes the unwinding of DNA.[73,176] Intercalation may result in subsequent DNA breakage and cell death, although the detailed mechanism is still unclear.

One pathway of ellipticine intercalation in DNA leads to the inhibition of topoisomerase II, leading to DNA strand breakage and causing cell death.[177] This results from the formation of a ternary complex between topoisomerase II, DNA and ellipticine as proposed by Froelich-Ammon *et al.*[178] They found that ellipticine stimulates DNA breakage by enhancing the forward rate of cleavage. In addition, the ternary complex formation does not require the presence of a preformed topoisomerase-II-DNA complex.

Apart from these two modes of action, ellipticine has recently shown to be involved in the induction of cell cycle apoptosis. It can upregulate the tumor suppressor protein p53 in hepatocellular carcinoma cell (HepG2) and breast cancer cells (MCF-7 and MDA-MB-231).[179-181] Besides, ellipticine can also trigger mitochondrial apoptotic pathway by regulating Bcl-2 family proteins expression, altering mitochondrial membrane potential, and activating caspase-9, caspase-8 and caspase-3. More recently, it has been found that ellipticine can covalently bind to DNA to form DNA adduct after being enzymatically activated.[182-185] The adduct formation starts with oxidation of ellipticine by cytochrome P450 and/or peroxidase. This new mode of action may explain the selective cytotoxicity of ellipticine towards specific cancer cells.

2.3.3 Current Advances in Ellipticine Delivery

As discussed earlier, low water solubility is one of the major challenges for the use of ellipticine. Although several ellipticine derivatives have shown enhanced water solubility via chemical modification without compromising the anticancer activity,[164,170,186] none were successful during clinical trials.[74,164-166] The early clinical trials with ellipticine and its derivatives (e.g., 2-methyl-9-hydroxyellipticinium, NSC 264137) encountered severe side effects on the cardiovascular system, including hemolysis, rapid hypotension and a decrease in heart rate. This was thought to result from the propensity of ellipticine to bind to membranes, causing an increase in membrane surface area and osmotic fragility.[173,187] Several other important toxicities to the patients were also displayed, such as xerostomia, vomiting, nausea, anorexia and immune-mediated hemolytic reactions.[188,189] These obstacles greatly hamper the development of ellipticine in cancer chemotherapy.

To overcome the low water solubility of ellipticine and possibly reduce its side effects, new approaches have emerged using polymeric micelle systems[71,190,191] as well as polymeric/peptide conjugation.[171,172,192,193] Vladimir *et al.*[190] reported that ellipticine can be successfully incorporated into phosphatidylethanolamine-polyethyleneoxide (PE-PEO) micelles for long-circulating delivery. C. Allen and coworkers[71] recently tested several polymeric systems for their compatibility with ellipticine. They compared different formulation characteristics regarding ellipticine solubility and release, and found that polycaprolactone (PCL)-based copolymer micelles (e.g., PEO-b-PCL) could be a promising delivery system for ellipticine. Such a system has a high ellipticine loading efficiency and can achieve controlled release. They also developed a new micelle system using methoxy (polyethylene glycol)-b-poly (5-benzyloxy-trimethylene carbonate) (MePEG-b-PBTMC), which had an enhanced ellipticine loading efficiency of 95%.[191] With the presence of serum proteins, the ellipticine release was accelerated although the interactions between micelles and proteins were found to be minimal and insignificant.

In addition to micelle systems, conjugation with polymers or peptides provides an alternative approach to deliver ellipticine. Searle *et al.*[172] prepared a series of novel N-(2-hydroxypropyl) methacrylamide (HPMA) copolymer conjugates with the 6-(3-aminopropyl)-ellipticine derivative (APE, NSC176328) using GFLG or GG peptide linkage; the aqueous solubility of APE can be significantly increased (>10 fold). It was found that HPMA-APE conjugates could significantly reduce hemolysis ~10 times less when compared with free APE. Moreover, the cytotoxicity of these conjugates was found to be much less than free drug against B16F10 melanoma *in vitro*; the *in vivo* studies showed a higher antitumor activity than free APE, indicating the potential of such conjugates in cancer treatments.

Peptides are attractive materials for conjugation because they often possess the capability of cellular recognition. An ellipticine derivative, 1-[3-[N-(3-aminopropyl)-N-methylamino]propyl] amino-9-methoxy-5,11-dimethyl-6H-pyrido[4,3-b] carbazole, was conjugated with a heptapeptide and its derivative that targeted the gastrin/cholecystokinin type B receptor.[192] The conjugated ellipticine derivative eradicated all receptor-positive tumor cells *in vivo* without producing any general toxicity. Another example was the vasoactive intestinal peptide (VIP)-ellipticine conjugates to selectively inhibit the growth of breast cancer cells MCF-7 and lung cancer cells NCI-H1299.[171,193] These peptide-ellipticine conjugates were internalized via receptor-mediated endocytosis, and active targeted delivery was achieved.

In summary, ellipticine has shown great anticancer ability since its discovery in 1959, but the clinical usage is limited due to intolerable side effects and lack of appropriate delivery systems. With fast development in nanobiotechnology, ellipticine and its derivatives could be a good choice for use in clinically applicable cancer chemotherapy. The fluorescence capability of ellipticine and its various modes of action enable its usage as a model drug for investigation of novel delivery vehicles for hydrophobic anticancer drug delivery.

Chapter 3*

Solvent Effect on the Photophysical Properties of the Anticancer Agent Ellipticine

3.1 Introduction

Many anticancer agents have been discovered and developed from natural sources,[35,157-159] as well as from the understanding of molecular genetics and cancer biology.[39,160-162] Among them, ellipticine, a natural plant alkaloid, and its derivatives have been found to have anticancer activity since the 1960's.[73,167,170,194] They are able to intercalate with DNA and inhibit topoisomerase II, leading to the inhibition of replication of DNA and transcription of RNA. While these compounds exhibit high cytotoxicity against tumor cells,[167,170,186,195,196] only a few clinical trials of ellipticine and its derivatives were attempted in the 1980s.[74,164-167] This is mainly due to the very low solubility of ellipticine and most of its derivatives in aqueous media and in many organic solvents.[71,167,172] In addition, severe side effects have been observed during clinical trials, including intravascular hemolysis, xerostomia and the decrease of heart beat.[73,74,167]

Recently, ellipticine and its derivatives have drawn renewed attention as new drug delivery technologies have emerged. Ellipticine can be covalently linked with polymers or peptides to form conjugates with significantly improved solubility.[171,172,190,192,193] Such conjugates have the potential to target specific cancer cells, thereby reducing side effects.[171,192,193] Micelles made of copolymers were also used to deliver ellipticine *in vitro* with some promising.[71,191] More recently, a special class of self-assembling peptides has been found to be a good candidate for carrying and delivering hydrophobic compounds.[51,59] These peptides were found to bind to ellipticine, showing great potential as a carrier of ellipticine.

*This chapter is based on a paper "S.Y. Fung, J. Duhamel, P. Chen, Solvent effect on the photophysical properties of the anticancer agent ellipticine, *J. Phys.Chem. A* 2006, 110, 11446-11454".

In order to characterize how ellipticine is transported to its target, it is useful to establish a relationship between the environment and photophysical properties of ellipticine. This will enable one to monitor the uptake of ellipticine by a given carrier and its release from the carrier to a target site by monitoring the change in absorption and emission spectra, as ellipticine migrates from the microenvironment of the carrier to that of the target site. Unfortunately, only a few scattered studies in the literature have reported the photophysical properties of ellipticine and its derivatives.[73,163,168,173,174] Some studies focused on the binding of ellipticine to DNA;[169,178,197] others monitored the ellipticine fluorescence inside cultured cells.[198-200] These studies provided a limited understanding of the photophysical properties of ellipticine. They are summarized hereafter. Ellipticine exhibits several UV absorption bands between 220 and 400 nm, with an extinction coefficient ranging from 3000 to 79000 1/(M·cm).[163] The UV absorption and fluorescence emission are highly dependent on solution pH.[163,168,174] Ellipticine exhibits a maximum of fluorescence at 520 nm in water (excitation at 304 nm), but an emission maximum at ~430 nm in ethanol (excitation at 294 nm). This dramatic spectral shift is attributed to the different structures adopted by ellipticine in different solvents. The protonation of the pyridine-like nitrogen (pKa 6-7.4)[73,168,169] results in an emission maximum at 520 nm while the neutral form of ellipticine emits fluorescence at ~430 nm.[168] The observation of the neutral form of ellipticine in ethanol and its protonated form in a more polar solvent (water) suggests that one may use the solvatochromic effects exhibited by ellipticine to determine its local environment. This would be a powerful investigation tool to describe the polarity of a medium in which ellipticine is located. Such a result would be expected to have immediate application to characterize the transfer mechanism of ellipticine in a given delivery system.

In the present study, the photophysical properties of ellipticine were determined in a series of organic solvents with different polarities. The UV absorption and fluorescence emission spectra were obtained in each solvent and analyzed in terms of the position of their peak maxima. The position of

the peak maxima was correlated to the solvent polarity using the Lippert-Mataga equation.[201,202] The extinction coefficient of ellipticine in each solvent was obtained by applying Beer-Lambert's law. Time-resolved fluorescence experiments were conducted to determine the lifetime of ellipticine. The trends obtained for the absorption and emission of ellipticine as a function of the solvent polarity enable one to use the photophysical properties of ellipticine as a tool to determine its location in a heterogeneous medium. For instance, ellipticine was found to reside close to the surface of the lipid membrane of egg phophatidylcholine (EPC) liposomes.

3.2 Materials and Methods

3.2.1 Materials

The solvents (Table 3.1) were obtained from Sigma-Aldrich (Oakville, Canada), Caledon Laboratories Ltd. (Georgetown, Canada) or EM Science (New Jersey, US) with a purity of 99+%. Dielectric constants (ε) and refractive indices (n) of the pure solvents were obtained from the literature,[203] and used to estimate these properties of the mixed solvents (ε_{mix} and n_{mix}) from Equations 3.1 and 3.2,[204-206]

$$\varepsilon_{mix} = f_a \varepsilon_a + f_b \varepsilon_b \tag{3.1}$$

$$n^2_{mix} = f_a n^2_a + f_b n^2_b \tag{3.2}$$

where the subscripts a and b represent the two different pure solvents, and $f_{a,b}$ is the volume fraction of each solvent. The polarities of the pure and mixed solvents could be estimated using the definition of the orientation polarizability (Δf) from the Lippert-Mataga Equation[201,202]

$$\Delta f = \frac{\varepsilon - 1}{2\varepsilon + 1} - \frac{n^2 - 1}{2n^2 + 1} \tag{3.3}$$

Table 3.1 Photophysical properties of ellipticine in different solvents

solvents	Δf	ε	n	λ_a (nm)	ν_a (1/cm)	λ_f	ν_f (1/cm)	ν_a-ν_f (1/cm)	e (1/(M·cm))
MeOH	0.308	32.70	1.3288	294	34014	434	23041	10972	62300
ACN	0.305	36.64	1.3442	291.5	34305	420	23810	10495	43500
EtOH	0.289	24.55	1.3611	294	34014	429	23310	10704	69900
$Hex_{15}EtOH_{85}$	0.281	21.15	1.3703	294.5	33956	426	23474	10482	
*i*PrOH	0.277	20.18	1.3776	294.5	33956	424	23585	10371	71300
DMF	0.274	36.70	1.4305	293.5	34072	425	23529	10543	53600
$Hex_{35}EtOH_{65}$	0.271	16.62	1.3708	294.8	33921	425	23529	10392	
BuOH	0.264	17.50	1.3988	295	33898	427	23419	10479	71500
DMSO	0.263	46.68	1.4793	295	33898	428	23364	10534	60000
$Hex_{50}EtOH_{50}$	0.260	13.225	1.3712	295	33898	423	23641	10257	
$Hex_{65}EtOH_{35}$	0.242	9.819	1.3716	295	33898	422	23697	10201	
*t*BuOH	0.238	12.47	1.4255	294.5	33956	420	23810	10146	70400
$Hex_{75}EtOH_{25}$	0.222	7.552	1.3718	295	33898	421	23753	10145	
THF	0.210	7.520	1.4050	293.3	34095	413	24213	9882	49600
Hex_1THF_{99}	0.209	7.464	1.4047	293	34130	412	24272	9858	
Hex_5THF_{95}	0.207	7.238	1.4034	293	34130	412	24272	9858	
$Hex_{80}EtOH_{20}$	0.206	6.420	1.3720	294.8	33921	420	23810	10111	
$Hex_{10}THF_{90}$	0.204	6.957	1.4018	293	34130	411	24331	9799	
EAce	0.201	6.081	1.3723	291.5	34305	410	24390	9915	47400
$Hex_{20}THF_{80}$	0.197	6.393	1.3986	293	34130	410	24390	9740	
$Hex_{30}THF_{70}$	0.188	5.830	1.3954	293	34130	410	24390	9740	
$Hex_{85}EtOH_{15}$	0.185	5.286	1.3721	294.8	33921	420	23810	10111	

*t*AmOH	0.184	5.780	1.4052	294.5	33956	419	23867	10089	70000
$Hex_{40}THF_{60}$	0.178	5.267	1.3922	293	34130	409	24450	9680	
$Hex_{50}THF_{50}$	0.165	4.703	1.3889	293	34130	409	24450	9680	
Ether	0.165	4.267	1.3526	291.5	34305	405	24691	9614	52100
$Hex_{90}EtOH_{10}$	0.154	4.153	1.3722	294.5	33956	419	23866	10090	
$Hex_{60}THF_{40}$	0.148	4.140	1.3857	292.5	34188	407	24570	9618	
$Hex_{70}THF_{30}$	0.127	3.577	1.3825	292.5	34188	406	24631	9557	
$Hex_{93}EtOH_{7}$	0.126	3.473	1.3723	294.5	33956	419	23866	10090	
$Hex_{95}EtOH_{5}$	0.102	3.020	1.3724	294.5	33956	418	23923	10033	
$Hex_{80}THF_{20}$	0.099	3.013	1.3792	292.5	34188	405	24691	9497	
$Hex_{97}EtOH_{3}$	0.070	2.566	1.3724	294	34014	418	23923	10091	
$Hex_{90}THF_{10}$	0.059	2.450	1.3760	292.5	34188	403	24814	9374	
$Hex_{98}EtOH_{2}$	0.051	2.340	1.3724	293.3	34095	416	24038	10057	
$Hex_{95}THF_{5}$	0.033	2.168	1.3743	292	34247	402	24876	9371	
$Hex_{99}EtOH_{1}$	0.028	2.113	1.3725	291	34364	407	24570	9794	
Diox	0.021	2.219	1.4224	292.5	34188	410	24390	9798	51800
$Hex_{98}THF_{2}$	0.014	1.999	1.3734	291.5	34305	401	24938	9367	
Tol	0.013	2.379	1.4961	293	34130	403	24814	9316	47400
$Hex_{99.6}EtOH_{0.4}$	0.012	1.977	1.3725	290.5	34423	403	24814	9609	
$Hex_{99}THF_{1}$	0.007	1.943	1.3730	291	34364	401	24938	9426	
$Hex_{99.8}EtOH_{0.2}$	0.006	1.932	1.3725	290.3	34447	402	24876	9571	
CHex	0	2.024	1.4235	290	34483	392	25510	8973	37700
Hex	0	1.887	1.3727	289.5	34542	390	25641	8901	32100
EPC				295	33898	436	22936	10962	
SDS				307	32573	520	19231	13342	

Notations: orientation polarizability, Δf; dielectric constant, ε; refractive index, n; absorption wavelength, λ_a; absorption wavenumber, ν_a; emission wavelength, λ_f; emission wavenumber, ν_f; extinction coefficient, e.

The anticancer agent ellipticine (99.8% pure) was purchased from Sigma-Aldrich (Oakville, Canada) and used without further purification. Egg phosphatidylcholine (EPC) and sodium dodecyl sulfate (SDS) were purchased from Avanti Polar Lipids, Inc. (Alabama, US) and EM Science (New Jersey, US), respectively. Ethylenediaminetetraacetic acid (EDTA) was supplied by Bio-Rad Laboratories. Tris(hydroxymethyl)methylamine (Tris) and acetic acid were obtained from BDH Inc. (Toronto, Canada).

The following abbreviations are used for the various solvents: methanol, MeOH; acetonitrile, ACN; ethanol, EtOH; *iso*-propanol, *i*PrOH; dimethylformamide, DMF; butanol, BuOH; dimethylsulfoxide, DMSO; *tert*-butanol, *t*BuOH; tetrahydrofuran, THF; ethyl acetate, EAce; *tert*-amyl alcohol, *t*AmOH; diethyl ether, Ether; 1,4-dioxane, Diox; toluene, Tol; cyclohexane, CHex; hexane, Hex; egg phosphatidylcholine, EPC; sodium dodecyl sulfate, SDS; the subscripts for the mixture represent the volume percentage of the two solvents in the mixture (i.e., $Hex_{99}THF_1$: the mixture contains 99% of hexane and 1% of THF)

The error for all absorption and emission data is within 0.2%, and that for extinction coefficients is less than 2.0%.

3.2.2 Sample Preparation

The ellipticine solutions were prepared from stock solutions (100 μM and 400 μM) dissolved in THF. Aliquots of the ellipticine stock solution (100 μM) in THF were transferred to a 20 mL vial. The vial

was then dried under a gentle flow of N_2. Solvents (5 mL) were added to the vial to obtain a solution with a final ellipticine concentration of 2 μM for all fluorescence studies. The same procedure was used to prepare higher ellipticine concentrations (4, 8, 10 and 20 μM) from the 400 μM stock solution for UV absorption experiments. All solutions were degassed prior to performing a steady-state or time-resolved fluorescence experiment.

A 25 mM Tris/acetic acid buffer at pH 7 with 0.2 mM EDTA was used in the dispersions of EPC liposomes. The preparation procedure was described in a previous publication:[51] EPC in chloroform (75 g) was added to a 1 L round-bottom flask. The chloroform was then evaporated off using a rotary evaporator to produce a thin film inside the round-bottom flask. The film was dispersed at room temperature in 310 mL of the buffer solution. The mixture was then sonicated for 25-30 min in a sonifier cell disrupter (Heat Systems-Ultrasonic Inc, model W-225) set at about 20 W output. The round-bottom flask was kept near 0 °C on ice above the lipid phase transition temperature (T_c = -15 °C to -7 °C) and nitrogen was bubbled into the mixture. This was followed by centrifugation at 7000 rpm for 1 h to eliminate the larger membranes and eventual titanium particles from the sonifier probe. The supernatant was collected and stored at 5 °C before use. The prepared liposomes were characterized as large unilamellar vesicles (LUVs) in terms of their sizes (70-130 nm in diameter).[51]

The lipid concentration was determined from the difference between the solid content of the vesicle solution and that of the buffer solution. The procedure was described in the following: three known masses of the vesicle solution were pipetted into preweighed 20 mL vials. Three aliquots of the buffer solution with masses close to the mass of the vesicle solution were also pipetted into preweighed 20 mL vials. This was done so that the solid content of the buffer solution could be withdrawn from the mass of the dried liposome and an accurate concentration of the EPC lipid could be determined. The three sets of vesicle and buffer solutions were set under a stream of nitrogen to obtain a film at the bottom of the vial. The vials were then placed in a vacuum oven overnight at 60

°C to remove any traces of water. The mass of the three sets of vesicle and buffer films were obtained to calculate the lipid concentration. The EPC concentration used in this study equaled 1.1 mM. Liposome dispersions (5 mL) were added to the sample vial containing a dry film of ellipticine to reach the set 2 μM ellipticine concentration.

3.2.3 UV Absorption

The extinction coefficient of ellipticine at the wavelength corresponding to the absorption maximum in each solvent was determined from the absorption of five ellipticine solutions (2, 4, 8, 10 and 20 μM). The absorption spectra were acquired on a UV-Vis spectrophotometer (Biochrom Ultraspec 4300 Pro, Cambridge, England) using a 1 cm path length quartz cell. The molar extinction coefficient (*e*) was obtained from Beer-Lambert's Law as follows:[202]

$$Absorbance(Abs) = ecd \tag{3.4}$$

where *c* is the molar concentration of ellipticine and *d* is the optical path length (cm). A plot of absorbance versus ellipticine concentration yields a straight line ($R^2 > 0.995$) with slope equal to *e* for a 1 cm light path length.

3.2.4 Steady-State and Time-Resolved Fluorescence

All steady-state fluorescence emission spectra were acquired on a Photon Technology International QM-4 spectrofluorometer (London, ON, Canada) with a continuous xenon lamp as the light source. For each sample, approximately 3 mL of solution was transferred from the sample vial into a square quartz cell (1 cm × 1 cm) through a Pasteur glass pipette. The sample was then excited at the wavelength corresponding to the position of the absorption maximum in different solvents (289-305 nm). The emission fluorescence spectra were collected at wavelengths ranging from 300 nm to 650 nm. Each spectrum was normalized according to its peak maximum. In the case of solutions

exhibiting multiple fluorescence peaks, the position of the far left fluorescence peak was used in the Lippert-Mataga Equation.

The time-resolved fluorescence decays were acquired on an IBH 5000U time-resolved fluorometer using the time-correlated single photon counting (TCSPC) technique. For each solvent, the excitation was set at the wavelength corresponding to the absorption maximum and the fluorescence was collected at the wavelength corresponding to the fluorescence maximum determined from the steady-state fluorescence spectra. All decay profiles were acquired over 1024 channels and the data collection was stopped when the peak maximum reached 20000 counts. A filter was applied with a cutoff of 370 nm to minimize potential light scattering leaking through the detection system. The decays were then fitted with a mono or bi-exponential function and the fitting parameters were optimized using the Marquardt-Levenberg algorithm.[207] The quality of all fits was determined by the χ^2 parameter, the random distribution of the residuals, and the autocorrelation function of the residuals.

3.3 Results and Discussion

3.3.1 Effect of Solvent on the Absorption Spectra

Typical absorption spectra of ellipticine in various solvents are shown in Figure 3.1. Ellipticine absorbs over a wide range of wavelengths from 220 nm to 400 nm. In methanol, three major absorption peaks are found at 294 nm, 285 nm and 276 nm. The peak locations are very close to the reported values.[163] When ellipticine is in a non-polar solvent, such as hexane, the absorption spectrum shifts toward the ultraviolet region (blue shift). The 294 nm peak (peak III) in methanol shifts to 289.5 nm in hexane, but it does not change much in the solvents with medium polarity such as THF

(absorption spectra for other solvents are not shown). The position of the absorption peak III in all tested solvents is listed in Table 3.1.

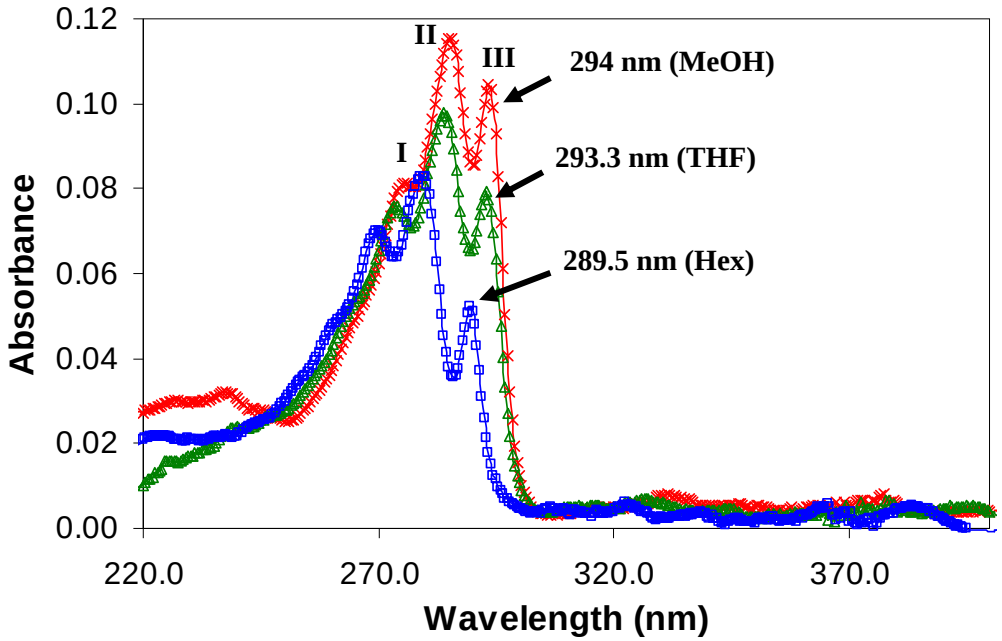

Figure 3.1 Absorption spectra of ellipticine in hexane (open squares), THF (open triangles) and methanol (crosses). The ellipticine concentration is 2 μM. The position of peak III was chosen as the excitation wavelength of ellipticine in each solvent.

The shift of the absorption spectrum with solvent polarity observed for a solvatochromic compound is a well-known phenomenon. The shift can be described as being hypsochromic or bathochromic depending on whether the absorption maximum occurs at a lower or higher wavelength, respectively. In the case of ellipticine, the absorption spectrum shifts to higher wavelengths with increasing solvent polarity, indicating a bathochromic shift. Normally, a bathochromic shift occurs when the dipole moment of the probe (ellipticine in the present case) increases during the electronic transition (i.e., the ground-state dipole moment μ_g < excited-state

dipole moment μ_e), and the excited state is formed in a solvent cage of already partly oriented solvent molecules.[208] Thus, more polar solvents favor the stabilization of the excited state of the probe. By examining the structure of ellipticine (Figure 3.2), the electrons are expected to be delocalized between the nitrogen atoms of the pyridine-like ring (ring 4) and of the pyrrole-like ring (ring 2). In addition, hydrogen bonding between the solvent and both nitrogen atoms of ellipticine may induce electron redistribution. This might be the reason why, in all protic solvents with strong hydrogen bonding ability, peak III shifts to higher wavelengths, but it remains fixed at low wavelengths in hexane and cyclohexane where the formation of hydrogen bonds is prevented. The effect of specific solvent interactions will be discussed later.

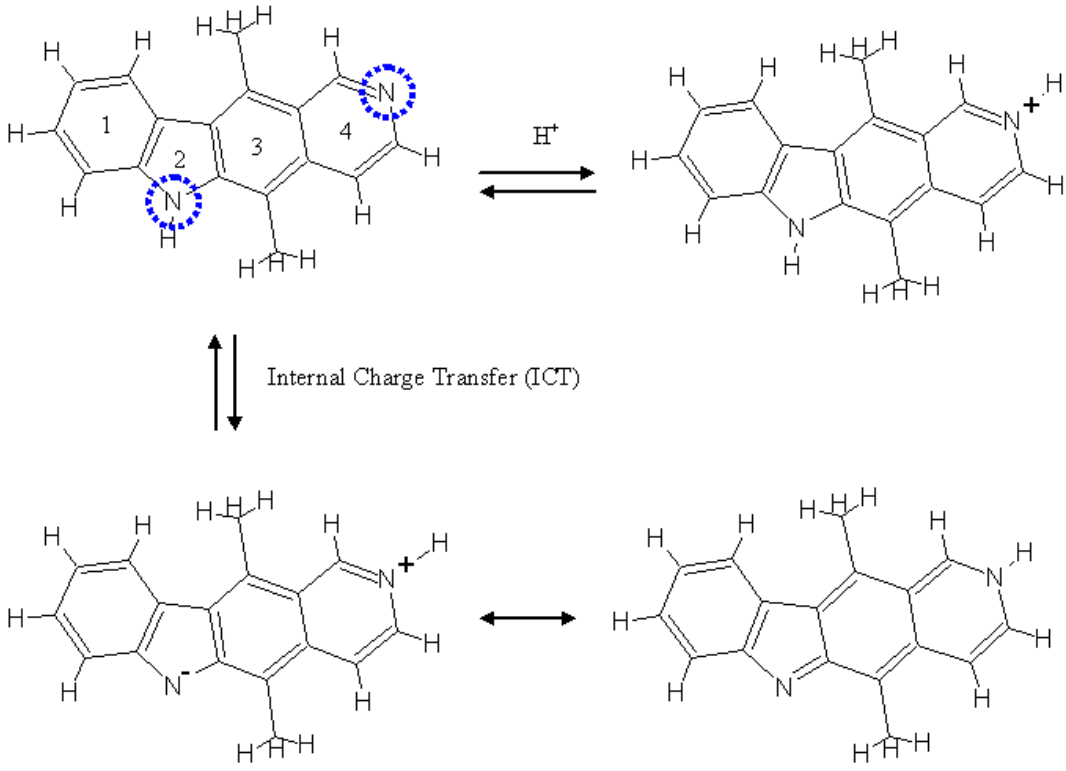

Figure 3.2 Different forms of ellipticine

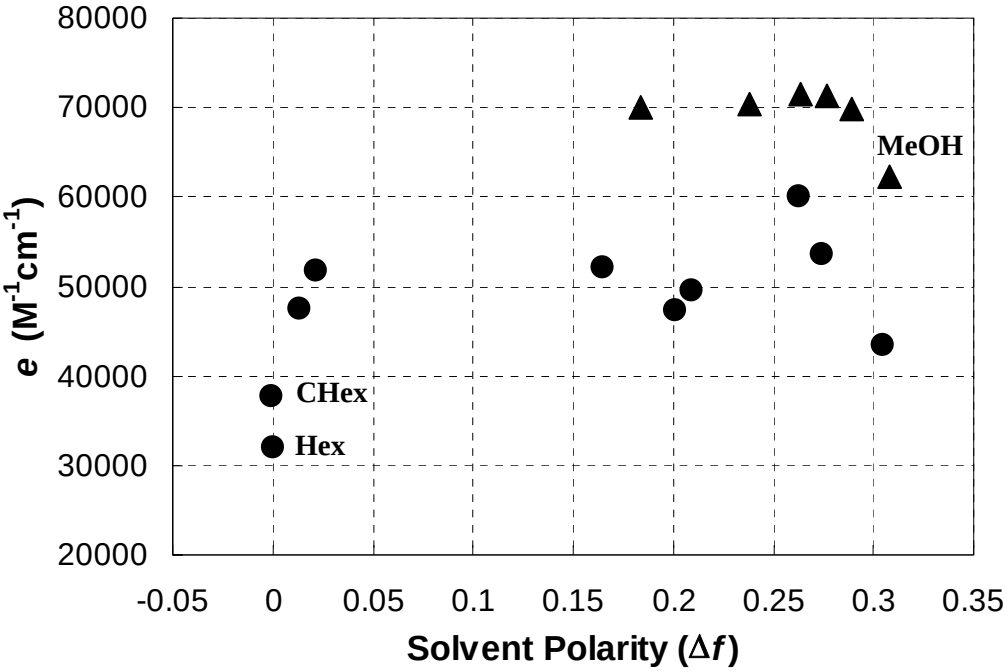

Figure 3.3 Extinction coefficients of ellipticine as a function of solvent polarity (Δ*f*) (alcohols, triangles). The ellipticine concentrations in hexane and cyclohexane varied from 1 to 5 μM (due to its low solubility in these two solvents) while those in other solvents varied from 2 to 20 μM. The data for each solvent followed a straight line, and the extinction coefficient was obtained through a linear fit of the data using Equation 3.4.

The extinction coefficients (*e*) at peak III in pure solvents are listed in Table 3.1 and plotted against the solvent polarity (Δ*f*) in Figure 3.3. It seems that there is no trend for the extinction coefficients as a function of solvent polarity. The values vary from 32000 in non-polar solvents up to ~70000 in protic solvents (alcohols). Interestingly, ellipticine has the highest extinction coefficients in all protic solvents (solid triangles) except methanol, intermediate ones in aprotic polar solvents, and the lowest ones in non-polar solvents. This trend seems to follow the hydrogen bonding ability of the solvents, where the alcohols exhibiting a hydroxyl group (OH) have the strongest hydrogen bonding

ability, but the non-polar solvents cannot form hydrogen bonds with ellipticine. The aprotic polar solvents contain either an ether group or an ester group, which can act as hydrogen acceptors for hydrogen bonding, resulting in an intermediate hydrogen bonding ability. These observations suggest that hydrogen bonding between the solvent and ellipticine affects its extinction coefficient.

3.3.2 Effect of Solvent on the Fluorescence Emission Spectra

Following the absorption experiments, steady-state fluorescence spectra of ellipticine were acquired in 16 different organic solvents. Some representative emission spectra are shown in Figure 3.4. The spectra were normalized with respect to their peak maxima. The peak maximum shifts to the right (red shift) as the solvent polarity increases (from hexane to methanol). Meanwhile, the spectra obtained in apolar solvents such as hexane exhibit several peaks which merged into a single broad peak when dissolved in more polar solvents. It is worth noting that the emission spectrum in methanol exhibits a red-shifted peak at ~510 nm. This peak is close to the one observed at 520 nm in SDS micelles and aqueous solutions, which has been identified as the protonated form of ellipticine (protonation of the nitrogen on the pyridine-like ring).[168,169,199] This might be due to the fact that methanol, having a smaller pKa, is more acidic than other alcohols. However, the real mechanisms behind this phenomenon are still unclear.

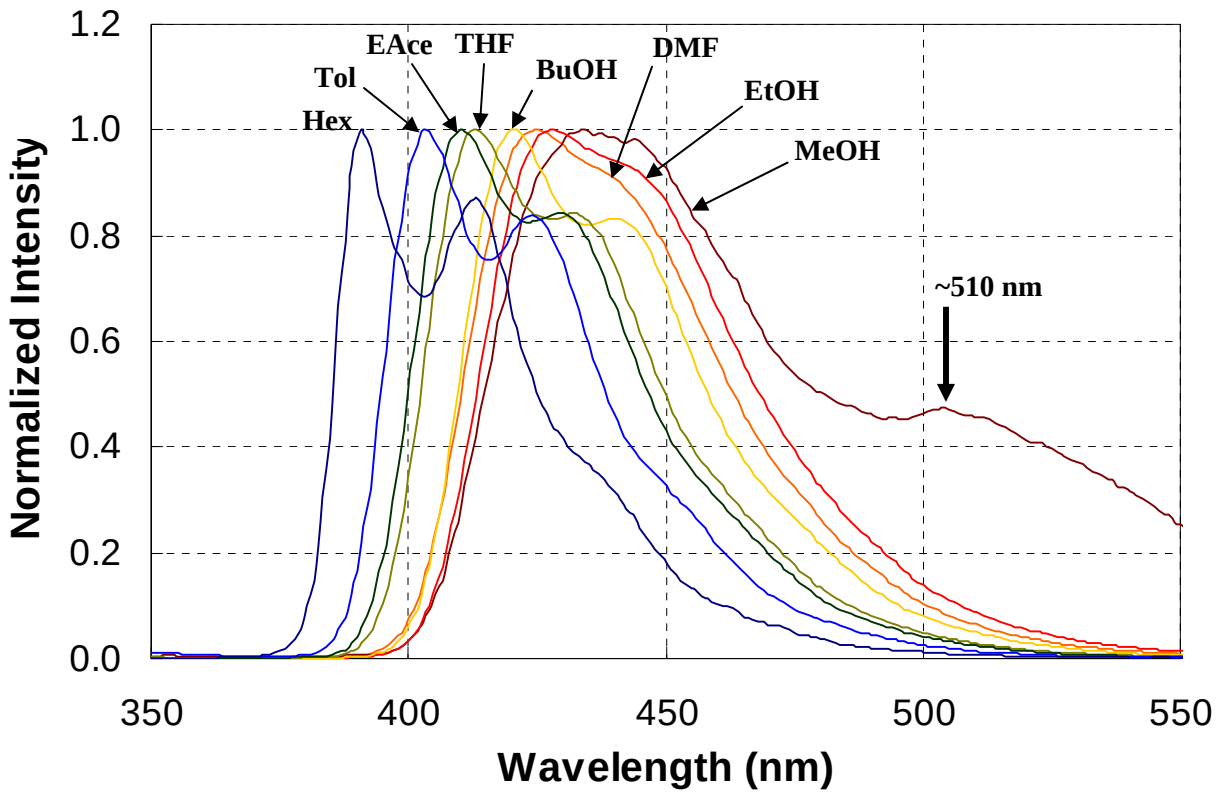

Figure 3.4 Fluorescence emission spectra of ellipticine (2 μM) in different solvents. All spectra were normalized with respect to the peak maximum.

Further experiments were conducted to investigate whether the 510 nm peak in methanol could be attributed to the formation of an ellipticine excimer. The fluorescence spectra of a series of ellipticine solutions in methanol with concentrations ranging from 2 to 100 μM were acquired. The ratio of the fluorescence intensity at the 436 nm peak to that at the 510 nm peak was found to remain constant and equal to 2.16 ± 0.02 for all ellipticine concentrations. This result suggests that the 510 nm peak is not due to the formation of an excimer since increasing the ellipticine concentration should have resulted in an increase of the ratio.[209]

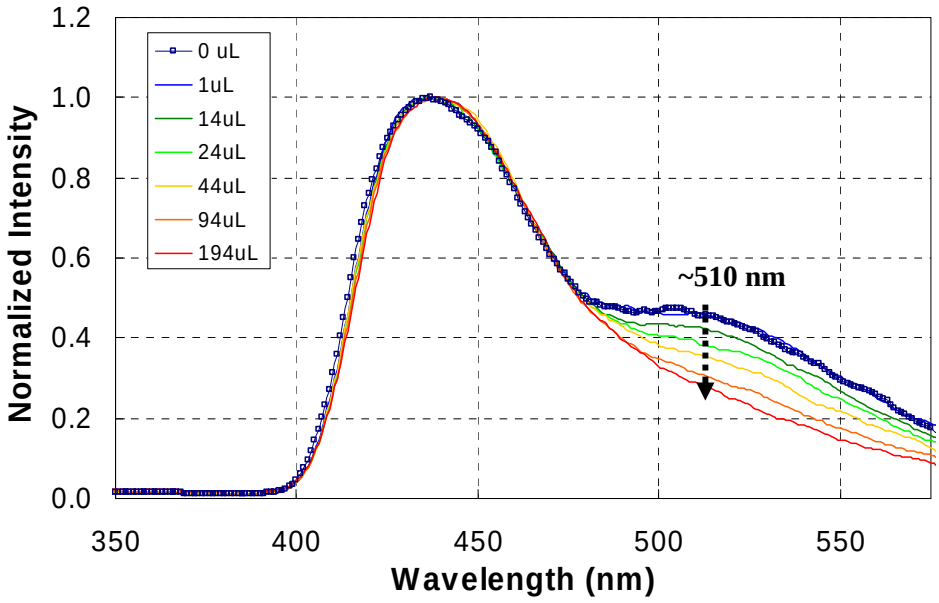

Figure 3.5 Fluorescence emission spectra of ellipticine (2 μM) in methanol upon addition of 1 M NaOH (top pure methanol, bottom 194 uL of 1M NaOH solution). All spectra were normalized with respect to their peak maxima.

To confirm that protonation resulted in the appearance of the 510 nm peak, a 5 mL methanol solution containing 2 μM ellipticine was titrated by adding 1-194 μL of 1.0 M NaOH solution. As shown in Figure 3.5, the 510 nm peak decreased with the addition of NaOH due to the deprotonation of ellipticine. Thus, it was concluded that the protonated ellipticine causes the emission peak at ~510 nm in methanol. This result is consistent with the earlier finding that ellipticine is protonated in SDS micelles giving a peak maximum at ~520 nm.[168]

3.3.3 General Solvent Effect and the Lippert-Mataga Relation

The position of the peak maximum (λ_f) for each fluorescence spectrum was plotted against the solvent dielectric constant (ε) in Figure 3.6a, and was listed in Table 3.1. A trend exists where the

peak maximum shifts from 390 nm to ~430 nm with increasing solvent dielectric constant. It seems that the profile reaches a plateau when the dielectric constant is larger than 20. Since the dielectric constant is a parameter often taken to represent the solvent polarity, Figure 3.6a confirms that the solvent polarity affects the fluorescence of ellipticine.

(a)

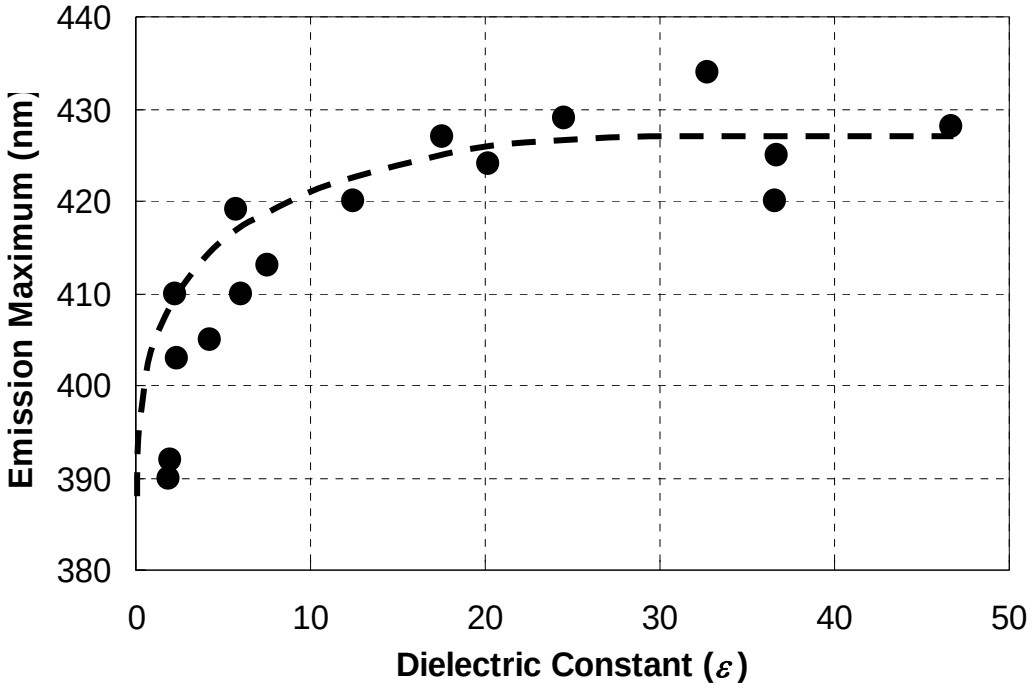

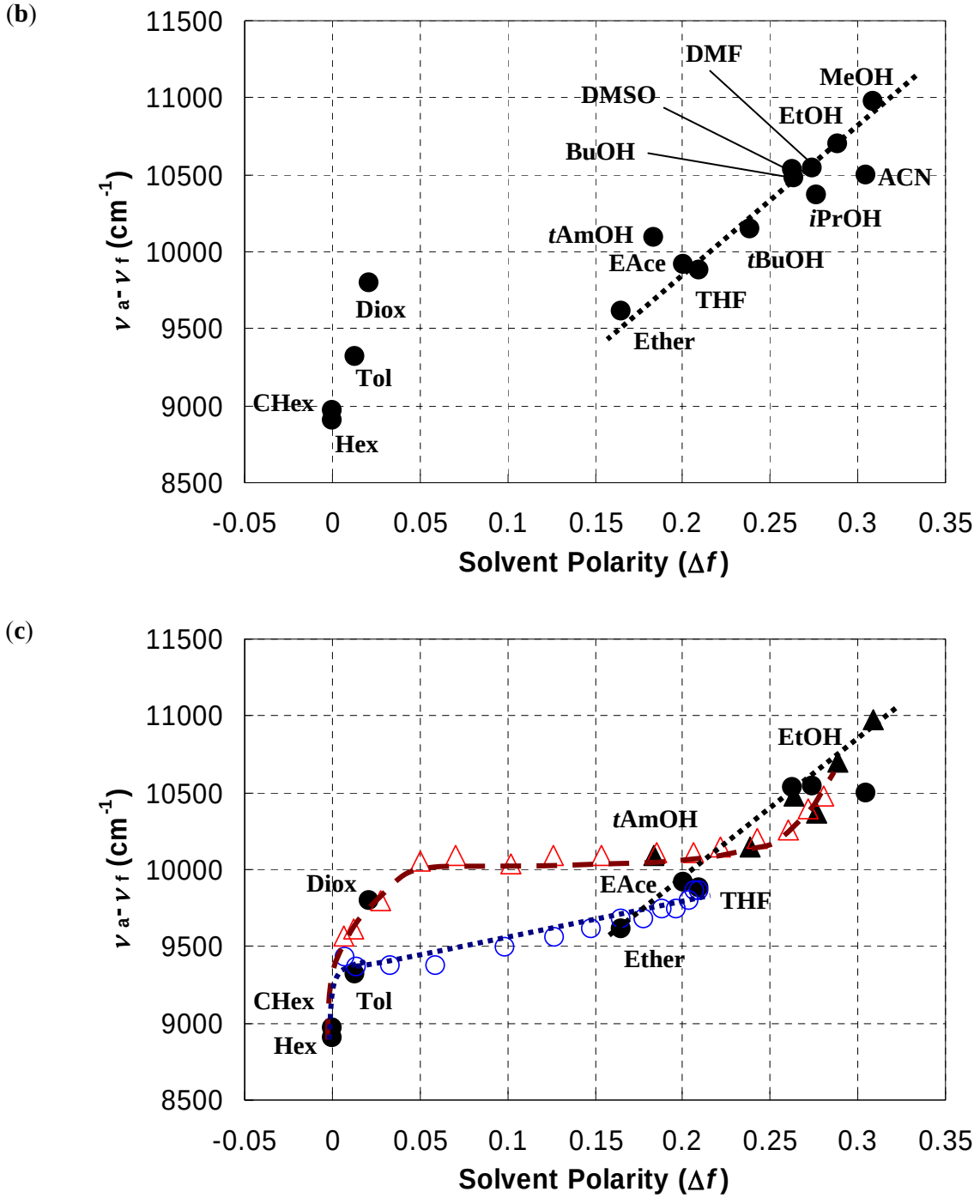

Figure 3.6 (a) Position of ellipticine fluorescence maximum as a function of solvent dielectric constants. (b) Lippert-Mataga plot of ellipticine in 16 pure solvents. The data are fitted to a straight line (slope = 9700 ± 990, $R^2 > 0.92$) for solvent polarity larger than 0.15. (c) Lippert-Mataga plot of

ellipticine in mixtures of hexane-THF (open circles) and hexane-ethanol (open triangles). The ellipticine concentration in each solvent and solvent mixture was set at 2 μM.

To better understand the solvent polarity effect, the Lippert-Mataga relation was applied. This relation has been widely used to correlate the energy difference between absorption ($h\nu_a$) and emission ($h\nu_f$), also known as Stokes' shift, with solvent polarity represented by Δf. This relation is given in Equation 3.5. It involves both the dielectric constant and the refractive index (n) of the solvents:[201,202]

$$\nu_a - \nu_f = \frac{2}{hc}\left(\frac{\varepsilon - 1}{2\varepsilon + 1} - \frac{n^2 - 1}{2n^2 + 1}\right)\frac{(\mu_E - \mu_G)^2}{a^3} + const. \qquad (3.5)$$

In Equation 5, ν_a and ν_f are the wavenumbers (1/cm) corresponding to the absorption and the emission, respectively, h is Planck's constant, c is the speed of light, and a is the radius of the solvent cavity in which the fluorophore resides. The term involving ε and n is called the orientation polarizability (Δf), which only accounts for the spectral shifts due to the reorientation of the solvent molecules. Therefore, the Lippert-Mataga relation is based on the assumption that the energy difference is only proportional to the solvent orientation polarizability (known as the general solvent effect). Inability of the Stokes' shift to increase linearly with Δf usually implies that specific solvent effects are involved.

Figure 3.6b shows the Lippert-Mataga plot of ellipticine in 16 organic solvents. The Stokes' shift increases with increasing solvent polarity. When the solvent polarity (Δf) is larger than 0.15, the data appears to fall on a straight line. From the Lippert-Mataga equation, the slope of this line yields

the dipole moment difference between the ground and excited states, $(\Delta\mu)^2$ according to Equation 3.6:[201,202]

$$slope = \frac{2(\Delta\mu)^2}{hca^3} \tag{3.6}$$

The estimated dipole moment difference is 12.2 D (debye) (slope 9700 ± 990, $R^2 > 0.92$), based on the assumption that the Onsager cavity radius *a* equals 5.35 Å, which is half of the optimized distance between the two farthest atoms of the molecule in the direction of charge separation (10.7 Å).[210] Although this $\Delta\mu$ value was obtained with an approximated cavity radius, it is quite comparable with those reported for other solvatochromic compounds (3~20 D).[210-217] This estimation from the Lippert-Mataga equation is based on the assumption that the photophysical properties of ellipticine can be described by the theory of general solvent effect; hence, it may not hold if specific solvent effects are involved. Actually, the Stokes' shifts observed for solvents with a polarity smaller than 0.03 do not follow the trend (Figure 3.6b). This suggests that the solvent polarity might not be the only factor affecting the spectral shifts. Specific solvent effects including hydrogen bonding, acid-base chemistry and charge-transfer interactions, can also result in nonlinear Lippert-Mataga plots.[202] As mentioned before, ellipticine can form hydrogen bonds with the solvent, and it can shuffle electrons between its two nitrogen atoms (Figure 3.2). This complicates the interpretation of how the solvent affects the absorption and emission spectra of ellipticine.

To better understand the factors that affect the Stokes' shifts of ellipticine, the data points in Figure 3.6b can be roughly divided into two groups corresponding to Δf values smaller than 0.03 and larger than 0.15. In the more polar region ($\Delta f > 0.15$), a linear trend was found and the corresponding dipole moment difference was estimated to be 12.2 D. Such a large dipole moment difference usually indicates the occurrence of intramolecular charge transfer (ICT) induced by the solvent after

excitation.[210,213-217] Figure 3.2 describes the mechanism by which the ICT occurs. In most cases, solvent polarity is believed to be the effect driving an ICT, but for ellipticine, another important factor – hydrogen bonding – should be considered as well. Most solvents used in this study can form hydrogen bonds with ellipticine except hexane and cyclohexane. Alcohols with a hydroxyl group (OH) together with solvents such as DMF and DMSO are expected to form strong hydrogen bonds with ellipticine, which, in addition to their large solvent polarity, may favor the occurrence of an ICT and result in the large 12.2D dipole moment difference. Although hydrogen bond formation may occur even in less polar solvents such as diethyl ether, THF and ethyl acetate, the strength of such hydrogen bonds is expected to be weaker;[208] as a result, these solvents will be much less effective at inducing an ICT (see below). In the less polar region ($\Delta f < 0.03$), the data fell on a second, steeper straight line. However, this steeper straight line is probably a coincidence because an ICT should not occur in the non-polar hexane and cyclohexane where no hydrogen bonds can be formed with ellipticine. In addition, the relatively larger Stokes' shift observed in toluene may be related to the presence of π-π staking, and that observed in 1,4-dioxane can be due to hydrogen bonding interactions (see below).

In order to bridge the gap between the non-polar ($\Delta f < 0.03$) and semi-polar ($0.15 < \Delta f < 0.2$) solvents in the Lippert-Mataga plot, ellipticine solutions were prepared with solvent mixtures of hexane and THF. Such binary mixtures provide a simpler means of studying solvent effects because it reduces the possibilities of specific solvent effects generated by different solvents. The results are listed in Table 3.1 and plotted in Figure 3.6c (open circles). The Stokes' shifts increases linearly with the solvent polarity, but the mixture containing the lowest volume fraction of THF (1 v/v %) exhibits a Stokes' shift substantially larger than that of hexane. The dramatic increase in Stokes' shift observed for 1 v/v % of THF in hexane cannot be due to an increase of the solvent polarity alone, but to specific interactions between THF and ellipticine. This statement is further illustrated in Figure

3.7a, where the position of the absorption and emission maxima is plotted as a function of solvent composition. Small addition of THF results in a substantial shift of the position of both the absorption and emission maxima.

(a)

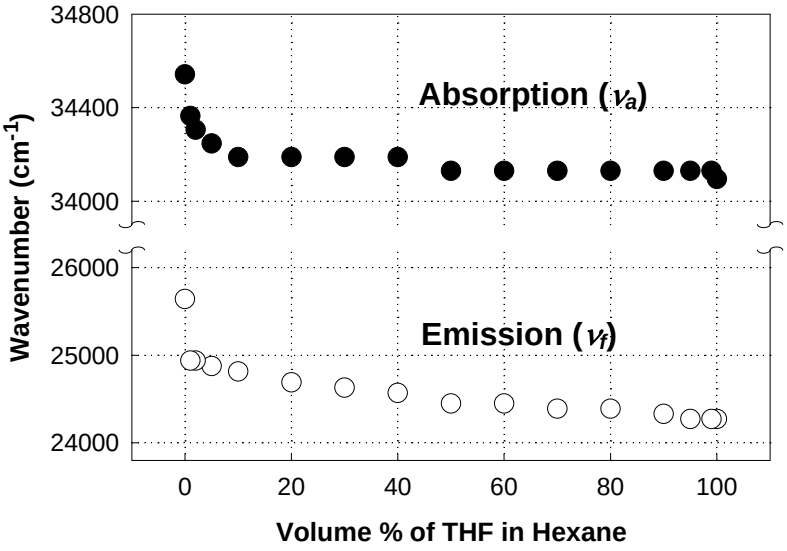

(b)

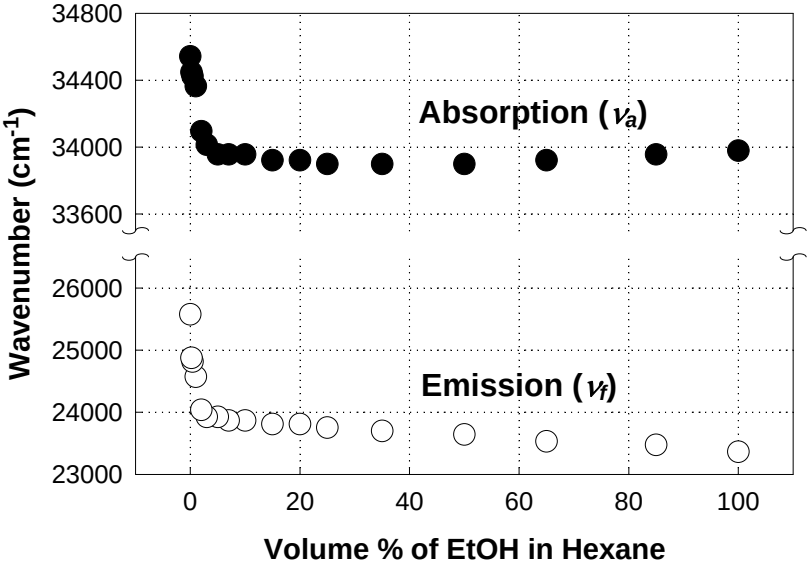

Figure 3.7 Position of the absorption peakIII and emission maximum of ellipticine (2 μM) in the hexane-THF mixtures (a) and in the hexane-ethanol mixtures (b).

One possible reason for this effect could be the formation of hydrogen bonds between THF and ellipticine. THF contains an ether group (C-O-C), which can serve as a hydrogen acceptor, so hydrogen bonds can be formed between the NH group on the pyrrole-like ring of ellipticine and the oxygen of THF. This interaction only requires minute amounts of THF since the ellipticine concentration is very low (2 μM), and that of THF in a 1 v/v % mixture is comparatively high (0.125 M). The presence of minute amounts of THF also affects the absorption of ellipticine (Figure 3.7a), suggesting that hydrogen bonding between THF and ellipticine must be occurring in the ground state.[202,208] When the amount of THF is greater than 5 v/v %, both absorption and emission shift gradually to lower wavenumbers due to the increase of solvent polarity.

Combining the data generated from the hexane-THF mixtures with that from 16 pure solvents, a transition is clearly seen at a solvent polarity around 0.2 (Figure 3.6c). This transition is thought to be an indication that an ICT happens when Δf is above 0.2. However, it is worth noting that the position of this transition is not fixed, and depends on different systems of solvent mixtures (see below). Furthermore, solvents with Δf values close to 0.2 (THF, ethyl acetate and diethyl ether) may be less effective at inducing an ICT as they are very close to the transition region.

The results obtained so far suggest that the Stokes' shift of ellipticine in solvents is governed by three factors: solvent polarity, hydrogen bonding and ICT. In the case of solvent mixtures between an alkane and a H-bond forming solvent, hydrogen bonding is expected to cause a sudden increase of the Stokes' shift in non-polar mixtures followed by a slight increase mainly due to the increase of the mixture polarity ($0.01 < \Delta f < 0.2$); an ICT induced by both hydrogen bonding and solvent polarity occurs when Δf is greater than ~0.2. To validate the transition described above, a series of binary mixtures of hexane and ethanol was prepared, covering a wider range of polarities from 0 to ~0.3. The resulting profile is shown as open triangles in Figure 3.6c. The previously described transitions are

also apparent in this profile. Comparing this profile to that generated with the series of mixtures of hexane and THF, one observes that both display a sudden increase of the Stokes' shift upon small addition of the polar cosolvent due to hydrogen bonding, followed by a slight increase for intermediate solvent polarities ($0.05 < \Delta f < 0.2$). When the solvent polarity of the hexane-ethanol mixtures is higher than 0.25, a steeper increase is observed due to an ICT. Overall, the profile obtained from the hexane-ethanol mixtures exhibits a much larger Stokes' shift in the apolar solvent region ($\Delta f < 0.05$) and reflects the occurrence of an ICT in the more polar solvent region ($\Delta f > 0.25$).

The relatively larger Stokes' shift observed with the hexane-ethanol mixtures comparatively to the hexane-THF mixtures is probably due to stronger hydrogen bond formation between ellipticine and ethanol than between ellipticine and THF. This can also be seen by comparing Figure 3.7a and b. As for THF, the hydrogen bonds were formed in the ground state with the presence of minute amounts of ethanol (less than 5 v/v % in Figure 3.7b). For Δf values between 0.05 and 0.25, the Stokes' shifts remains almost constant regardless of increasing solvent polarity. This result suggests that, in the moderate polarity range, the Stokes' shift of ellipticine in the hexane-ethanol mixtures is predominantly determined by hydrogen bonding rather than by solvent polarity. When the polarity is larger than 0.25, ellipticine undergoes an ICT resulting in a large increase of the Stokes' shift.

The above discussion rationalizes why some of the data points in Figure 3.6b, (i.e., hexane, cyclohexane, 1,4-dioxane, *tert*-amyl alcohol and acetonitrile), are scattered and away from the master line obtained for solvents with polarity between 0.15 and 0.32. The non-polar solvents, hexane and cyclohexane, do not have specific interactions with ellipticine; hence the Stokes' shift in these non-polar solvents is small. A similar observation was reported from Pal and his group when studying coumarin and its derivatives.[218-220] They found that the unusual behavior of coumarin and its derivatives in non-polar solvents is due to the absence of ICT (i.e., locally excited (LE) state). A

much larger Stokes' shift observed in 1,4-dioxane, which is comparable to that obtained with THF and diethyl ether, is probably due to a similar ability of forming hydrogen bonds between ellipticine and the ether oxygen of 1,4-dioxane, THF or diethyl ether. Similarly, the OH group of *tert*-amyl alcohol may induce stronger hydrogen bonding with ellipticine, so that a larger Stokes' shift than expected from the Δf value is observed. In fact, both 1,4-dioxane and *tert*-amyl alcohol yield Stokes' shifts that fall on the profile generated by the hexane-ethanol mixtures, suggesting the presence of stronger hydrogen bonds between ellipticine and these two solvents. In the region of polar solvents, the Stoke's shift of acetonitrile is somewhat lower than its value expected from the linear trend line shown in Figure 3.6b. This effect may be a result of the weaker hydrogen bonds formed between ellipticine and the CN group than the hydroxyl group (OH) of alcohols, even though acetonitrile is the second most polar solvent in this study.

3.3.4 Solvent Effect on Fluorescence Lifetime

The lifetimes of ellipticine in pure solvents are listed in Table 3.2. Most decay curves can be well fitted with a single exponential with a χ^2 smaller than 1.3. The others are fitted with a sum of two exponentials. The solvents in which ellipticine has two lifetimes are methanol, toluene, cyclohexane and hexane. These "abnormal" solvents are either very polar (methanol) or non-polar (toluene, cyclohexane and hexane). The data in Table 3.2 indicate that the lifetime of ellipticine falls in two categories: the longer lifetime ranges from 15 to 29 ns depending on the solvent polarity; the shorter one is around 5 ns. In very polar methanol, ellipticine exhibits a decay time around 3 ns. The reason for the biexponential decay of ellipticine is still unclear. One may speculate that there exist two different forms of ellipticine in methanol, i.e., the protonated and neutral forms as mentioned before; however, such speculation does not hold in non-polar solvents where two lifetimes are observed because ellipticine cannot be protonated in non-polar solvents.

Table 3.2 Lifetime of ellipticine in different solvents

Solvents	Δf	τ_1 (ns)	a_1	τ_2 (ns)	a_2	τ_{avg} (ns)	χ^2
DMSO	0.263	24.4	1.00				1.23
DMF	0.274	25.7	1.00				1.22
$MeOH_{(434)}$	0.308	3.4	0.70	5.3	0.30	4.0	1.10
EtOH	0.289	29.8	1.00				1.21
BuOH	0.264	28.3	1.00				1.10
*t*BuOH	0.238	27.4	1.00				1.16
THF	0.210	21.7	1.00				1.25
EAce	0.201	23.5	1.00				1.19
*t*AmOH	0.184	26.2	1.00				1.22
Ether	0.165	15.4	1.00				1.17
Diox	0.021	21.2	1.00				1.15
Tol	0.013	18.3	0.83	13.2	0.17	17.4	1.24
CHex	0	15.1	0.92	4.6	0.08	14.2	1.00
Hex	0	16.5	0.87	4.4	0.13	14.9	1.16
EPC		28.5	0.84	5.8	0.16	24.9	1.19
$MeOH_{(510)}$		9.2	0.89	2.0	-0.11	-	1.24
SDS		8.5	1.00				1.20

Note: the average lifetime is calculated from Equation 3.7. The subscripts for MeOH represent the wavelengths at which the fluorescence decay was collected. The time-resolved fluorescence data were fitted with the equation: $I(t) = a_1 e^{(-t/\tau_1)} + a_2 e^{(-t/\tau_2)}$

The effect of solvent on the lifetimes is illustrated in Figure 3.8, where the lifetimes are plotted as a function of solvent polarity. When two lifetimes were needed to fit the fluorescence decays, the number average lifetime was calculated with Equation 3.7:

$$\tau_{avg} = \frac{a_1}{a_1 + a_2}\tau_1 + \frac{a_2}{a_1 + a_2}\tau_2 \qquad (3.7)$$

where a_1 and a_2 are the contributions of the two decay times obtained from the curve fitting. The average lifetime of ellipticine shown in Figure 3.8 is scattered between 15 and 30 ns. Interestingly, ellipticine has the longest lifetime in all alcohols (triangles) except in methanol ($\Delta f = 0.308$).

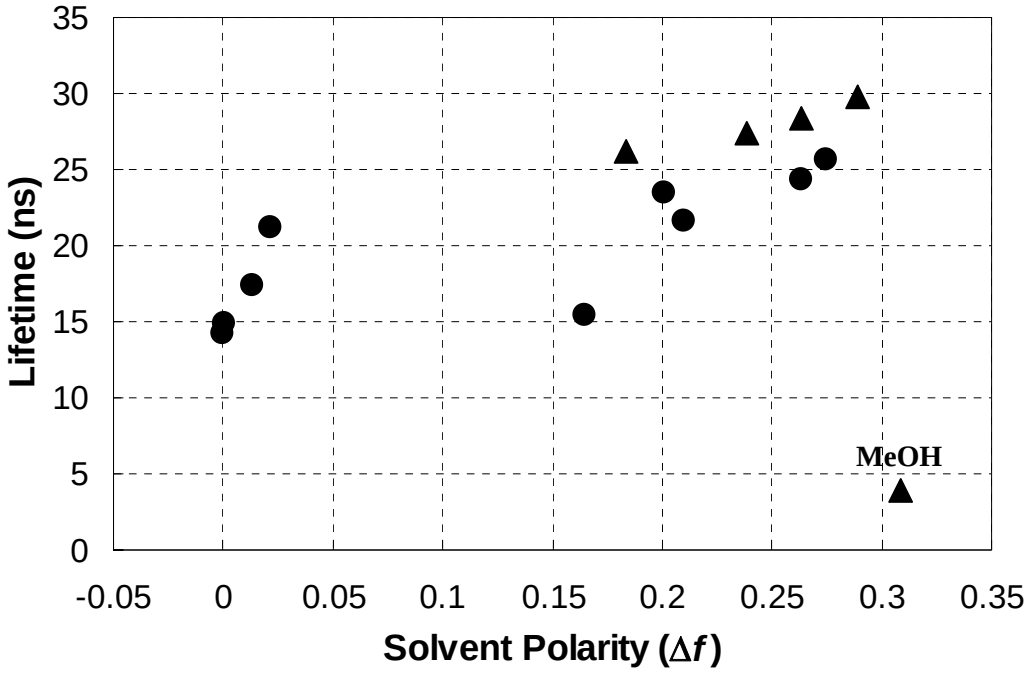

Figure 3.8 Ellipticine lifetime as a function of solvent polarity. The lifetime increases with increasing solvent polarity. Ellipticine in methanol is an exception with a very short lifetime. Triangles represent alcohols. The ellipticine concentration was set at 2 μM

It was shown in Figure 3.4 that ellipticine exhibits two fluorescence peaks in methanol. To further confirm whether the emission of ellipticine at the 434 nm and 510 nm peaks came from two different ellipticine species, a fluorescence decay experiment was carried out at 510 nm in addition to 434 nm. The decay time of ellipticine at 510 nm was found to be ~9.2 ns, which is much longer than that at 434 nm (~4.0 ns) (Table 3.2). Furthermore, the decay acquired at 510 nm displayed a rise time,

suggesting that the formation of the species that emitted with a 9.2 ns decay time was delayed. These results clearly show that the fluorescence emission at 434 nm and 510 nm comes from two different species of ellipticine in methanol. In addition, the species (species II) having a 9.2 ns decay time were formed after those (species I) with a shorter decay time (~4.0 ns) were excited. In fact, the excitation spectra acquired at both emission maxima of 434 nm and 510 nm overlapped after normalization, which supports the statement that species I of ellipticine is generated prior to species II. The decay time of the protonated form of ellipticine at 520 nm was found to equal ~8.5 ns in SDS micelles, which is comparable to that of ellipticine at 510 nm in methanol. Therefore, these results suggest that the 510 nm fluorescence maximum of ellipticine in methanol is due to the protonated form of ellipticine.

3.3.5 Ellipticine in Lipid Bilayers

The photophysical behavior of ellipticine was investigated in aqueous dispersions of EPC liposomes. Since ellipticine can be classified as being extremely hydrophobic considering its very low water solubility (6.2×10^{-7} M)[71], it was expected to reside in the hydrophobic regions of the EPC liposomes. The location of ellipticine in the lipid bilayers might be inferred by comparing the spectral shift of ellipticine in the liposome dispersions with those obtained in organic solvents of known polarity.

The emission spectra of ellipticine in different solvents and in the EPC liposomes were normalized to 1.0 and plotted in Figure 3.9. The emission band of ellipticine in the liposomes is located at 436 nm (λ_{ex} = 295 nm), a wavelength very close to that obtained in methanol. The spectrum shows a relatively large red shift, suggesting that a more polar microenvironment is surrounding the ellipticine molecules. For comparison, the fluorescence spectrum of ellipticine in pH 7 Tris/acetic acid buffer solution was acquired. The intensity of this emission spectrum was normalized according to that of ellipticine in EPC liposomes. It is clearly seen that ellipticine in the buffer solution exhibits

an emission band at ~520 nm corresponding to its protonated form (Figure 3.9 inset), and does not dissolve well in aqueous solution resulting in a very low fluorescence signal. These results indicate that the EPC liposomes can efficiently dissolve ellipticine, but that the local environment experienced by ellipticine in the liposomes is rather polar, different from that expected of ellipticine located inside the hydrophobic lipid bilayer. Consequently, ellipticine dissolved in the liposomes must be located at or close to the interface between the lipid membrane and water. This could be due to the fact that the dipole and quadrupole moments of the indole ring (a combination of rings 1 and 2 in Figure 3.2) of ellipticine are more suited to interacting with charged and polar groups in the phospholipids than with the hydrophobic acyl chains; in addition, the flat rigid shape of ellipticine may limit its access to the hydrocarbon core. Such phenomena have also been found with the amino acid tryptophan (Trp), which consists of an indole ring and has a preference for membrane interfaces.[221] The location of ellipticine at or close to the membrane surface combined with its sensitivity to the local environment suggests that ellipticine might also serve as a surface probe for studying biological phenomena occurring at a membrane interface.

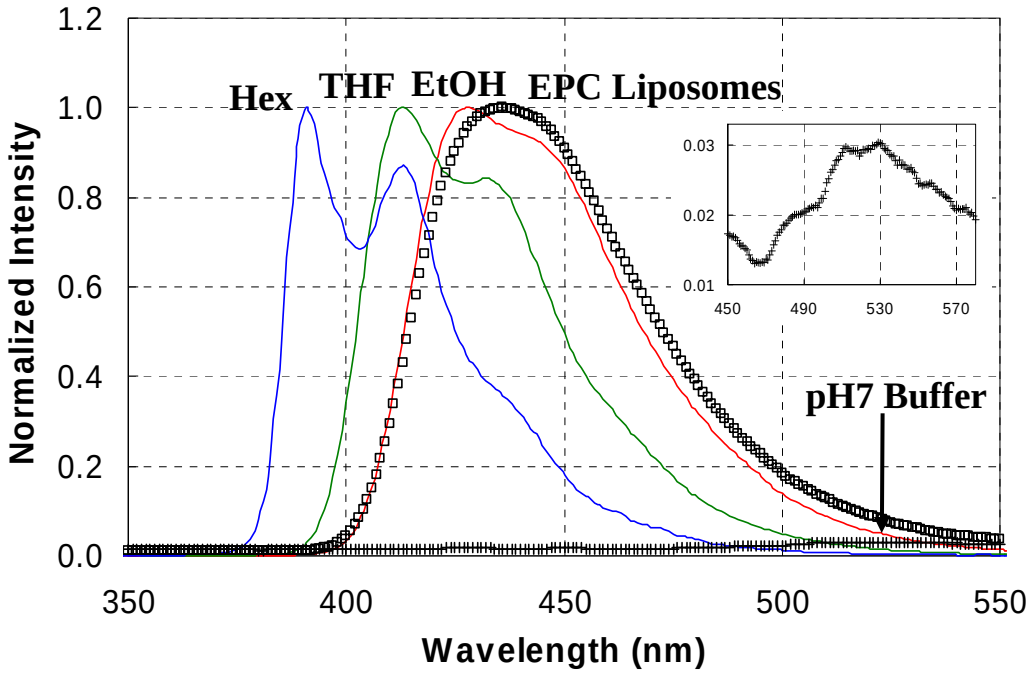

Figure 3.9 Fluorescence emission spectra of ellipticine (2 μM) in different solvents and EPC liposomes. The spectrum of ellipticine in pH 7 buffer was normalized with respect to the peak maximum in EPC liposomes. The spectrum of ellipticine in buffer is enlarged in the inset.

3.4 Conclusions

The photophysical properties of the anticancer agent ellipticine were systematically studied in 16 organic solvents and some of their mixtures. The UV absorption and fluorescence emission of ellipticine were found to be solvent dependent. As the solvent polarity increased, ellipticine exhibited a spectral shift to the red for both absorption and emission. The spectral shifts could be correlated with the solvent dielectric constants and the solvent polarity using the Lippert-Mataga equation. The presence of a non-linear trend in the Lippert-Mataga plot indicated the existence of specific solvent effects. Such effects were thought to result in an intramolecular charge transfer (ICT) due to the large

dipole moment difference between the ground state and the excited state. Hydrogen bonding between the solvent and ellipticine can also be related to the specific solvent effects. The formation of stronger hydrogen bonds in alcohols led to larger extinction coefficients and longer lifetimes, although methanol was an exception. Ellipticine exhibited an emission band at 436 nm in EPC liposomes. The emission band of ellipticine at 436 nm in the liposomes indicated that ellipticine is located in a rather polar environment, presumably close to the hydrophilic surface of the liposomes rather than buried in the hydrophobic interior of the liposome membrane. This study not only provides detailed information on the photophysical properties of ellipticine in many solvents, but also suggests that the dependence of the spectral shift of ellipticine with solvent can be a good indicator of where ellipticine is located in a heterogeneous medium such as the one offered by EPC liposomes.

Chapter 4*
Complexation of Ellipticine with a Self-Assembling Peptide and Its Release into a Cell Membrane Mimic

4.1 Introduction

The slow progress in treating severe diseases such as cancer has suggested a growing need for novel approaches to the effective delivery of therapeutics to physiological targets. Drug delivery systems are essential to control pharmacokinetics, non-specific toxicity, immunogenecity, biorecognition, and drug efficacy.[151] In order to develop novel drug delivery systems for clinical use, the design and/or discovery of effective delivery vehicles play an important role. The ideal delivery vehicle should have the following properties: biocompatibility, biodegradability, suitable size, high loading capacity, extended circulation time, and ability to accumulate at required pathological sites in the body.[25]

Peptides have shown much potential for drug delivery. The most attractive aspect of peptide-mediated drug delivery is the natural propensities of many peptides for cell penetration and targeting.[112,153,154] As a result, many novel delivery systems involve peptides to achieve targeted delivery[15,16,112,222] for anticancer therapeutics and to cross the cell membrane barrier[223-226] for gene/siRNA delivery. Peptide-based delivery systems have also shown the potential to deliver therapeutic proteins, bioactive peptides, small molecules and nucleic acids.[112,154,227]

A special class of self-assembling, ionic-complementary peptides[228] could be a new and promising biomaterial for constructing drug delivery carriers. The unique amphiphilic structure and the ability of self-assembly of these peptides allow them to encapsulate both hydrophobic chemotherapeutics and hydrophilic protein and oligonucleotides.[57,58,228] Moreover, no detectable immune response was observed when these peptides were introduced into animals.[61,64,134] These

*This chapter is based on a paper "S.Y. Fung, H. Yang, P. T. Bhola, P. Sadatmousavi, E. Muzar, M. Liu and P. Chen, Self-assembling peptide as a potential carrier for hydrophobic anticancer drug ellipticine: complexation and release, submitted to *ACS Nano*, 2007".

peptides can spontaneously organize themselves into nano/micro structures that may provide a protected and stable environment for the therapeutic molecules. An additional advantage of using such peptide-based carriers is the ease of sequence modification and design to incorporate peptide cell penetration and targeting capabilities.

A typical self-assembling, ionic-complementary peptide, EAK16-II, has been shown to readily encapsulate hydrophobic compounds and stabilize them in aqueous solution. Recent work using pyrene as a model hydrophobic compound demonstrated the promising potential of this peptide for the delivery of hydrophobic anticancer drugs.[51,56] EAK16-II was shown to stabilize pyrene microcrystals in aqueous solution at a concentration ten-thousand fold beyond its solubility in water, indicating a very high loading efficiency. The encapsulated pyrene from the peptide coatings can be released into liposomes and the release rate can be controlled by changing the peptide-to-pyrene ratio during the encapsulation.[51] More recently, this peptide has been used to stabilize microcrystals of the anticancer agent ellipticine in aqueous solution.[56] The stabilized ellipticine microcrystals can have a concentration several hundred times larger than its solubility in water.

Ellipticine is selected as the model hydrophobic anticancer drug in our studies for the following reasons: first, the fluorescence property of ellipticine enables us to monitor the interaction of ellipticine with the peptide and its location in different micro-environments (Chapter 3). Second, ellipticine is extremely hydrophobic with a low water solubility of ~0.62 μM at neutral pH,[71] which is comparable with that of the model hydrophobic compound pyrene.[72] Third, its great anticancer activity makes ellipticine one of the promising candidates in cancer chemotherapy.[73] Fourth, the discovery of severe side effects of ellipticine derivatives during clinical trials suggests that a novel delivery system is required.[73,74]

In this study, we investigate the effect of peptide and ellipticine concentration on the formation of stable peptide-ellipticine complexes in aqueous solution over time. This will elucidate the kinetics of complex formation in relation to peptide self-assembly. A new methodology developed in our recent work[51] is applied to study the release kinetics of ellipticine from the stable peptide-ellipticine complexes to egg phosphatidylcholine (EPC) vesicles as cell membrane mimics. The fluorescence technique is the primary tool to characterize the complex formation and the release kinetics, where the change of ellipticine fluorescence is monitored over time. A calibration curve is constructed to relate the fluorescence of ellipticine in vesicles to ellipticine concentration. The UV-Vis absorption as a complementary method is adopted to verify the trend of the calibration curve and the corresponding ellipticine concentration. Scanning electron microscopy (SEM) is applied to characterize the dimensions of the peptide-ellipticine complexes. This work will provide comprehensive knowledge on the formation of peptide-ellipticine suspensions and ellipticine release kinetics, paving the way for future cellular and animal studies in the development of self-assembling peptide-based delivery of hydrophobic anticancer drugs.

4.2 Materials and Methods

4.2.1 Materials

The peptide EAK16-II (Mw = 1657 g/mol, crude) was purchased from CanPeptide Inc. (Montreal, Canada) and used without further purification. It has a sequence of AEAEAKAKAEAEAKAK (Figure 4.1), where A corresponds to alanine, E to glutamic acid and K to lysine. The N-terminus and C-terminus of the peptide were protected by acetyl and amino groups, respectively. The anticancer agent ellipticine (99.8% pure) was purchased from Sigma-Aldrich (Oakville, Canada) and used as received. Egg phosphatidylcholine (EPC, powder, 99+% pure) was obtained from Avanti Polar Lipids, Inc. (Alabaster, AL). Ethylenediaminetetraacetic acid (EDTA) was from Bio-Rad

Laboratories (Mississauga, Canada). Tris(hydroxymethyl)methylamine (Tris) and glacial acetic acid were bought from BDH Inc. (Toronto, Canada). Tetrahydrofuran (THF, reagent grade 99%) was obtained from Calendon Laboratories Ltd. (Georgetown, Canada).

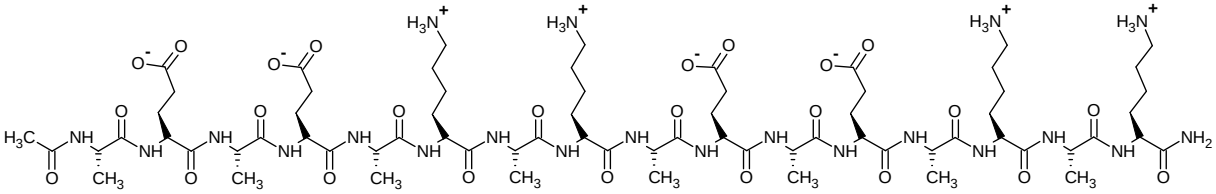

Figure 4.1 Molecular structure of EAK16-II structure.

4.2.2 Liposome Preparation

EPC powders (~5 g) were weighed and dissolved in 125 mL of a buffer solution containing 25 mM Tris/acetic acid (pH = 7.0) and 0.2 mM EDTA.[51] The mixture was then extruded using a LiposoFast-Basic extruder (Avestin Inc., Ottawa, Canada) with a polycarbonate membrane (100 nm pore size) to obtain uniform liposome dispersions at room temperature. The dispersions were further diluted (4x) with the same Tris/acetic acid buffer. This was followed by centrifugation at 4000 rpm for 1 h to eliminate the larger vesicles and possible contaminants. The supernatant was collected and stored at 4°C before use. The EPC concentration was determined to be 7.1×10^{-4} M using the method described in our previous publication (Also see Section 3.2.2).[51] The size of the EPC liposomes was characterized by Dynamic Light Scattering (DLS).

4.2.3 Formation of Peptide-Ellipticine Complexes

To make peptide-ellipticine complexes, certain amounts of ellipticine crystals were added into fresh EAK16-II solutions (0.05-0.5 mg/mL) to obtain ellipticine concentrations of 0.1-1.0 mg/mL. The fresh peptide solutions were prepared by dissolving peptide powder in pure water (18.2 MΩ, Milli-Q A10 synthesis), followed by sonication for 10 min. The peptide-ellipticine mixtures were stirred at 900 rpm on a magnetic stir plate throughout the complexation experiment. At specified times, the mixtures were transferred to a quartz cuvette to acquire fluorescence spectra of ellipticine on a steady-state spectrofluorometer (Photon Technology International, London, Canada). The test was performed once every hour for the first 20 h and less frequently for the remaining period until an equilibrium state was reached. A 1 mg/mL solution of ellipticine in pure water was prepared as a control.

Since the peptide can self-assemble over time, it is expected that a competition may exist between the peptide-peptide association and the peptide-ellipticine complexation during the drug formulation. To better understand such a complicated process, peptide assembly without ellipticine was investigated. For this purpose, 0.2 mg/mL of fresh EAK16-II solution was prepared and stirred for 30 h at 900 rpm. The peptide assembly was characterized by static light scattering (at 400 nm) acquired on the steady-state spectrofluorometer and compared with the fresh peptide solution (0 h). The light scattering intensity of air was obtained as the standard to correct for the lamp fluctuations.

For the ellipticine release experiments, the complexes were newly prepared with a fixed ellipticine concentration of 0.1 mg/mL and various peptide concentrations ranging from 0.05 to 0.5 mg/mL. The samples were continuously stirred for 24 h to ensure that equilibrium was reached. They were then photographed with a digital camera (Cannon PowerShot A95). The steady-state fluorescence spectra of the complexes were acquired just before the release experiments (to show the states of ellipticine in complexes different from that in EPC vesicles).

4.2.4 Ellipticine Release into Liposome Vesicles

The release of ellipticine from the complex into the EPC vesicles was continuously monitored on the spectrofluorometer over time. The experiments were conducted with the following procedure: 100 μL of the peptide-ellipticine dispersion were transferred into a quartz cuvette and mixed with 2.9 mL of EPC vesicles. The 30 times dilution of the complex upon mixing with the vesicles was to ensure that the final ellipticine concentration was low enough to be in the range of the calibration curve. The cuvette was then put in the spectrofluorometer with gentle magnetic stirring, covered with a parafilm (to eliminate water evaporation during the course of measurement) before collecting the fluorescence intensity over time. The time required to prepare the sample before starting a time-dependent fluorescence measurement was less than 30 s.

4.2.5 Calibration Curve

In order to relate the fluorescence signals of ellipticine in the EPC vesicles to the ellipticine concentration, a calibration curve of ellipticine fluorescence from the ellipticine-EPC suspensions is needed. The concentration range of ellipticine was selected to be 10^{-6}-10^{-4} M based on our previous experience on pyrene release experiments.[51] The ellipticine-EPC suspensions were prepared using the following procedure: ellipticine crystals were dissolved in THF to make the ellipticine-THF stock solution with ellipticine concentration of 1 mM. Aliquots of ellipticine-THF solution were put into a 4 mL vial and THF was evaporated under a stream of filtered air (0.45 μm) to have a film of ellipticine at the bottom of the vial. 3 mL of the EPC dispersions were added and the samples were stirred for ~24 h to allow the saturation of ellipticine in the EPC vesicles. The ellipticine fluorescence was then acquired. It should be noted that ellipticine at high concentrations may not completely dissolve in the vesicles made of 7.1×10^{-4} M EPC. Therefore, the UV-Vis absorption of the ellipticine-EPC

suspensions was acquired and plotted as a function of ellipticine concentration to show whether ellipticine was completely dissolved in the EPC dispersions.

To ensure that the fluorescence signal of ellipticine-EPC dispersions was from the ellipticine in the vesicles, the fluorescence of a control sample made of the buffer saturated with ellipticine was acquired. The fluorescence of the control was found to be ~280 fold smaller than that of 1 μM ellipticine in the EPC dispersion. Such a small fluorescence signal can be neglected. Thus, the observed fluorescence of the ellipticine-EPC dispersions should represent the fluorescence of ellipticine in the vesicles.

4.2.6 Dynamic Light Scattering (DLS) Measurements

The hydrodynamic diameter of the EPC vesicles was obtained on a Zetasizer Nano ZS (Malvern Instruments, Worcestershire, U.K.) with the appropriate viscosity and refractive index settings, at a fixed temperature of 25 °C during the measurement. A small-volume (45 μL) black quartz cuvette with a 3 mm light path was used. The scattered light intensities of the samples at the angle of 173 degree were collected. The intensity-based size distribution of the EPC vesicles was obtained with the multimodal algorithm CONTIN,[229] provided in the software package Dispersion Technology Software 5.0 (Malvern Instruments, Worcestershire, U.K.). Six measurements were performed to generate the intensity-based size distribution plot reported herein.

4.2.7 Steady-State Fluorescence Measurements

The ellipticine fluorescence was acquired on the Photon Technology International spectrofluorometer (Type QM4-SE, London, Canada) with a continuous xenon lamp as the light source. For each sample, approximately 3mL of solution were transferred from a vial into a square quartz cell (1 cm × 1 cm) through a pasteur glass pipette. All samples containing ellipticine were excited at 294 nm and the

emission spectra were collected from 320 to 650 nm. The excitation and emission slit widths were set at 0.25 mm and 0.5 mm, respectively (0.25 mm corresponds to 1 nm band path). The fluorescence intensity at 468 nm and 520 nm were obtained by taking the average from 458 to 478 nm and 510 to 530 nm, respectively. A standard (2 μM ellipticine in ethanol, sealed and degassed) was used in each run to correct for the lamp intensity variations. The standard fluorescence intensity I_s was obtained by taking the average of the fluorescence signal from 424 to 432 nm (peak at ~428 nm).

In order to generate an accurate calibration curve, the emission fluorescence of ellipticine in EPC vesicles was collected at 436 nm over 1 min and averaged to yield the intensity for each ellipticine concentration. The excitation and emission slit widths were set at 0.5 mm and 0.25 mm, respectively. The intensities were corrected with an ellipticine standard (2 μM in ethanol, sealed and degassed) to account for lamp fluctuations. The I_s was obtained by taking the average of fluorescence at 428 nm over 1 min after each run.

The kinetics of the ellipticine release from the complex into the EPC vesicles was monitored by acquiring the time-dependent ellipticine fluorescence at 436 nm over a 7 h time span at 5 s intervals. All solutions reached equilibrium within 7 h as the fluorescence intensities reached a plateau during the experimental time span. The same standard sample as described above was used to obtain I_s (at 428 nm over 10 min) to correct for the day-to-day fluctuations. For each release experiment, the fluorescence was recorded while the solution was gently stirred in the spectrofluorometer.

4.2.8 Scanning Electron Microscopy (SEM)

A LEO model 1530 field emission SEM (GmbH, Oberkochen, Germany) was employed to study the morphology and dimensions of the peptide-ellipticine complex. The SEM samples were prepared by depositing 20 μL of the complex suspensions on a freshly cleaved mica surface. The mica was affixed on an SEM stub using a conductive carbon tape. The sample was placed under a Petridish-cover for

10 min to allow the complexes to adhere to the mica surface. It was then washed once with a total of 100 μL pure water and air-dried in a dessicator overnight. All samples were coated with a 20 nm thick gold layer prior to imaging; the images were acquired using the secondary electron (SE2) mode at 5 kV.

4.3 Results and Discussion

The self-assembling peptide EAK16-II has shown the capability of stabilizing a hydrophobic compound and the anticancer agent ellipticine in aqueous solution from our previous studies.[56] Here we report the details of the complexation between EAK 16-II and ellipticine, concentration effects on the complex formation and the release kinetics of ellipticine from the complexes to the liposomes.

4.3.1 Time-Dependence of the formation of Peptide-Ellipticine Complexes

To investigate the details of the complexation kinetics, the change in the ellipticine fluorescence of the peptide-ellipticine dispersions was monitored over time. Figure 4.2a shows the fluorescence spectra of the complex suspension with 1.0 mg/mL ellipticine and 0.2 mg/mL EAK16-II at different times. Initially, the fluorescence spectrum exhibits the characteristics of protonated ellipticine with a peak located near 520 nm after 0.5 h stirring.[168] This peak rises with time and reaches a maximum after 6 h before decreasing. Meanwhile, a shoulder located at ~468 nm becomes pronounced with time and eventually forms a peak after 9 h. The band at 468 nm is characterized as the crystalline form of ellipticine.[56] Note that there was no trace of fluorescence at 468 nm (crystalline ellipticine) initially, although ellipticine was in crystalline form when just mixed with the peptide solution; the ellipticine crystals were large, unable to be suspended in solution, and thus settled to the bottom of the sample vial, and did not contribute to the fluorescence signal detected.

(a)

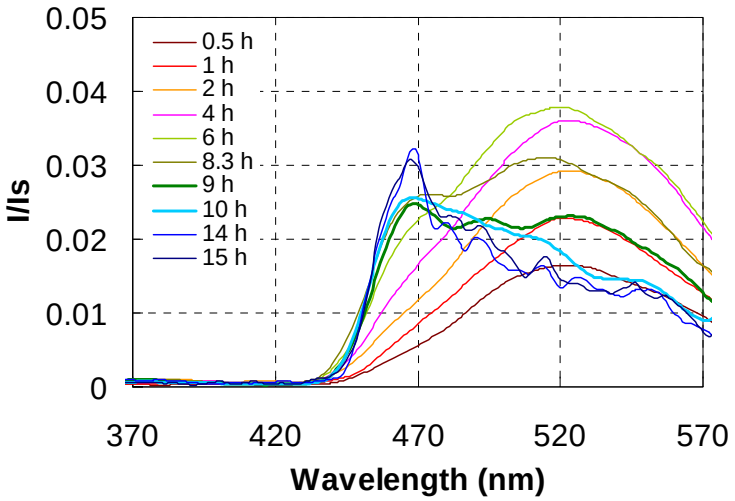

(b)

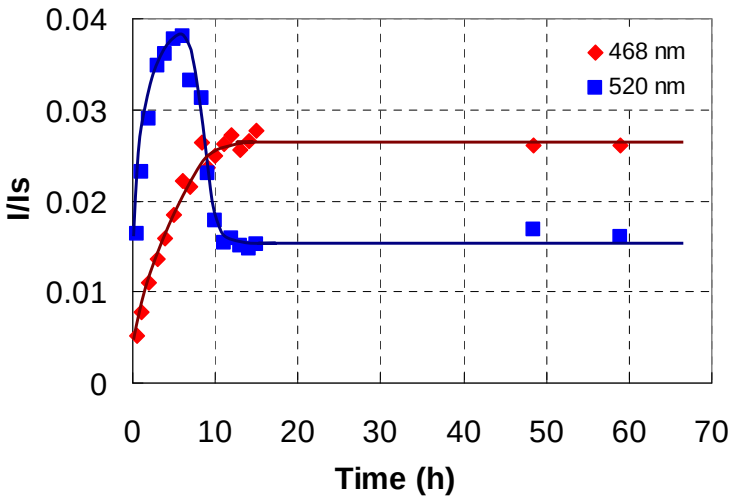

Figure 4.2 The ellipticine fluorescence from the peptide-ellipticine suspension over time. (a) Fluorescence spectra of ellipticine as a function of time; (b) the normalized fluorescence intensities at 468 nm (diamonds) and 520 nm (squares) as a function of time. The ellipticine concentration is 1.0 mg/mL (4 mM) and the peptide concentration is 0.2 mg/mL (0.12 mM).

The intensity changes of the two peaks at 468 and 520 nm are plotted with time in Figure 4.2b. It can be clearly seen that the intensity at 520 nm increases for the first 6 h to a maximum and then decreases to the initial level after 10 h. On the other hand, the intensity at 468 nm increases with time

and reaches a plateau after ~15 h. The latter indicates that ellipticine crystals or microcrystals are gradually stabilized in aqueous solution, to form peptide-ellipticine complexes with time. The final state of stabilized ellipticine is in crystalline form and equilibrium is reached after ~15 h (considering both I_{468} and I_{520} reaching equilibrium).

The trend in the change of the fluorescence of protonated ellipticine shown in Figure 4.2b may indicate a special mechanism for complex formation. It is speculated that the fresh peptide solution could facilitate the formation of protonated ellipticine. Since ellipticine has a pKa of ~6 (pyridine-like nitrogen), it can be protonated in a weak acidic environment.[73,168,169] A fresh 0.2 mg/mL EAK16-II in pure water has a pH value of ~4.6, which can cause the protonation of ellipticine. In addition, the peptide molecules consisting of negatively charged glutamic acid residues may help stabilize the protonated ellipticine upon interaction. A similar phenomenon has been reported that highly negatively charged SDS micelles can stabilize protonated ellipticine in pure water (Chapter 3).[168] The amount of protonated ellipticine increases during the first several hours to a maximum and then disappears when the equilibrium is established. The diminishing of the protonated ellipticine prior to equilibrium may be related to the dynamics of peptide self-assembly and its associated events. As shown in Figure 4.3, the scattered light intensity of a 0.2 mg/mL EAK16-II solution can significantly increase 30 h after preparation to a level 6 fold higher than that of a fresh peptide solution. This is the evidence of peptide assembly over time under constant mechanical stirring. The formation of EAK16-II assemblies may consume the negatively charged glutamic acid residues as they are complementary to the lysine residues in the assemblies. This in turn reduces the amount of free glutamic acid residues that are able to stabilize the protonated ellipticine. Meanwhile, the pH of the EAK16-II solution was found to increase from ~4.6 (fresh) to 6.4 (30 h after preparation), which is slightly above the pKa of ellipticine. The combination of these two effects can induce deprotonation of ellipticine, thereby explaining the disappearance of protonated ellipticine over time. Note that an occurrence of “inner

filter effect" due to the increase of protonated ellipticine concentration might also result in the decrease in fluorescence signals of the protonated ellipticine. However, more experiments are required to verify such an effect.

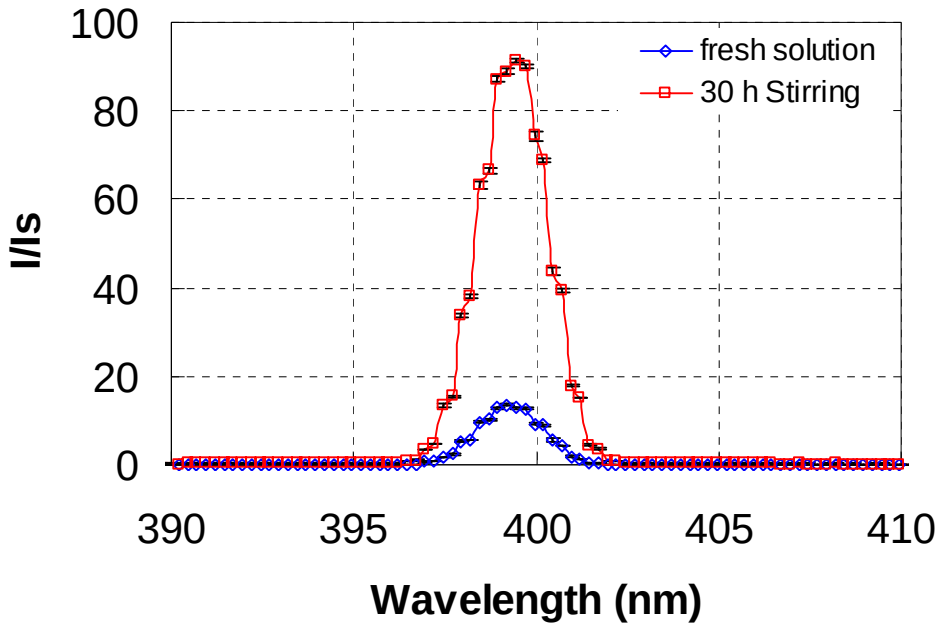

Figure 4.3 Static light scattering of 0.2 mg/mL (0.12 mM) EAK16-II solution at 400 nm before (diamonds) and after mechanical stirring for 30 h (squares).

On the other hand, the peptide assembly does not likely inhibit the formation of stable ellipticine microcrystals. In fact, these peptide assemblies are mainly made of β-sheets, which are amphiphilic with hydrophobic and hydrophilic regions on the opposite sides.[67,68] The hydrophobic region can still interact with hydrophobic ellipticine microcrystals to form stable peptide-ellipticine suspensions. It has been shown that EAK16-II can adsorb on hydrophobic surfaces and assemble into stable β-sheet rich nanostructures.[56,67]

4.3.2 Concentration Effect on the Complex Formation

Figure 4.4 shows the peptide concentration effect on the formation of peptide-ellipticine complexes at a fixed ellipticine concentration of 1.0 mg/mL. The peptide concentration ranges from 0.05 to 0.5 mg/mL. The fluorescence intensity at 468 nm (crystalline ellipticine) increases with time and reaches a plateau for all peptide concentrations used, but the time required to reach equilibrium is dependent on the peptide concentration (Figure 4.4a). The equilibration time is at minimum (~5 h) when the peptide concentration is around 0.1 mg/mL, which is the reported critical aggregation concentration (CAC) of the peptide.[40] When the peptide concentration is above or below the CAC, the equilibration time increases (> 10 h). The change in the fluorescence intensity at 520 nm (protonated ellipticine) is also strongly dependent on the peptide concentration as shown in Figure 4.4b. Above the CAC, the protonated ellipticine can be seen to form over time and then disappear. The protonated ellipticine stays for a longer time (40 h) with a higher peptide concentration (0.5 mg/mL). At the CAC, the fluorescence of protonated ellipticine only appears in the first 2 h and quickly disappears afterwards. Below the CAC, no significant protonation of ellipticine is observed.

(a)

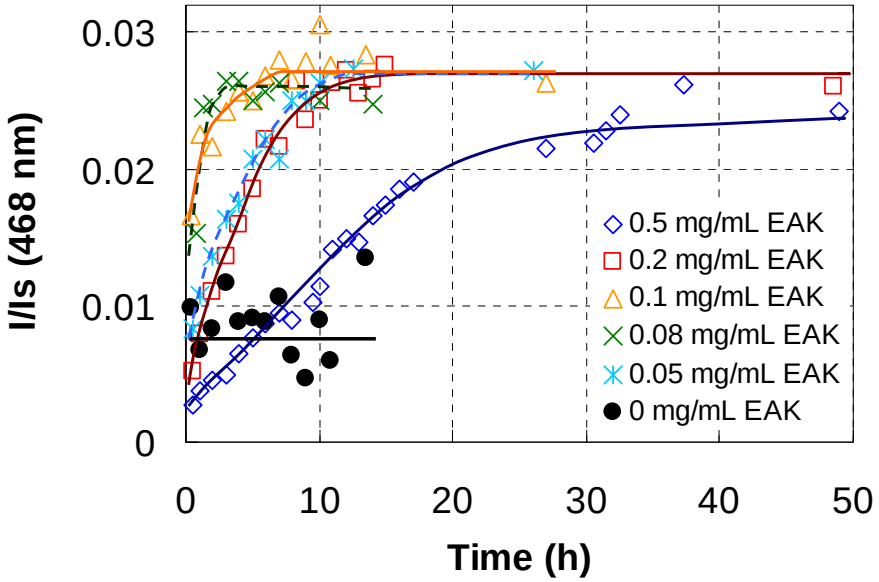

(b)

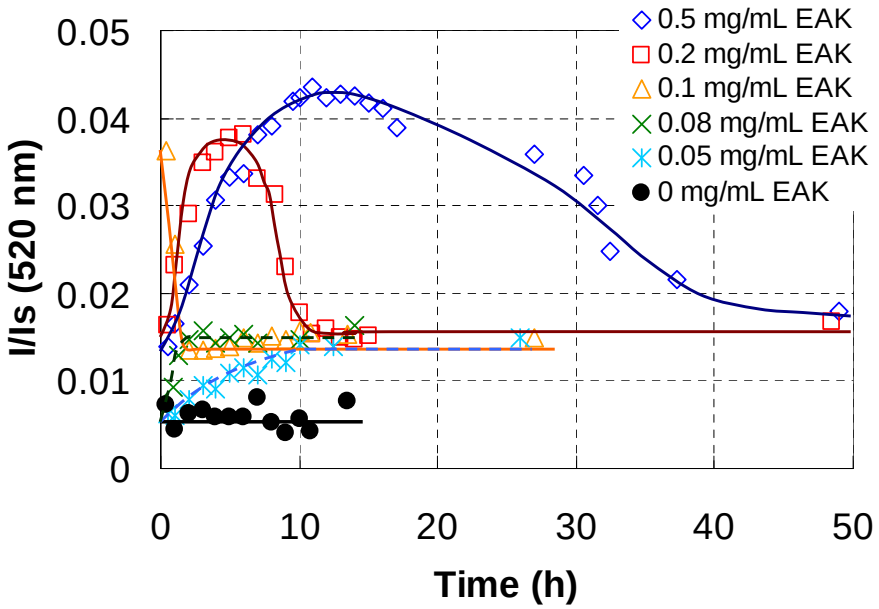

Figure 4.4 Effect of peptide concentration on the complex formation. The normalized fluorescence intensities of peptide-ellipticine suspensions as a function of time at 468 nm (a) and 520 nm (b). The ellipticine concentration was fixed at 1.0 mg/mL (4 mM) with various EAK16-II concentrations ranging from 0 to 0.5 mg/mL (0-0.3 mM).

The overall equilibration time of the peptide-ellipticine complexation at different EAK16-II concentrations is list in Table 4.1. The reported values were estimated from Figure 4.4, considering that both processes of ellipticine protonation and formation of stable ellipticine microcrystals have reached steady-state or equilibrium. Note that when the equilibrium of both processes is reached, the final state of the stabilized ellipticine is mainly in crystalline form. It can be clearly seen that the overall equilibration time is strongly dependent on the peptide concentration and approaches a minimum when the peptide concentration is close to the CAC. This phenomenon may be related to the solution pH at various peptide concentrations and the peptide self-assembly.

Table 4.1 Peptide concentration-dependent equilibration time and solution pH

[EAK] (mg/mL)	Estimated equilibration time (h)	pH of fresh peptide solution
0.50	40	3.9
0.20	15	4.6
0.10	7	5.2
0.08	4	5.5
0.05	12	6.0

Notes:

1. The equilibration time was estimated from Figure 4.4, considering that both I_{468} and I_{520} reach equilibrium.
2. The pH was measured from freshly prepared peptide solutions.

At peptide concentrations below the CAC, the peptide solution has a relatively high pH, which prohibits ellipticine protonation. But under such a condition, microcrystals of ellipticine can form over time. Such formation of ellipticine microcrystals becomes faster with increasing peptide concentration up to its CAC. At the CAC, a low pH, below the pKa of ellipticine, is observed. Such a low pH allows protonated ellipticine to form (Figure 4.4b). However, over time peptide assemblies start to appear at this concentration; meanwhile the solution pH starts to increase and the number of available glutamic acid residues reduces. (Note that the glutamic acid residues can stabilize the protonated ellipticine.) As a result, deprotonation of ellipticine occurs shortly after the initial protonation.

At peptide concentrations above the CAC, a longer equilibration time is observed. This is probably due to the combined effects of the ellipticine protonation and microcrystal formation. The pH of a fresh peptide solution decreases with an increase in peptide concentration as shown in Table 4.1. At a concentration above the CAC, the solution has a pH below 5, which can induce the protonation of ellipticine. The lower the solution pH is, the more ellipticine can be protonated. The protonated ellipticine will gradually disappear with time while more stable ellipticine microcrystals form. It takes a longer time for protonated ellipticine to disappear at a higher peptide concentration, leading to a longer equilibration time.

The peptide EAK16-II is capable of stabilizing ellipticine microcrystals and protonated ellipticine in aqueous solution in a time-dependent and peptide concentration-dependent manner. The state of ellipticine could be critically important in its function as a therapeutic agent. It has been reported that the neutral form of ellipticine is active against various tumors.[73,167] Further *in vitro* and *in vivo* studies will elucidate the effects of the different states of ellipticine on its activity against cancer cells.

(a)

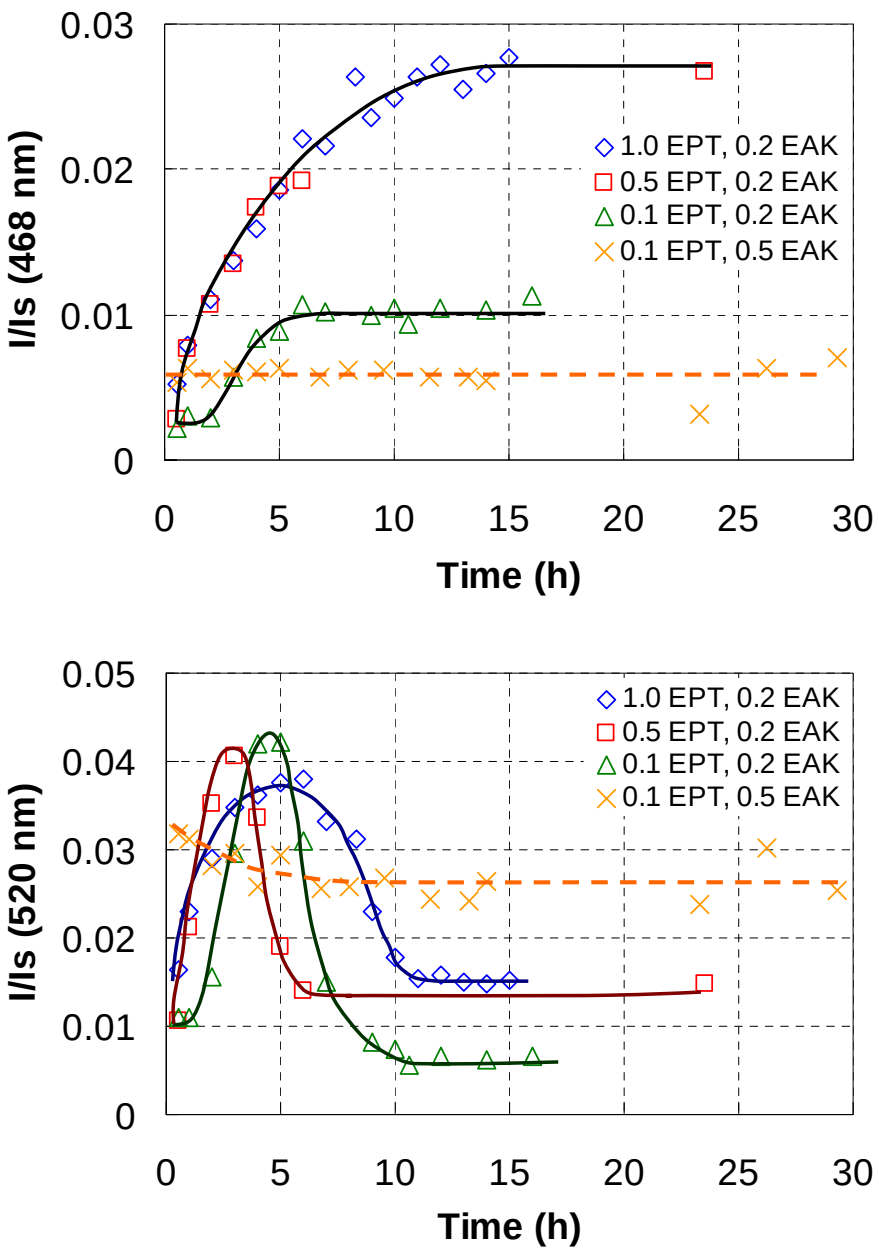

Figure 4.5 Effect of ellipticine concentration on the complex formation. The normalized fluorescence intensities of peptide-ellipticine suspensions as a function of time at 468 nm (a) and 520 nm (b). The 0.2 (0.12 mM) and 0.5 mg/mL (0.3 mM) EAK16-II were used with different ellipticine concentrations from 0.1 (0.4 mM) to 1.0 mg/mL (4 mM).

The ellipticine concentration effect on the complex formation was investigated with 0.2 mg/mL EAK16-II and three ellipticine concentrations: 1.0, 0.5 and 0.1 mg/mL. The change in fluorescence of crystal and protonated ellipticine is shown in Figure 4.5a and b, respectively. At this peptide concentration, the ellipticine concentration does not seem to affect the overall equilibration time significantly. The time for the peptide-ellipticine suspension formation (both ellipticine protonation and formation of ellipticine microcrystals should reach equilibrium) is all ~10 h.

Interestingly, a particular combination of 0.1 mg/mL ellipticine with 0.5 mg/mL EAK16-II, increased from 0.2 mg/mL, can stabilize protonated ellipticine for a prolonged time (Figure 4.5, crosses). The intensity at 520 nm decreases slightly at the beginning and reaches a plateau after 10 h, while that at 468 nm remains constant at a low value with time. The very low intensity at 468 nm has comparable level to that of the background noise, indicating that no ellipticine microcrystals can be detected. This result shows that most ellipticine is protonated and solubilized in the solution. The slight initial decrease in intensity of the protonated ellipticine is likely the results of inner-filter effect as the solution solubilizes more ellipticine with time. The protonated ellipticine is stable for at least 50 h, the duration of the experiment, under continuous mechanical stirring. During this time period, the solution remains clear with a yellow-orange color. This particular combination of ellipticine and peptide concentrations suggests that a prolonged state of protonated ellipticine can be established. This will affect ellipticine release kinetics, and probably its therapeutic efficiency.

4.3.3 Release of Ellipticine from the Complexes into EPC Vesicles

So far, we have shown the formation of stable peptide-ellipticine dispersions in water, either in microcrystal or protonated form. It is important to investigate how ellipticine releases from the peptide complex, and the release kinetics. This was done by mixing the complex with liposome vesicles, which mimic the cell membrane.[51]

The EPC vesicles were made by manual extrusion passing a polycarbonate filter for 10 cycles. The sizes of the vesicles were determined by DLS to be ~200 nm in diameter as shown in Figure 4.6. The liposomes with such a size using the extrusion method are classified as large unilaminar vesicles (LUVs).[230-232]

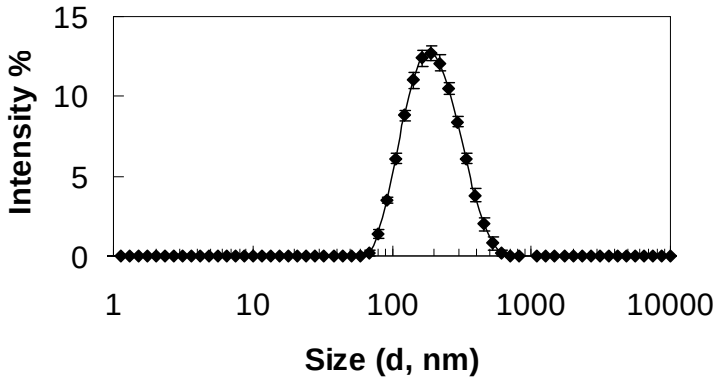

Figure 4.6 Intensity-based size distribution of the EPC vesicles.

Four peptide concentrations (0.05, 0.1, 0.2 and 0.5 mg/mL) were used to form stable peptide-ellipticine dispersions with 0.1 mg/mL of ellipticine in study of release kinetics. The samples were stirred for 24 h to ensure that equilibrium was reached. As shown in the photographs (Figure 4.7a), the stable complex suspensions are formed with the presence of EAK16-II compared to ellipticine only in water (far left vial). At 0.5 mg/mL of EAK16-II, the dispersion looks more yellow and less turbid compared to others at lower peptide concentrations. This exceptional appearance is the additional evidence to the results of Figure 4.5 that the 0.5 mg/mL EAK16-II solution can stabilize protonated ellipticine for a prolonged time. The different states of ellipticine at equilibrium are also shown in Figure 4.7b. The suspension with 0.5 mg/mL EAK16-II has a pronounced peak located

~525 nm (protonated state) while those with peptide concentrations ranging from 0.05 to 0.2 mg/mL exhibit a peak of ~468 nm (crystalline state) (Figure 4.7b, inset). The very different properties of the complex suspensions according to the peptide concentration could also have significant effects on the ellipticine release (see below).

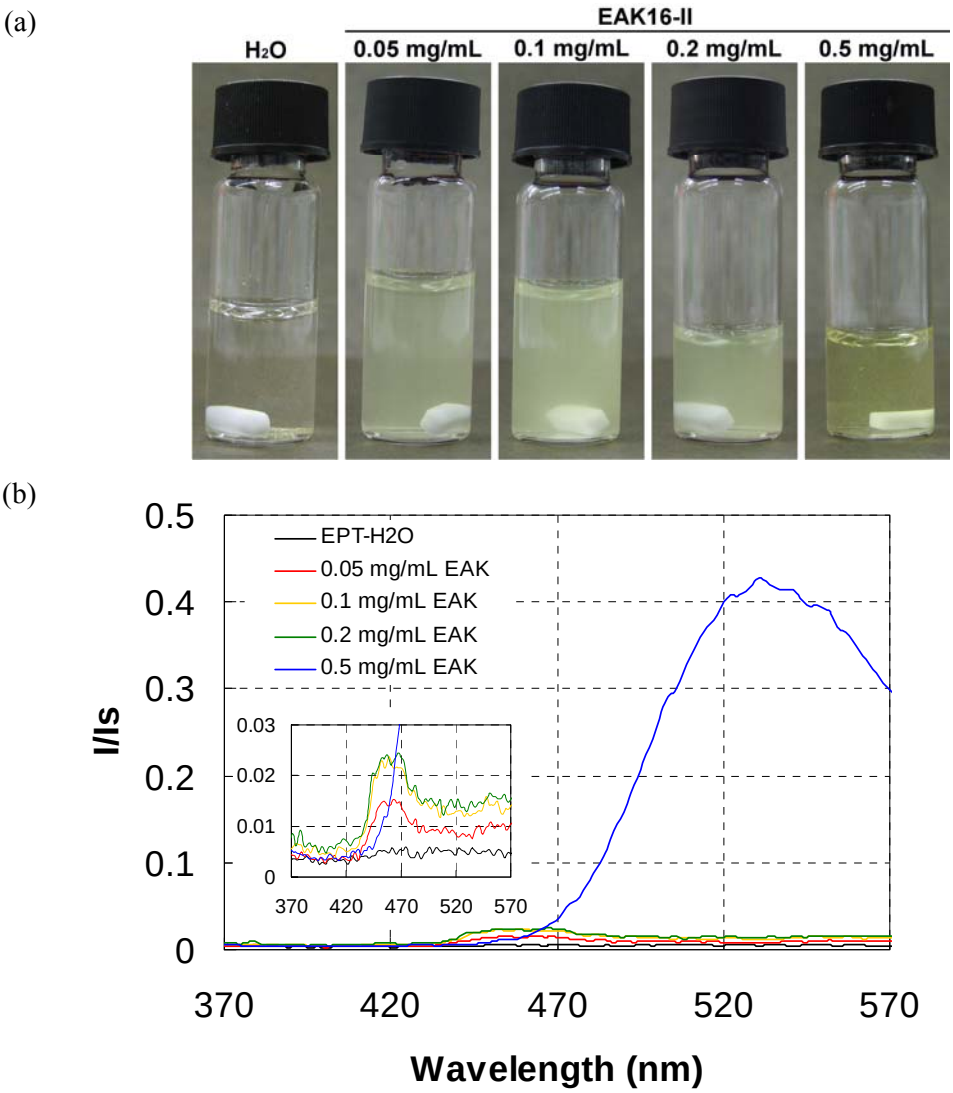

Figure 4.7 (a) Photographs of the peptide-ellipticine suspensions after 24 h stirring with 0.1 mg/mL (0.4 mM) ellipticine and various peptide concentrations of 0-0.5 mg/mL (0-0.3 mM). (b) The corresponding fluorescence spectra of the peptide-ellipticine suspensions in (a).

It is worth noting that the fluorescence of ellipticine, either protonated or in crystal form upon interaction with peptides, is very different from that of ellipticine in EPC vesicles. Ellipticine in the vesicles exhibits a strong fluorescence signal at ~436 nm, which is characterized as neutral, monomeric ellipticine (Chapter 3). Such a signal can be well distinguished from those of the protonated ellipticine (~520 nm) and ellipticine crystals (weak fluorescence at ~468 nm) (Figure 4.7b). The transfer of ellipticine from the complex into the vesicles can be monitored by the change in ellipticine fluorescence at 436 nm over time.

A typical transfer curve of ellipticine from the complex to the EPC vesicles, or liposomes, is shown in Figure 4.8a. The complex was made with 0.05 mg/mL EAK16-II and 0.1 mg/mL ellipticine in pure water after 24 h stirring (second vial to the left in Figure 4.7a). The fluorescence intensity at 436 nm increases with time and approaches a plateau after 20,000 s. The reason that the initial point starts slightly above zero (t = 0) is probably due to the burst release of ellipticine into the vesicles during the initial sample mixing time (< 30 s).

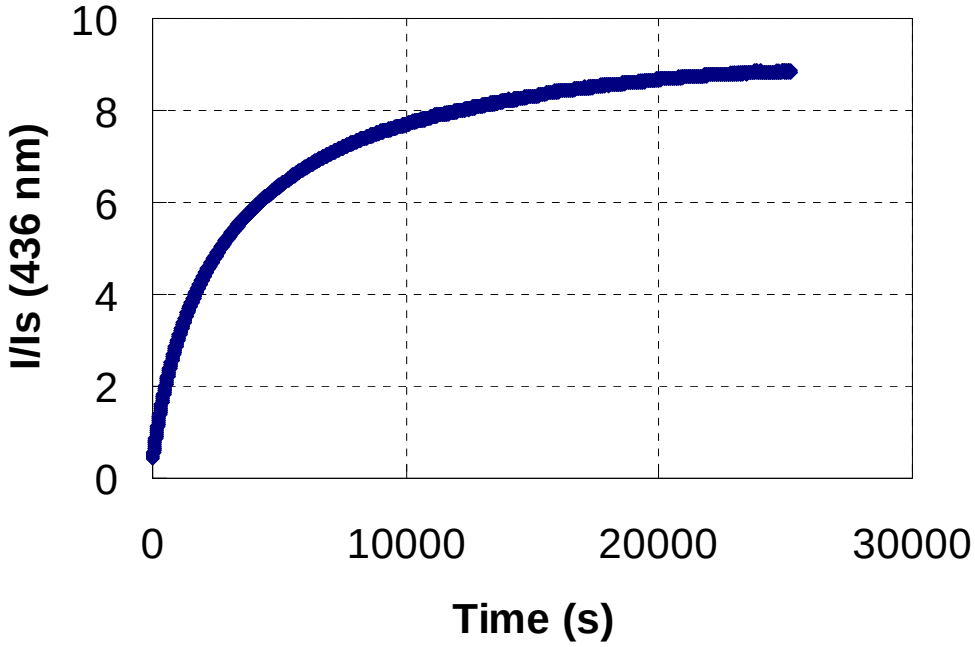

(a)

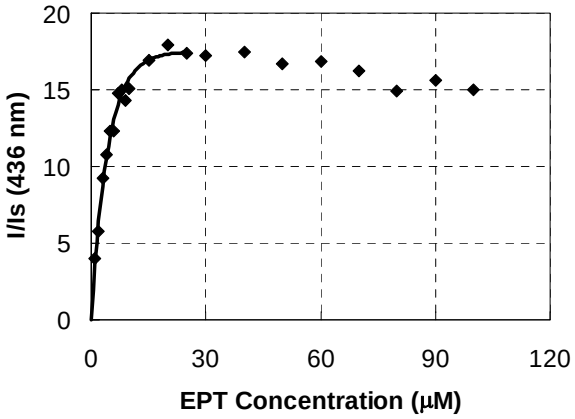

(b)

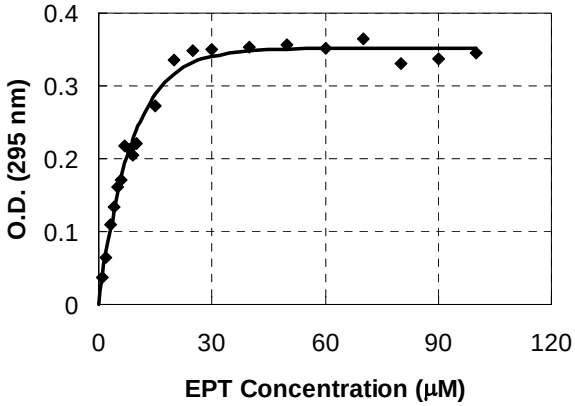

(c)

Figure 4.8 (a) The time-dependent ellipticine fluorescence showing the release of ellipticine from the complex made of 0.05 mg/mL (0.03 mM) EAK16-II and 0.1 mg/mL (0.4 mM) ellipticine into the EPC vesicles. (b) Calibration curve of various ellipticine concentrations in the EPC vesicles. (c) Corresponding UV absorption of ellipticine in (b).

In order to relate the transfer curve based on the ellipticine fluorescence to the concentration accumulation of ellipticine in vesicles, a calibration curve was generated as shown in Figure 4.8b. The ellipticine fluorescence in EPC vesicles increases to a maximum with the increase of ellipticine concentration from 1 to ~20 μM; it then slightly decreases with a further increase in ellipticine concentration (up to 100 μM). Normally, the decrease of ellipticine fluorescence at high ellipticine concentrations can be related to the inner-filter effect. This usually occurs when the concentration of a fluorophore is high enough with right angle detection.[51,202] However, the decrease of the fluorescence due to the inner-filter effect is usually more dramatic (~50%), which does not seem to match with the present case.

Figure 4.8c shows the concentration-dependent UV absorption of the ellipticine in EPC vesicles used for generating the calibration curve. It can be seen that the ellipticine absorbance at 295 nm increases initially and reaches a plateau when the ellipticine concentration is greater than 20 μM. This trend correlates well with that of the calibration curve. A plateau observed in Figure 4.8c indicates that ellipticine is saturated in the vesicles (formed at this particular lipid concentration of 7.1×10^{-4} M). This confirms that the inner-filter effect is not the cause of the slight decrease in the calibration curve at ellipticine concentrations above 20 μM. In addition, the molar ratio of ellipticine to the EPC lipid can be roughly estimated to be 0.028. Such a small number reflects the fact that such liposomes may not be an effective carrier for ellipticine when loading capacity is concerned. However, the exact reason for the slight decrease in the ellipticine fluorescence at high ellipticine concentrations (> 20 μM) in Figure 4.8b is still under study.

The rising region in the calibration curve can be used to convert the fluorescence signals from the transfer profile to the ellipticine concentration in vesicles. This can be done by using a simple exponential equation to fit the rising region in Figure 4.8b (1-20 μM):

$$I = A\left(1 - e^{B[EPT]}\right) \tag{4.1}$$

The fitting parameters A and B are 17.5 ± 0.36 and 230000 ± 13400 (1/M), respectively. [EPT] represents the concentration of ellipticine within the range of 0-20 μM. For a given fluorescence intensity of ellipticine (I/I_s < 17.5), one can obtain the corresponding ellipticine concentration using Equation 4.1.

Figure 4.9 shows four transfer profiles of ellipticine concentration in the vesicles ([EPT_v]) with time (h). Each curve corresponds to the transfer of ellipticine into the vesicles from different peptide-ellipticine complexes made with various EAK16-II concentrations. All profiles have a similar trend with a fast increase initially and gradually approaching a plateau. The very high initial values of the transfer profile from the complexes with 0.5 mg/mL EAK16-II indicate a burst release of ellipticine from the complex into the vesicles within 30 s. This is reasonable since the 0.5 mg/mL EAK16-II solution can stabilize protonated ellipticine (Figures 4.5 and 4.7b). These protonated ellipticine molecules may easily migrate into the lipid bilayers, causing a sudden increase in the ellipticine concentration in the vesicles. On the other hand, other peptide concentrations (0.05-0.2 mg/mL) stabilize ellipticine microcrystals rather than protonated ellipticine. The migration of ellipticine molecules from the microcrystals to the vesicles involves the molecularly dissolving of ellipticine, which is time consuming. Therefore, their transfer profiles do not have a large sudden increase at the onset, with initial ellipticine concentration close to zero.

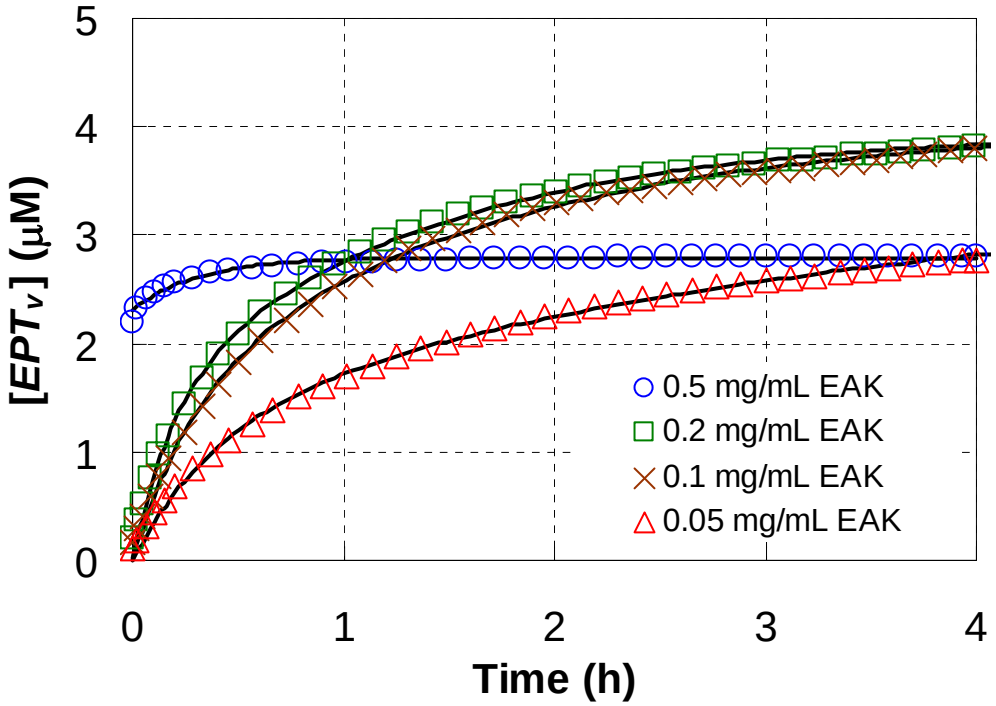

Figure 4.9 The transfer profiles of ellipticine from different peptide-ellipticine complexes to the EPC vesicles. The complexes were made of 0.1 mg/mL (0.4 mM) ellipticine with various EAK16-II concentrations: 0.05 (triangles, 0.03 mM), 0.1 (crosses, 0.06 mM), 0.2 (squares, 0.12 mM) and 0.5 mg/mL (circles, 0.3 mM). The solid lines represent the fitting curves to the data points using either Equation 4.2 or Equation 4.3. The excitation and emission wavelengths are 295 and 436 nm, respectively.

To better compare the transfer kinetics for the four different EAK16-II concentrations, the profiles were fitted to one of the following exponential equations. The second equation was used if the first could not satisfactorily describe the dynamics:[51]

$$[EPT_v](t) = [EPT_v]_{eq} - \left([EPT_v]_{eq} - [EPT_v]_0\right)e^{-kt} \quad (4.2)$$

$$[EPT_v](t) = [EPT_v]_{eq}\left(1 - a_1 e^{-k_1 t} - a_2 e^{-k_2 t}\right) \quad (4.3)$$

where $[EPT_v](t)$, $[EPT_v]_{eq}$ and $[EPT_v]_0$ are the ellipticine concentration in the vesicles at time t, at equilibrium and at time zero, respectively; k, k_1 and k_2 are the rate constants; a_1 and a_2 are the pre-exponential factors and $a_1 + a_2 = 1$. The particular transfer profile with 0.5 mg/mL EAK16-II was fitted with Equation 4.2 where $[EPT_v]_0 \neq 0$ due to an initial burst transfer of ellipticine into the vesicles; the other three profiles were fitted well with Equation 3 as the initial transfer in these cases was very small and can be negligible. The rate constants are summarized in Table 4.2. Comparing the average rate constants for each transfer profile, it can be seen that the rate of transfer of ellipticine from the complexes into the vesicles increases with the peptide concentration during the preparation of peptide-ellipticine complexes.

Table 4.2 Transfer rates of ellipticine from peptide-ellipticine complexes to EPC liposomes

[EAK]	0.5 mg/mL*	0.2 mg/mL	0.1 mg/mL	0.05 mg/mL
k_1 (1/h)	3.13 ± 0.14	5.20 ± 0.04	3.52 ± 0.03	2.53 ± 0.02
a_1		0.363 ± 0.002	0.345 ± 0.002	0.348 ± 0.003
k_2 (1/h)	n/a	0.75 ± 0.002	0.62 ± 0.002	0.30 ± 0.003
a_2		0.637 ± 0.002	0.655 ± 0.003	0.652 ± 0.002
k_{avg}	3.13 ± 0.14	2.36 ± 0.02	1.62 ± 0.01	1.08 ± 0.01
R^2	0.976	0.999	0.999	0.999

*Denotes the fitting with Equation 4.2; all others with Equation 4.3. All the fitting parameters are significantly different from the statistical analysis.

$k_{avg} = a_1k_1 + a_2k_2$; $a_1 + a_2 = 1$

This trend is opposite to that of our previous studies on the pyrene release from the EAK16-II coatings into the EPC vesicles.[51] The higher EAK16-II concentration used to form peptide-pyrene complexes results in a thicker coating on the pyrene microcrystals, which in turn causes a slower release rate. In the present case of ellipticine, the higher peptide concentration induces the protonation of ellipticine and formation of smaller complexes as visualized by the SEM images in Figure 4.10. The size of the complexes with 0.5 mg/mL EAK16-II (Figure 4.10a) is much smaller than that with 0.2 mg/mL EAK16-II (Figure 4.10b). Further decrease in the peptide concentration (0.05 mg/mL) will result in a bigger size of the complexes as shown in Figure 4.10c. Since the ellipticine in the vesicles is molecularly solubilized, the transfer process must involve the release of individual ellipticine molecules from the complexes; the bigger the complexes are, the longer the release of ellipticine from the complexes will be. Therefore, a slower transfer rate of ellipticine was observed at low peptide concentrations.

This study demonstrates that a self-assembling, ionic-complementary peptide, EAK16-II, can stabilize the hydrophobic anticancer agent ellipticine in aqueous solution. Different combinations of peptide and ellipticine concentrations can stabilize either protonated ellipticine or ellipticine microcrystals for an extended time. The ellipticine can be released from the complexes into a cell membrane mimic. The release rate is related to the peptide concentration used in the complexation. By optimizing the process of complex formation, one could obtain desired complex dimensions and release property.

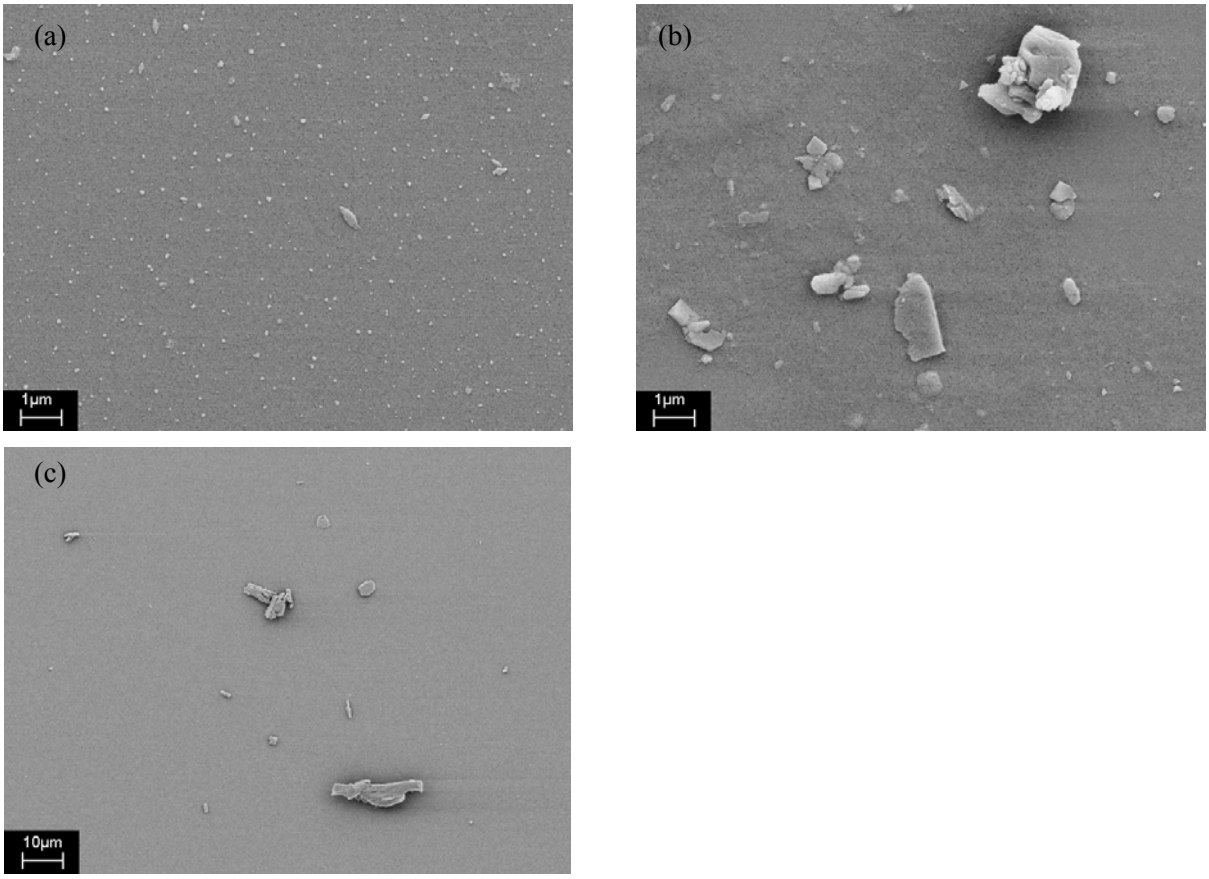

Figure 4.10 SEM images of the peptide-ellipticine complexes with 0.1 mg/mL (0.4 mM) ellipticine and different EAK16-II concentrations: (a) 0.5 mg/mL (0.3 mM), (b) 0.2 mg/mL (0.12 mM) and (c) 0.05 mg/mL (0.03 mM).

The results obtained here will be important in the next phase studies on the peptide-based delivery of ellipticine *in vitro* and *in vivo*. First, the size of the peptide-ellipticine complexes can be manipulated from micrometers to hundreds of nanometers. The particle size will significantly affect the circulation in the blood stream, the binding to the cells and the uptake by the cells.[233-236] Second, the different states of stabilized ellipticine in solution can be obtained depending on the peptide and ellipticine concentrations in the formulation. This will have a varying impact on the anticancer activity and therapeutic efficacy.[157,237,238] Third, the release rate of ellipticine from the complex can be

tuned, in relation to the size of the complex and the state of stabilized ellipticine. The cellular toxicity and uptake as well as *in vivo* animal studies are currently under investigation.

4.4 Conclusions

The ionic-complementary self-assembling peptide EAK16-II was found to be able to stabilize the hydrophobic anticancer agent ellipticine in aqueous solution. Both microcrystal and protonated forms of ellipticine can be obtained. The formation of peptide-ellipticine suspensions in water is peptide concentration-dependent. The equilibration time can be as short as 5 h when the peptide concentration is close to its critical aggregation concentration (~0.1 mg/mL). At higher and lower peptide concentrations, the time required to reach equilibrium is much longer. High peptide concentrations (> 0.1 mg/mL) facilitate the formation of protonated ellipticine during the complexation. With a combination of 0.1 mg/mL ellipticine and 0.5 mg/mL EAK16-II, protonated ellipticine can be stabilized at equilibrium. The transfer rate of ellipticine from its peptide complexes into EPC vesicles is highly dependent on the peptide concentration used in the formulation. A higher peptide concentration results in a faster release rate. This relates to the fact that a higher peptide concentration favors the protonation of ellipticine and the formation of smaller complexes. In addition, the peptide-ellipticine complex size can be tuned with the concentration ratio in the formulation. This study demonstrates an excellent potential of ionic-complementary, self-assembling peptides as carriers for hydrophobic anticancer drug delivery.

Chapter 5*

Cellular Toxicity and Uptake of EAK16-II-Ellipticine Complexes

5.1 Introduction

The self-assembling peptide EAK16-II has recently shown its potential for the delivery of hydrophobic compounds.[51,56] Further studies have demonstrated that EAK16-II can stabilize a hydrophobic anticancer agent, ellipticine, in either protonated or crystalline form (Chapter 4). The release kinetics of ellipticine can be tuned by adjusting the peptide-to-ellipticine ratio during formulation. It will be critical to further evaluate the therapeutic effect of the formulated peptide-drug complexes *in vitro* in order to develop self-assembling peptide-based delivery of hydrophobic anticancer drugs.

Here we investigate the cellular toxicity and uptake of the EAK16-II-ellipticine complexes. Two cancer cell lines, the non-small cell lung cancer cell A549 and breast cancer cell MCF-7, were used in this study. The complexes were first prepared at five different peptide-to-ellipticine ratios, where either protonated or crystalline ellipticine was stabilized. Their toxicity to both cell lines was then tested in relation to the cell viability obtained from the MTT assay. The complex stability upon dilution was also studied since such information is essential for future preclinical tests. To better understand the therapeutic effect of the two molecular states of ellipticine in complexes, cellular uptake experiments were performed by a fluorescence imaging technique based on the well-characterized ellipticine fluorescence properties (Chapter 3). The measurements were conducted in different time periods and at different temperatures in order to characterize the internalization pathway. This research will provide important information on drug formulation and design of peptide nanocarriers.

*The cellular uptake experiments of this chapter were done and contributed by our collaborators at the University of Toronto, P. Tang, R. Bawa, B. Han and M. Liu.

5.2 Materials and Methods

5.2.1 Materials

The self-assembling ionic-complementary peptide EAK16-II (Mw = 1657 g/mol, crude) was obtained from CanPeptide Inc. (Pointe-Claire, Quebec, Canada) and used without further purification. It has an amino acid sequence: n-AEAEAKAKAEAEAKAK-c, where A corresponds to alanine, E to glutamic acid and K to lysine. The N-terminus and C-terminus of the peptide were protected by acetyl and amino groups, respectively. At pH~7, A is neutral, while E and K are negatively and positively charged, respectively. The anticancer agent ellipticine (99.8% pure) was purchased from Sigma-Aldrich (Oakville, ON, Canada) and used as received. Paraformaldehyde (PFA, reagent grade) was obtained from Sigma-Aldrich (Oakville, ON, Canada). Cell culture reagents including Dulbecco's modified eagle medium (DMEM), fetal bovine serum (FBS) and trypsin-ETDA were purchased from Invitrogen Canada Inc. (Burlington, ON, Canada). Phosphate buffer saline (PBS) and penicillin-streptomycin (p/s, 10000 U) were obtained from MP Biomedicals Inc. (Solon, OH, USA).

5.2.2 Sample Preparation

Fresh EAK16-II solutions were prepared in pure water (18 MΩ; Millipore Milli-Q system) at concentrations of 0.02, 0.1, 0.2, 0.5 and 1.0 mg/ml. The solution was then sonicated in a bath sonicator (Branson, model 2510) for 10 min to ensure complete dissolution of the peptide powders. Appropriate amounts of the fresh peptide solutions at each concentration were added into a glass vial containing ellipticine crystals to yield an ellipticine concentration of 0.1 mg/mL, generating five peptide-to-ellipticine ratios of 10:1, 5:1, 2:1, 1:1 and 1:5 (by mass). The EAK16-II-ellipticine mixtures were under mechanical stirring at 900 rpm for 24 h to allow the complex formation. An ellipticine control in pure water (with the absence of EAK16-II) at the same ellipticine concentration

was prepared for comparison, following the same procedure. The complexes at a 5:1 ratio were diluted serially (2x, 4x, 8x and 16x) in pure water to study the complex stability. All vials and solvents were sterilized and the samples were prepared in a biological safety cabinet to avoid possible contamination. The complexes were photographed with a digital camera (Cannon PowerShot A95); the appearance of the peptide-ellipticine suspensions could reveal certain information on the molecular states of ellipticine in the complexes.

5.2.3 Cellular Toxicity Tests

Two cancer cell lines, non-small cell lung cancer cell A549 and breast cancer cell MCF-7 (courtesy from Dr. Mingyao Liu at the University of Toronto), were used for *in vitro* cellular toxicity studies on the EAK16-II-ellipticine complexes. The cells were cultured in DMEM containing 10% FBS and 1% p/s at 37°C and with 5% CO_2. When the cells grew to reach ~95% confluence, they were detached from the cell culture dishes with trypsin-EDTA, centrifuged at 500 rpm for 5 minutes, and resuspended in fresh cell culture media at concentrations of 5×10^4 and 1×10^5 cells/mL for A549 and MCF-7 cells, respectively. For each type of cell, 200 μL of the cell suspensions were added into each well of a clear, flat bottom 96-well plate (Costar) and incubated for ~24 h. The old media were taken out and replaced with 150 μL fresh culture media, followed by an addition of 50 μL treatments (including the complexes and control samples) into each well, resulting in a 4-fold dilution of the treatments. The plates were incubated for 4, 8, 12, 24 and 48 h prior to performing the cell viability assay. The experimental setup contained several control groups for each plate, including negative control (medium), solvent control, peptide control and drug control.

MTT assay (TOX1 from Sigma-Aldrich, Oakville, ON, Canada) was used to determine the cell viability after different treatments. 5 mg of solid MTT was first dissolved in 3 mL PBS solution, followed by a 10-time dilution in the culture medium. All the treatments were taken out, and 100 μL

of the MTT solution was then added to each well of the treated plates. The plates were incubated for 4 h prior to the addition of 100 μL solubilization solution (anhydrous isopropanol with 0.1 N HCl and 10% Triton X-100). After overnight incubation, the absorbance at 570 nm was collected on a microplate reader (BMG FLUOstar OPTIMA) and subtracted by the background signals at 690 nm. The absorption intensities were averaged from 4 replicates for each treatment and normalized to that obtained from the untreated cells (negative control) to generate the cell viability (i.e., the cell viability of the negative control is 1).

5.2.4 Cellular Uptake Studies

Two cancer cell lines, A549 and MCF-7 (from ATCC), were used to investigate the uptake of EAK16-II-ellipitcine complexes *in vitro*. They were cultured in DMEM with 10% FBS at 37 °C with 5% CO_2. The cells were then seeded on a 12-well plate with cell densities of 5×10^4 and 1×10^5 cells/well for A549 and MCF-7, respectively, followed by 48 h incubation prior to the treatments. The prolonged incubation time was to enhance the cell adhesion and avoid significant cell loss under intensive rinsing during the subsequent cell fixing procedure. The treatments were added into each well and incubated for 5, 15 and 30 min. Four treatments were tested: the complexes at two peptide-to-ellipticine ratios, 5:1 (125 μg/mL:25 μg/mL) and 1:1 (25 μg/mL:25 μg/mL), the ellipticine control (25 μg/mL), and the peptide control (125 μg/mL). The treated cells were washed with PBS 3 times, and fixed with 4% PFA in PBS, followed by another 3 times washing with PBS. The cells were examined with a fluorescence microscope (Nikon Eclipse 80i); a green fluorescence filter was used to collect the fluorescence signals of ellipticine, and phase contrast images were acquired to observe the cell morphology.

The temperature-dependent cellular uptake of ellipticine was conducted at 37 °C and 4 °C to examine whether the internalization of ellipticine occurs through an endocytosis pathway.[239,240] The

same cell density (as above) was used for cell seeding with 48 h incubation. Prior to treating the cells, the plates were incubated at 37 °C or 4 °C for 30 min, allowing the culture media to reach the equilibrium temperature. The same treatments (two complexes, ellipticine control and peptide control) were applied with an incubation time of 30 min. The cells were then fixed following the same procedure as before, and examined with the fluorescence microscope.

5.3 Results and Discussion

The previous studies (Chapter 4) have shown that EAK16-II can stabilize ellipticine in protonated or crystalline form in aqueous solution, depending on the peptide and ellipticine concentrations. Protonated ellipticine can be stabilized in the complexes formulated with a combination of 0.5 mg/mL EAK16-II and 0.1 mg/mL ellipticine. When the ratio of peptide-to-ellipticine is smaller than 5:1 (by mass), the stabilized ellipticine is predominantly in crystalline form in the complexes. This may indicate that 5:1 ratio is important in determining the molecular states of ellipticine in the complexes.

Here we report a series of peptide-to-ellipticine ratios (at a fixed ellipticine concentration of 0.1 mg/mL) on their complex formation and *in vitro* therapeutic effect against two cancer cell lines, A549 and MCF-7. Figure 5.1 shows the photographs of the EAK16-II-ellipticine complexes at different peptide-to-ellipticine ratios. It is clearly seen that the solutions turn yellow and transparent at ratios of 5:1 and 10:1, indicating the formation of protonated ellipticine in the complexes. At ratios below 5:1, the solutions appear to be turbid as the stabilized ellipticine is predominantly in crystalline form. However, the ellipticine control sample remains transparent with chunks of ellipticine crystals floating on top or at the bottom of the vial (far right), owing to its extreme hydrophobicity with a very low solubility in water (~0.6 μM).[71] These results confirm our previous observations (Chapter 4, Figure 4.7a) and provide evidence that whether protonated or crystalline ellipticine can be stabilized is related to the peptide-to-ellipticine ratio.

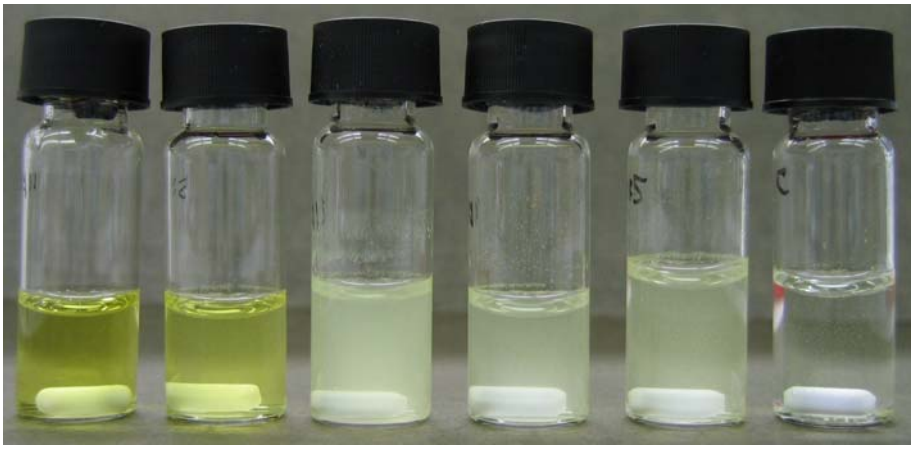

10:1 5:1 2:1 1:1 1:5 EPT-H_2O

Figure 5.1 Photographs of EAK16-II-ellipticine complexes at different peptide-to-ellipticine ratios (by mass). The ellipticine concentration is fixed at 0.1 mg/mL. An ellipticine control in pure water (EPT-H_2O) is also tested for comparison.

5.3.1 Cellular Toxicity of EAK16-II-Ellipticine Complexes

The toxicity of the complexes at different peptide-to-ellipticine ratios against both A549 and MCF-7 cells is shown in Figure 5.2a. The complexes at the ratios of 5:1 and 10:1 are effective at killing both cancer cells, leading to low cell viability (less than 0.25). Below the 5:1 ratio, the anticancer activity of the complexes decreases significantly, and is similar to the ellipticine control. The dramatic change in the complex toxicity is probably related to the molecular state of ellipticine in the complexes. The protonated ellipticine appears to be more effective at killing cancer cells than crystalline ellipticine. This may be due to fast release kinetics of protonated ellipticine from the complexes (Chapter 4, Figure 4.9). In addition, protonated ellipticine tends to interact with negatively charged cell membranes, and accumulate at the membrane surface; the hydrophobic moiety of ellipticine further helps it cross the cell membrane. This also implies that the internalization of ellipticine may not be through energy-dependent endocytosis (see Section 5.3.2).

(a)

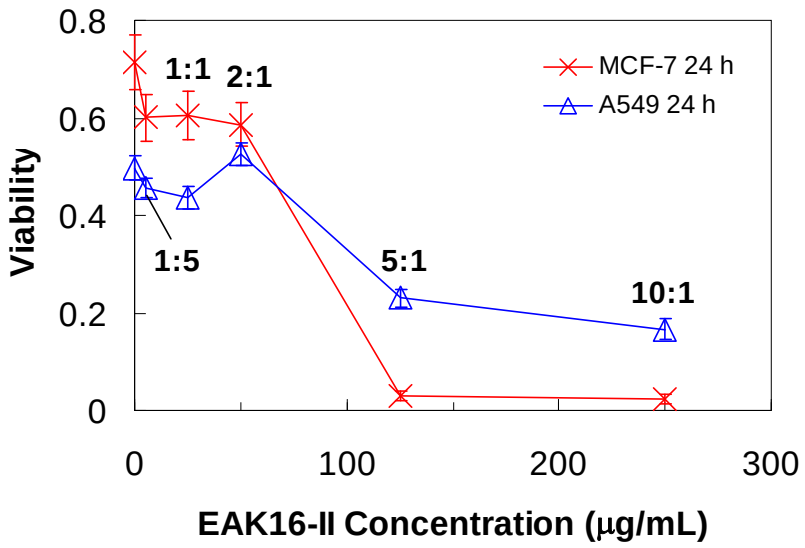

(b)

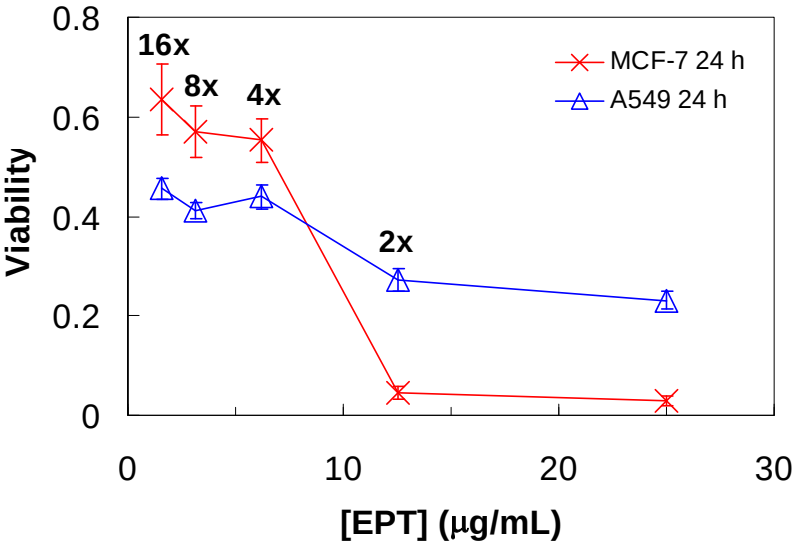

Figure 5.2 Viability of MCF-7 and A549 cells treated with the complexes at different peptide-to-ellipticine ratios (a) and upon serial dilution (b). The complex at 5:1 ratio was used for the serial dilution. The complexes were prepared with a fixed ellipticine concentration of 0.1 mg/mL (0.4 mM) with various EAK16-II concentrations of 0.02-1.0 mg/mL (0.012-0.6 mM)

Note that the protonated ellipticine seems to be more active at killing MCF-7 cells than A549 cells, causing an almost zero MCF-7 cell viability. Such an effect may be due to the fact that MCF-7 cells are more sensitive to protonated ellipticine. Thus, these results may lead to a notion of selecting appropriate formulations to treat different cancer cells. By adjusting the mass ratio of EAK16-II versus ellipticine, one can obtain different molecular states of ellipticine in the complexes as well as the complex dimensions (Chapter 4, Figure 4.10), for specific cancer cells.

The stability of a given formulation upon dilution is an important factor in determining its applicability in clinical usage.[241] Since the complexes at 5:1 ratio show a good anticancer activity against both cancer cell lines, we further carry out serial dilution of such complexes in pure water and test their stability in relation to the cellular toxicity. Figure 5.2b shows the toxicity of the complex at 5:1 ratio and its serial dilution in water (2, 4, 8 and 16 times). The 2 times dilution does not affect the toxicity of the complex significantly for both cells. Further dilution greatly reduces the complex toxicity against MCF-7 cells; it also decreases the toxicity against A549 cells, but to a lesser degree. Normally, the decrease in cell viability should be gradual and smooth due to the decrease in drug concentration upon dilution. However, the observed trend is not gradual, but rather has a dramatic change at a more than 2x dilution. This may be related to the instability of the complexes upon dilution in water. One possible reason is that the complex containing protonated ellipticine is pH sensitive; extensive dilution is expected to increase the solution pH, leading to the deprotonation of ellipticine to form ellipticine microcrystals. As a result, the toxicity of the diluted complexes reduces, similar to that of the complexes at a lower peptide-to-ellipticine ratio. A drastic decrease in complex toxicity upon dilution for MCF-7 cells provides additional evidence that MCF-7 cells are more sensitive to protonated ellipticine.

In order to find a proper time-window for cellular uptake, time-dependent toxicity tests are conducted. In principle, a proper time-window should allow drug to enter the cells but not cause cell

death. The time-dependent toxicity of the complexes is shown in Figure 5.3. Two ratios, 1:1 (squares) and 5:1 (circles), are used to examine the difference in toxicity of crystalline and protonated ellipticine, respectively. They are compared with the ellipticine control (crosses) in the absence of EAK16-II. It can be seen that the two different cell lines exhibit different patterns in the time-dependent viability in response to the treatments. For MCF-7 cells (Figure 5.3a), the complexes at the 5:1 ratio are so effective that the cell viability decreases to less than 0.5 after 4 h treatment; it decreases further to almost zero after 24 h treatment. Meanwhile, the complexes at the 1:1 ratio and ellipticine control have almost no effect at 4 h, before gradually decreasing the viability to about 0.5 by 48 h. On the other hand, no distinguishable difference in cell viability can be observed among the three treatments at 4 h for A549 cells (Figure 5.3b); with time, all treatments cause significant cell death, although the effect is more pronounced for the complexes at 5:1 ratio. Almost zero viability is achieved after 48 h treatment of the complexes with protonated ellipticine (5:1 ratio).

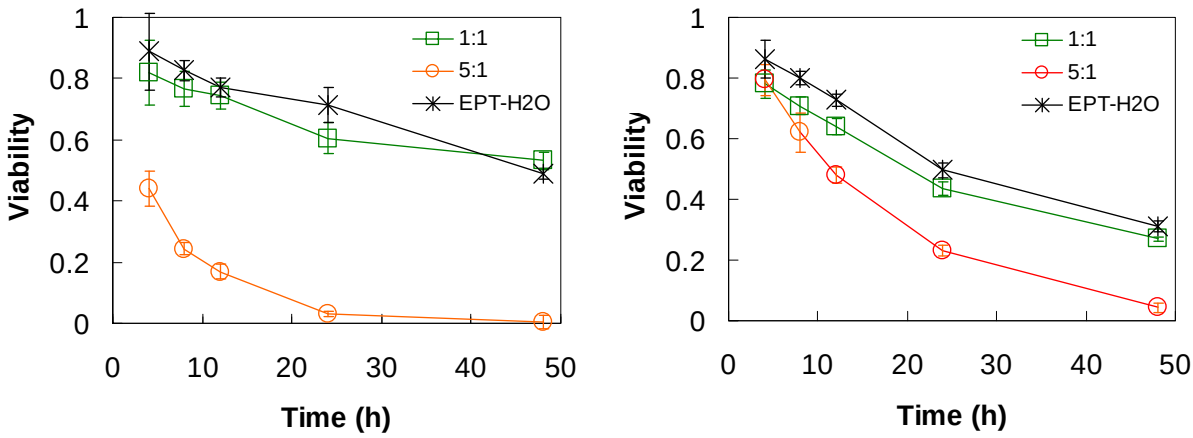

(a) (b)

Figure 5.3 Time-dependent toxicity of the EAK16-II-ellipticine complexes against MCF-7 (a) and A549 (b) cells. EPT-H2O: ellipticine control (in pure water).

The above results indicate that the appropriate time-window for cellular uptake should be within 4 h. In addition, MCF-7 cells are very sensitive to protonated ellipticine while both protonated and crystalline ellipticine are effective at killing A549 cells (Figure 5.2). However, the reason behind this is still unclear. One may speculate that such a phenomenon probably results from the differences in uptake of the complexes by A549 and MCF-7. To clarify this, fluorescence imaging technique is applied to characterize the internalization of ellipticine by the two cell lines.

5.3.2 Cellular Uptake of Ellipticine in A549 and MCF-7 Cells

The uptake of ellipticine by the two cell lines is shown in Figure 5.4. The cells are treated with complexes at two ratios of 5:1 and 1:1, the ellipticine control and the peptide control for 5, 15 and 30 min. For A549 cells (Figure 5.4a), the treatment with peptide alone does not exhibit any fluorescence (1st column, insets), which is reasonable since there is no ellipticine in the system and EAK16-II is not fluorescent. When the cells are treated with ellipticine control, the fluorescence signals are too dim to be seen initially, but increase with time. A stronger fluorescence signal can be observed for the treatments of complexes at 5 min and become more pronounced at later times. After 30 min treatment of the complexes at the 5:1 ratio, the ellipticine fluorescence seems to accumulate in the cell nuclei. Similar phenomena are observed for MCF-7 cells (Figure 5.4b).

These results show that the uptake of ellipticine is fast. This is likely because ellipticine is a small hydrophobic molecule, and can easily cross the cell membrane barrier once reaching its outer surface. However, the presence of peptides appears to enhance the rate of uptake. One reason is that peptides can stabilize large amounts of protonated or crystalline ellipticine in aqueous solution. The high concentration of ellipticine in solution facilitates its diffusion into the cells. In addition, protonated ellipticine seems to have a much stronger tendency to be taken up by both cell lines, especially MCF-7 cells. This may due to a stronger interaction between positively charged ellipticine

and negatively charged cell membranes. Besides, protonated ellipticine is released much faster from the complexes than crystalline ellipticine (Chapter 4, Figure 4.9). It is worth noting that the subtle difference in ellipticine uptake from the complexes at two different ratios cannot explain the much higher toxicity of the complexes at the 5:1 ratio over the other as shown in Figure 5.2a. Other factors may determine the toxicity of protonated and crystalline ellipticine. The toxicity difference may be related to variations in the amount of ellipticine uptaken at the two ratios, although it is not directly reflected from these fluorescence images.

(a)

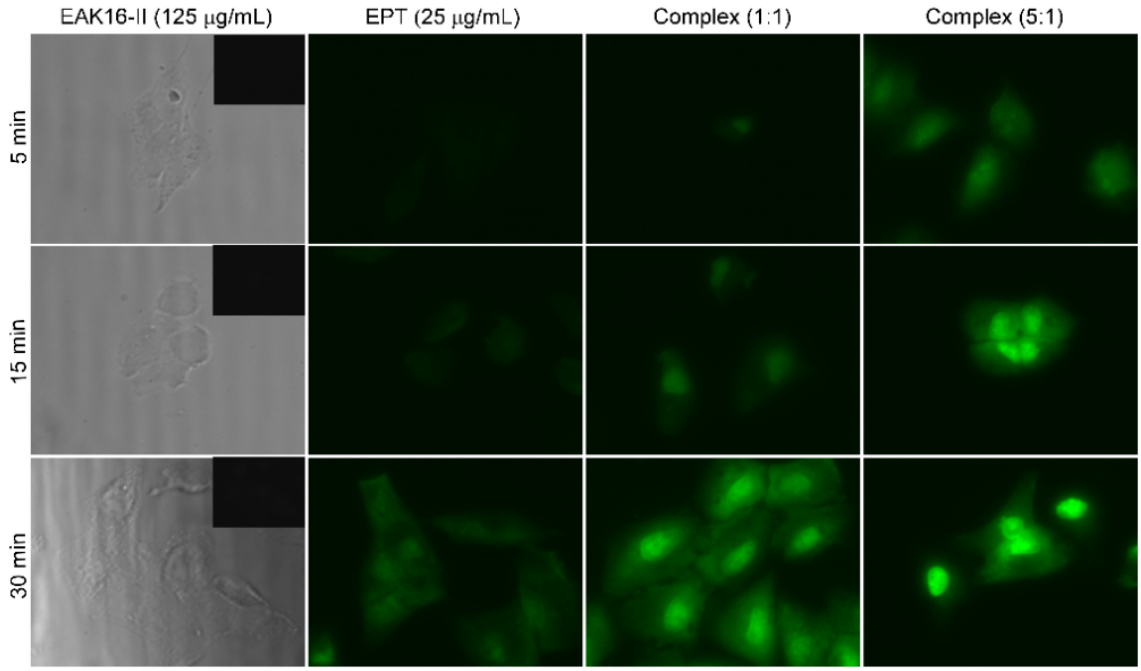

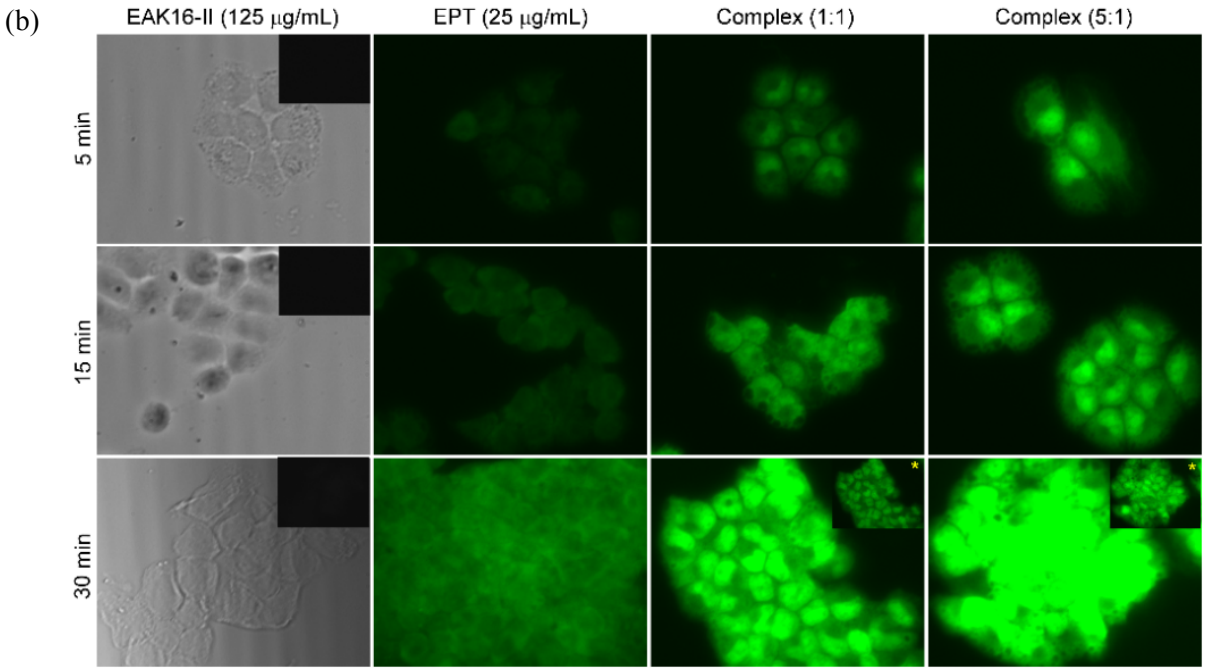

Figure 5.4 Fluorescence images showing cellular uptake of ellipticine in A549 (a) and MCF-7 (b) cells. Green color is from ellipticine fluorescence. The first column shows the phase contrast images with corresponding fluorescence images as the insets. * denotes half exposure time.

To confirm whether the internalization of ellipticine is through direct permeation across the cell membranes, the uptake of ellipticine is conducted at two different temperatures, 37 °C and 4 °C. Most cellular uptake through the endocytosis pathway is energy dependent, which can be blocked at a temperature as low as 4 °C.[224,225,242] As shown in Figure 5.5, the uptake of ellipticine in both cancer cells can be observed after 30 min treatments with the complexes as well as the ellipticine control. Evidently, there are no significant differences in ellipticine uptake between 37 °C and 4 °C, although the ellipticine fluorescence is weak at 4 °C for the treatment of ellipticine control. The temperature-independent uptake of ellipticine indicates that the passive diffusion of ellipticine into the cells is probably the primary cell internalization mechanism.

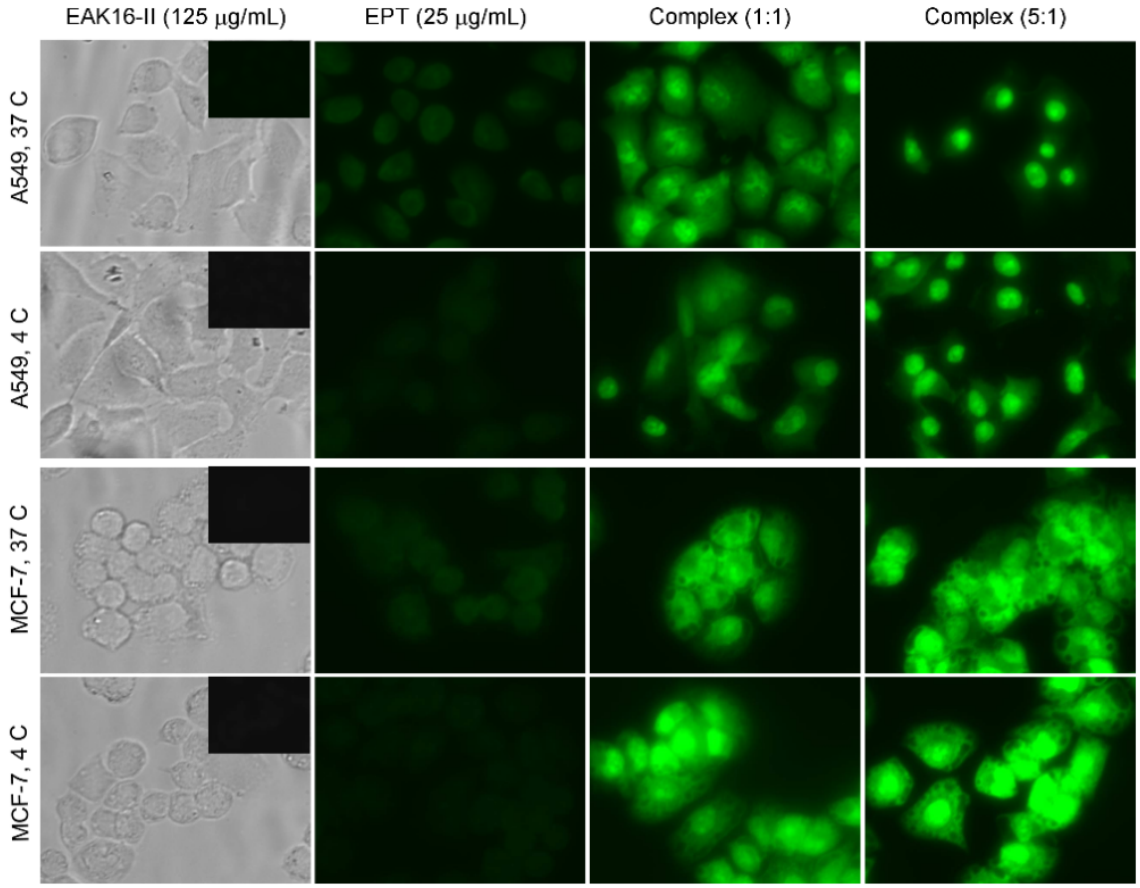

Figure 5.5 Fluorescence images showing cellular uptake of ellipticine at 37 °C and 4 °C in A549 and MCF-7 cells with different treatments. Green color represents ellipticine fluorescence. First column shows phase contrast images, and the insets are the corresponding fluorescence images.

From these results, the complexation of ellipticine with EAK16-II seems not to alter the internalization pathway of ellipticine; however, it enhances the rate of cellular uptake by increasing the amount of ellipticine suspended in solution. Note that such a fast and unspecific cellular uptake may not be ideal for anticancer drug delivery as it would cause harmful side effects to healthy tissue during delivery. To overcome this problem, one could increase the interaction between ellipticine and peptides to slow the release process. For example, one could increase the hydrophobicity of the peptide through sequence design, which may increase the interaction between the hydrophobic

ellipticine and peptides. On the other hand, unspecific uptake may be solved by introducing cell targeting moieties onto the peptide sequence to achieve active targeting. An example is the cyclic peptide motif c-NGRGEQ-c, which has been found to strongly bind to several non-small cell lung cancer cell lines including A549, Calu-1 and H178.[112] A vasoactive intestinal peptide (VIP) can selectively bind to many breast cancer cell lines such as MCF-7.[171,193] Thus, a proper design of peptide sequence becomes very important in the development of self-assembling peptide-mediated delivery for hydrophobic anticancer drugs.

5.4 Conclusions

From this study, it can be concluded that EAK16-II is capable of stabilizing protonated or crystalline ellipticine in aqueous solution depending on the peptide-to-ellipticine ratio during the formulation. Above the ratio of 5:1 (by weight), the stabilized ellipticine is protonated; below this ratio ellipticine is in crystalline form in the complexes. The two molecular states of stabilized ellipticine in the complexes exhibit different toxicity against two cancer cell lines, A549 and MCF-7, with the protonated being more toxic. Such an effect is more pronounced for MCF-7 cells than for A549 cells. This is probably due to the fact that MCF-7 cells are more sensitive to protonated ellipticine. The complexes with protonated ellipticine are not stable upon dilution in water. The uptake of ellipticine in both cell lines appears to follow a diffusion mechanism. It is found that ellipticine can still be taken up by both cancer cells at 4 °C, where the energy-dependent endocytosis pathway is blocked. The complexation of ellipticine with EAK16-II seems not to alter the internalization pathway of ellipticine. However, it significantly enhances the uptake over a shorter time period (~5 min). These results demonstrate that the EAK16-II-ellipticine complexes with protonated ellipticine are effective at killing cancer cells *in vitro*; the existence of some unfavorable properties of the complexes, such as

unspecific cellular uptake, suggests that appropriate design of the peptide sequence is essential for future development of self-assembling peptide carriers.

Chapter 6*

Sequence Effect of Self-Assembling Peptides on the Complexation and *In Vitro* Delivery of the Hydrophobic Anticancer Drug Ellipticine

6.1 Introduction

Self-assembling peptides are emerging nano-biomaterials with promising biomedical and bioengineering applications.[59,116,243] Among them is a special class of ionic-complementary peptides discovered from a yeast Z-DNA binding protein.[61] These peptides have a unique amphiphilic structure resulting from an alternative arrangement of hydrophobic and hydrophilic amino acids in sequence. They also consist of alternating positive and negative charges under physiological conditions, resulting in ionic complementarity. These peptides are capable of self-assembling into very stable nanostructures or macroscopic membranes, which can withstand high temperature, extreme pH, many digesting enzymes and denaturation agents.[61,62] Moreover, they exhibit good biocompatibility with many cultured mammalian cells[64] and do not have detectable immune responses when introduced into animals[61,63,244] These properties make them ideal materials for tissue scaffolding,[134,135,245] regenerative medicine[63,126,244] and drug delivery.[51,57,58,154]

The ionic-complementary self-assembling peptides have recently been used as novel nano-biomaterials in the local delivery of hydrophilic peptide/protein drugs[57,58] and the formulation of hydrophobic chemotherapeutics.[56] The biotinylated, self-assembling peptide RADA16-II was found to be able to locally deliver insulin-like growth factor 1 (IGF-1) to the myocardium, and provide sustained release of IGF-1 for 28 days.[58] These peptide nanofibers can also bind with a human platelet derived growth factor (PDGF-BB) and deliver it *in vivo* with sustained release to successfully decrease cardiomyocyte death and preserve systolic function.[57] In addition to the delivery of peptide/protein drugs, it has recently been demonstrated that a self-assembling peptide, EAK16-II,

*This chapter is based on a paper draft "S.Y. Fung, H. Yang and P. Chen, Sequence effect of self-assembling peptides on the complexation and *in vitro* delivery of the hydrophobic anticancer agent ellipticine, accepted by *PLoS ONE*, 2008".

can stabilize hydrophobic compounds in aqueous solution and release them into a cell membrane mimic in a controlled manner.[51,56] Further studies revealed that such a peptide can stabilize the hydrophobic anticancer agent ellipticine with different molecular states in aqueous solution depending on the peptide and ellipticine concentration, which in turn affects the ellipticine release from the complexes (Chapter 4). These studies have shown great potential for the use of the self-assembling peptides in drug delivery.

However, current studies of using self-assembling peptides for drug delivery are still at their early stage. The development of a self-assembling peptide-based delivery system requires better design of peptide sequences for specific delivery goals. Previous studies have shown that a difference in the charge distribution of the self-assembling peptides significantly alters the nanostructure of the peptide assemblies.[45,46] In addition, the charge distribution affects the peptide assemblies in response to solution pH.[45] The variations in peptide length, hydrophobicity and ionic complementarity have been applied to control the formation of self-assembling peptide matrices.[128] The resulting structure of peptide assemblies will impact the design of delivery vehicles for different therapeutics. For example, delivery of protein or siRNA drugs requires cell penetration while cell recognition is critical to achieve targeted delivery of anticancer therapeutics.[15,225,226] Therefore, proper design of peptide sequences becomes crucial to build functional peptide-based carriers for effective drug delivery.

In this work, we carry out the study of peptide sequence effects on the drug formulation and *in vitro* delivery. Three self-assembling peptides, EAK16-II, EAK16-IV and EFK16-II, are chosen to investigate the effects of charge distribution (type II vs. type IV) and hydrophobicity (alanine A vs. phenylalanine F). A hydrophobic anticancer agent, ellipticine, is selected as a model drug, following our early studies. The self-assembled nanostructures of these peptides are first characterized by atomic force microscopy (AFM); the hydrophobicity of the peptides dissolved in aqueous solution is studied via surface tension measurements, and fluorescence spectroscopy using a hydrophobic

fluorescent probe. These characteristics of the three peptides are expected to impact their complexation with ellipticine, in terms of ellipticine molecular states and the size of the resulting complexes. The anticancer activity of the formulation is tested *in vitro* against two cancer cell lines: non-small cell lung cancer cell A549 and breast cancer cell MCF-7. The stability of the complexes after serial dilutions in aqueous solution is further investigated. The information obtained in this study is aimed at providing appropriate design principles for selecting peptide sequences and fabricating advanced functional peptide carriers for anticancer drug delivery.

6.2 Materials and Methods

6.2.1 Materials

Three self-assembling, ionic-complementary peptides EAK16-II (Mw = 1657 g/mol, crude), EAK16-IV (Mw = 1657 g/mol, crude) and EFK16-II (Mw = 2265 g/mol, crude) were obtained from CanPeptide Inc. (Pointe-Claire, Quebec, Canada) and used without further purification. Their sequences and molecular structures are shown in Figure 6.1, where A corresponds to alanine, F to phenylalanine, E to glutamic acid and K to lysine. The N-terminus and C-terminus of the peptide were protected by acetyl and amino groups, respectively. At pH~7, A and F are neutral, while E and K are negatively and positively charged, respectively. The anticancer agent ellipticine (99.8% pure) and 1-anilinonaphthalene-8-sulfonic acid (ANS) were purchased from Sigma-Aldrich (Oakville, ON, Canada) and used as received. Tetrahydrofuran (THF, reagent grade 99%) and dimethyl sulfoxide (DMSO, spectral grade 99+%) were acquired from Caledon Laboratories Ltd. (Georgetown, ON, Canada) and Sigma-Aldrich (Oakville, ON, Canada), respectively. Cell culture reagents including Dulbecco's modified eagle medium (DMEM), fetal bovine serum (FBS) and trypsin-ETDA were purchased from Invitrogen Canada Inc. (Burlington, ON, Canada). Phosphate buffer saline (PBS) and penicillin-streptomycin (p/s, 10000 U) were obtained from MP Biomedicals Inc. (Solon, OH, USA).

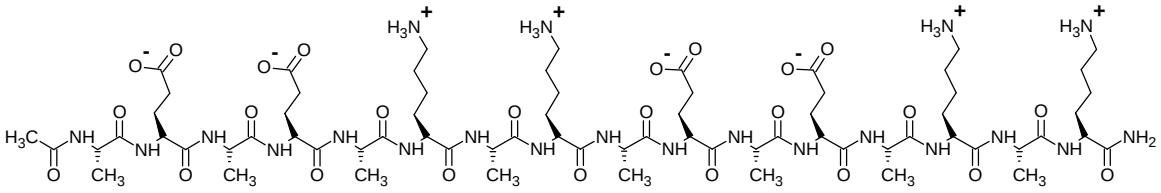

EAK16-II: n-AEAEAKAKAEAEAKAK-c

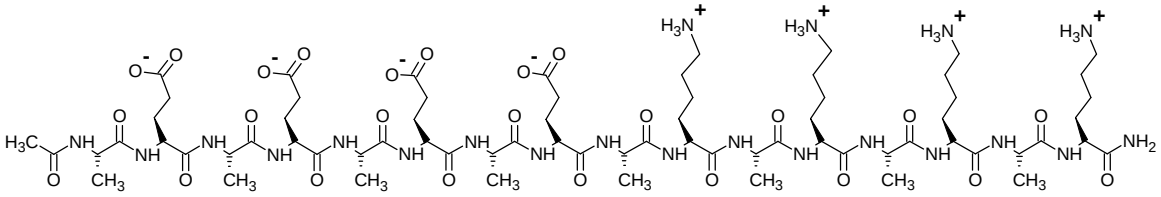

EAK16-IV: n-AEAEAEAEAKAKAKAK-c

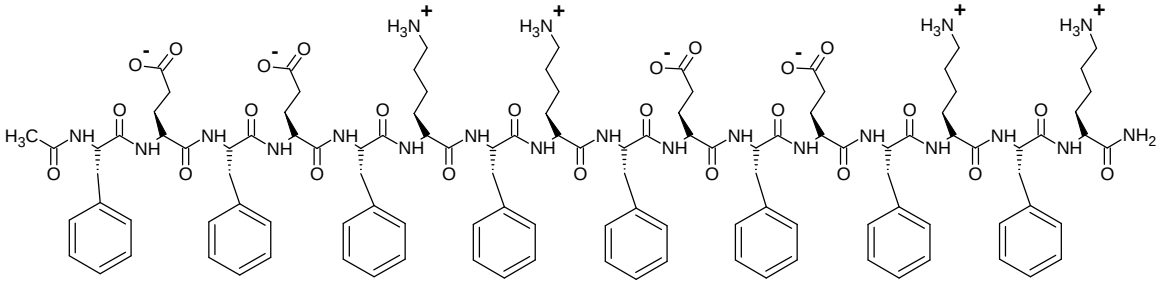

EFK16-II: n-FEFEFKFKFEFEFKFK-c

Figure 6.1 Molecular structures and sequences of EAK16-II, EAK16-IV and EFK16-II. N and C termini are protected by acetylation and amidation, respectively.

6.2.2 Sample Preparation

Appropriate amounts of the peptide powder were first dissolved in pure water (18 MΩ; Millipore Milli-Q system) to obtain fresh peptide solutions at concentrations of 0.5, 0.2 and 0.04 mg/ml. The solution was then sonicated in a bath sonicator (Branson, model 2510) for 10 min. The peptide

solution at a concentration of 0.5 mg/mL was used to study the differences among the three peptides in terms of their self-assembled nanostructures, hydrophobicity and surface activity.

The peptide-ellipticine complexes were prepared by adding 1 mL of the fresh peptide solution into a glass vial containing a thin film of 0.04 mg ellipticine at the bottom, followed by mechanical stirring at 900 rpm for 24 h. 1 mL of pure water, instead of peptide solution, was also added to another vial to make a control sample. The purpose of using a relatively low ellipticine concentration of 0.04 mg/mL in this study was to obtain more distinguishable cellular toxicity levels in the complexes and the control sample. To make a thin film of ellipticine at the bottom of the vials, 100 μL of 0.4 mg/mL ellipticine stock solution in THF was transferred to the vials, and dried by gently blowing filtered air (0.22 μm pore size filter) for ~5 min. All the vials and solvents were sterilized and the samples were prepared in a biological safety cabinet to avoid possible contamination, for especially cell culture experiments. For dynamic light scattering (DLS) measurements, the solvents were filtered, and the samples were made in the biosafety cabinet to eliminate potential dust contamination. The complexes were photographed with a digital camera (Cannon PowerShot A95) and characterized using several techniques to obtain complex dimensions and molecular states of the ellipticine in the complexes.

6.2.3 Determining the Maximum Suspension Concentration of Ellipticine

The amount of suspended ellipticine in solution was determined by UV-absorption. The peptide-ellipticine suspension was diluted 20 times in DMSO (resulting in a solvent mixture of 95% DMSO and 5% water by volume) to dissolve ellipticine from the complexes. 80 μL of the solution were then transferred to a quartz microcell (70 μL) with a 1 cm light path and tested on a UV-Vis spectrophotometer (Biochrom Ultraspec 4300 Pro, Cambridge, England). The absorbance at 295 nm was converted to the ellipticine concentration using Beer-Lambert's law: absorbance (Abs) = εcd,

where ε is the molar extinction coefficient, c is the molar concentration of ellipticine, and d is the optical path length (cm).[202] The extinction coefficient was determined to be 59000 ± 1100 (R^2 > 0.995) from the linear fitting of ellipticine absorption as a function of ellipticine concentration (2-20 μM) prepared in a mixture of 95% DMSO and 5% water. The suspension concentration of ellipticine was averaged from 3 measurements, and compared with the given ellipticine concentration of 0.04 mg/mL. Since not all ellipticine in the thin film at the bottom of the vials could be stabilized and suspended in solution, the comparison of the suspension concentration with the given ellipticine concentration (0.04 mg/mL) would thus provide the maximum percentage of the ellipticine suspension at each formulation condition.

6.2.4 Atomic Force Microscopy (AFM)

The self-assembled peptide nanostructures were imaged on a PicoScan™ AFM (Molecular Imaging, Phoenix, AZ) in pure water. The samples were prepared with the following procedure: 10 μL of 0.5 mg/mL peptide solution were put on a freshly cleaved mica substrate, which was fixed on an AFM sample plate; a custom made AFM liquid cell was fastened on top of the mica substrate. The solution was incubated for 10 s to allow the peptide assemblies to adhere to the mica surface. The surface was then washed with pure water 15 times, before adding 500 μL of pure water into the cell prior to AFM imaging. A scanner with a maximum scan area of 6 × 6 μm^2 was used to acquire the AFM images. It was operated with a tapping mode using silicon nitride cantilevers with a nominal spring constant of 0.58 N/m (DNP-S, Digital Instruments, Santa Barbara, CA) and a typical tip radius of 10 nm. For the best imaging quality, the tapping frequency was typically set between 16 kHz and 18 kHz and the scan rates controlled between 0.8 and 1 line/s. The experiments were conducted in an environmentally-controlled chamber at room temperature to avoid evaporation of the solution. All AFM images were obtained at a resolution of 256 × 256 pixels.

6.2.5 Surface Tension Measurements

The dynamic surface tension of fresh peptide solutions was measured over a period of 2 h using the Axisymmetric Drop Shape Analysis-Profile (ADSA-P) technique. The experimental setup and operation of ADSA-P were described in an earlier publication[41] and references therein.

6.2.6 Fluorescence Spectroscopy

The hydrophobicity of the three peptides and their assemblies was investigated via ANS fluorescence.[246,247] 10 μM ANS solution was prepared in a 10 mM phosphate buffer at pH 6. The fresh peptide solutions were mixed with the same volume of the ANS solution on a vortex mixer for 10 s. The ANS solution was also mixed with the same volume of pure water as a control sample. 60 μL of the mixed solution were transferred to a quartz microcell and tested on a spectrofluorometer (Photon Technology International, Type QM4-SE, London, Canada) with a continuous xenon lamp as the light source. The sample was excited at 360 nm and the emission spectra were collected at wavelengths from 420 to 670 nm. The excitation and emission slit widths were set at 0.5 mm and 1.25 mm, respectively (0.5 and 1.25 mm corresponds to 2 and 5 nm band path). The spectra were normalized with the intensity of light scattering of air at 360 nm, to correct for the lamp fluctuations.

To study the molecular states of ellipticine in the complexes, 60 μL of the peptide-ellipticine suspensions were transferred to a microcell and tested on the spectrofluorometer. The excitation wavelength was set to be 294 nm and the emission was collected from 320 to 650 nm. The excitation and emission slit widths were set at 0.5 mm and 0.25 mm, respectively. The intensities were corrected with an ellipticine standard (2 μM in ethanol, sealed and degassed), to account for lamp fluctuations.

6.2.7 Dynamic Light Scattering (DLS)

The dimension of the peptide assemblies (0.5 mg/mL) and the complexes from the peptide-ellipticine suspensions was measured with a Zetasizer Nano ZS (Malvern Instruments, Worcestershire, U.K.) with appropriate viscosity and refractive index settings. The temperature was maintained at 25 °C during the measurement. A quartz microcell (45 μL) with a 3 mm light path was used. The scattered light intensities of the samples at the angle of 173° were collected. The intensity-based size distribution was obtained with the multimodal algorithm CONTIN,[229] provided in the software package Dispersion Technology Software 5.0 (Malvern Instruments, Worcestershire, U.K.). Each of the intensity-based size distribution reported herein corresponds to the average of three replicate measurements.

6.2.8 Scanning Electron Microscopy (SEM)

A LEO model 1530 field emission SEM (GmbH, Oberkochen, Germany) was employed to study the morphology and dimensions of the peptide-ellipticine complexes. The SEM sample was prepared by depositing 10 μL of the peptide-ellipticine suspensions on a freshly cleaved mica surface. The mica was affixed on an SEM stub using conductive carbon tape. The sample was placed under a Petridish-cover for 10 min to allow the complexes to adhere onto the mica surface. It was then washed once with a total of 100 μL pure water and air-dried in a dessicator overnight. All samples were coated with a 20 nm thick gold layer prior to SEM imaging; the images were acquired using the secondary electron (SE2) mode at 5 kV.

6.2.9 *In Vitro* Cell Viability Studies

Two types of cancer cells, non-small cell lung cancer cell A549 and breast cancer cell MCF-7 (courtesy from Dr. Mingyao Liu at the University of Toronto), were used for *in vitro* cellular toxicity

studies on the peptide-ellipticine complexes. The cells were cultured in DMEM containing 10% FBS and 1% p/s at 37°C and with 5% CO_2. When cells grew to reach ~95% confluence, they were detached from the cell culture flasks with trypsin-EDTA and resuspended in the cell culture media at concentrations of 5×10^4 and 1×10^5 cells/mL for A549 and MCF-7 cells, respectively. For each type of cell, 200 μL of the cell suspensions were added into each well of a clear, flat bottom 96-well plate (Costar) and incubated overnight. 50 μL of the treatments (including the complexes and control samples) were then added to the wells each containing 150 μL of fresh culture media. The plates were incubated for 48 h prior to perform the cell viability assay.

MTT assay was used to determine the cell viability after different treatments. 5 mg of solid MTT was dissolved in 3 mL PBS solution, followed by 10-fold dilution in the culture medium. All the treatments were taken out before 100 μL of the MTT solution was added to each well of the treated plates. The plates were incubated for 4 h prior to the addition of 100 μL of the solubilization solution (anhydrous isopropanol with 0.1 N HCl and 10% Triton X-100). After overnight incubation, the absorbance at 570 nm was recorded on a microplate reader (BMG FLUOstar OPTIMA) and subtracted by the background signals at 690 nm. The absorption intensities were averaged from 4 replicates for each treatment and normalized to that obtained from the untreated cells (negative control) to generate the cell viability.

6.3 Results and Discussion

The self-assembling peptide EAK16-II has been found to be able to stabilize the hydrophobic anticancer agent ellipticine in aqueous solution;[56] the ellipticine release kinetics from the complexes into a cell membrane mimic has also been determined (Chapter 4). Here, we report how the subtle differences in the peptide sequence affect the properties of the peptide assemblies, the formation of the peptide-ellipticine complexes, and the cellular toxicity of the complexes.

6.3.1 Sequence Effect on the Peptide Assemblies

Three self-assembling, ionic-complementary peptides, EAK16-II, EAK16-IV and EFK16-II, are used in this study. The latter two peptides are derived from the first one EAK16-II. All three peptides have 16 amino acids in sequence with 3 amino acid components: E, K and A or F, as shown in Figure 6.1. EAK16-IV has a different charge distribution of type IV ($---++++$) from EAK16-II as type II ($--++--++$), while the difference between EFK16-II and EAK16-II is a more hydrophobic residue F replacing A in EAK16-II. The slight differences in sequence among the three peptides may significantly affect their assemblies and further complexation with the hydrophobic molecules.

First, the self-assembled nanostructures formed by these peptides are found to be different. The distribution of negative and positive charges towards the two ends of an EAK16-IV molecule at neutral pH is reported to cause the folding of the peptide molecule to form a β-turn structure, resulting in the formation of globular nanostructures.[45,46] EAK16-II, on the other hand, has the preference for a stretched molecular structure and likely self-assembles into β-sheet rich nanofibers.[46] The nanostructures of the two peptides are shown in Figure 6.2a and b at a peptide concentration of 0.5 mg/mL. EAK16-II forms straight nanofibers, connecting to networks (Figure 6.2a), whereas EAK16-IV self-assembles into many more globular aggregates and some short nanofibers (Figure 6.2b). The formation of short nanofibers of EAK16-IV may be due to a relatively low pH (< 5) at such a high peptide concentration: when the pH is low enough, some of the negatively charged residues can be neutralized so that the intramolecular ionic interaction is weakened. Thus, some peptides remain in a stretched form, facilitating the formation of nanofibers.[45]

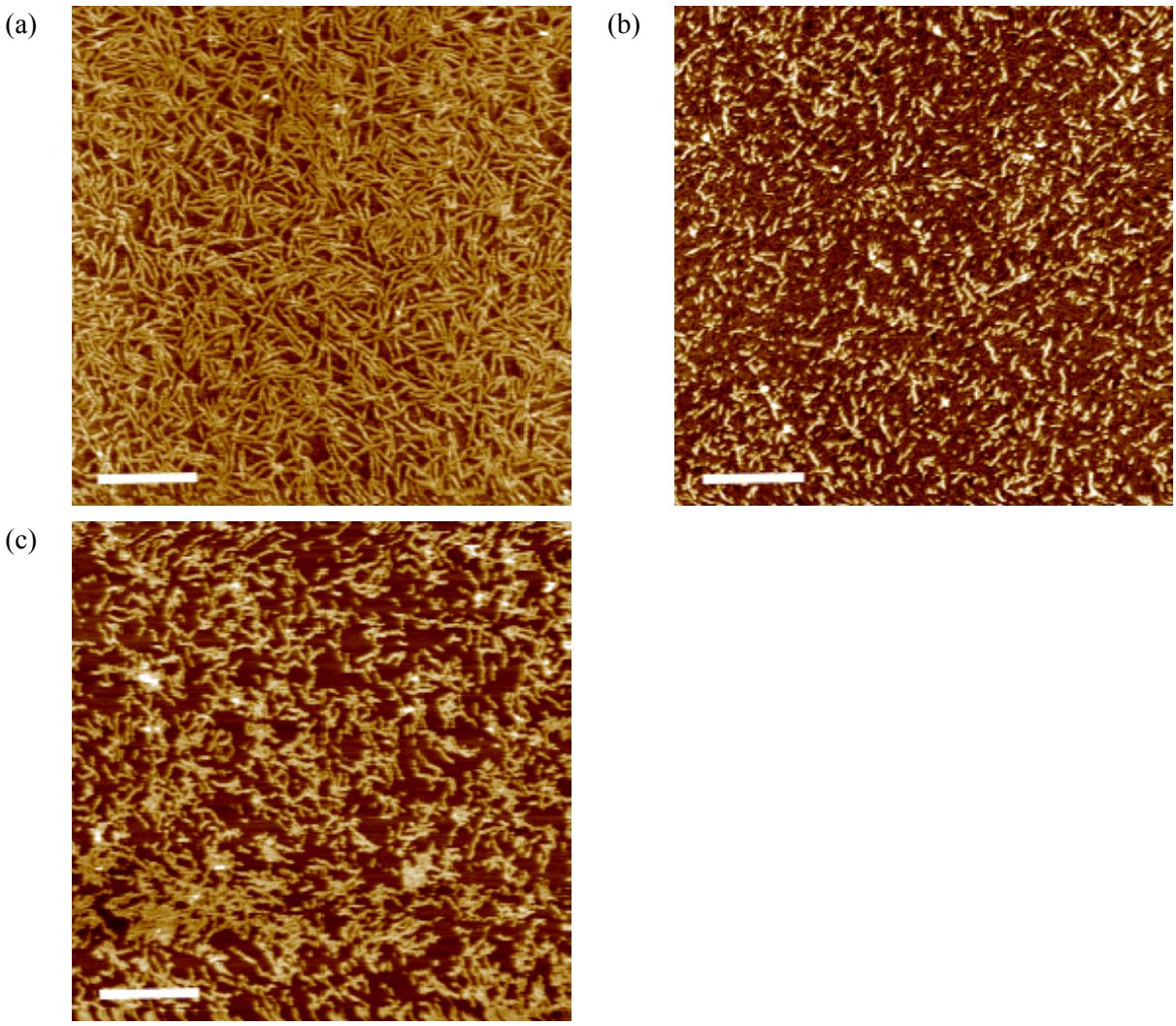

Figure 6.2 AFM images of the peptide nanostructures: (a) EAK16-II; (b) EAK16-IV; (c) EFK16-II. The peptide concentration is 0.5 mg/mL. The scale bar is 200 nm.

The nanostructures of EFK16-II are also different from those of EAK16-II as shown in Figure 6.2. EFK16-II forms predominant nanofibers and these fibers tend to aggregate into fiber clusters. This aggregation of nanofibers is probably due to a stronger hydrophobic interaction between them. Such a stronger hydrophobic interaction is expected to come from the more hydrophobic phenylalanine (F) residues in the EFK16-II sequence than the alanine (A) residues in EAK16-II. This

is probably why the nanofibers of EFK16-II tend to form fiber clusters, but those of EAK16-II are dispersed and form fiber networks.

The hydrophobicity of the three peptides and their assemblies is further characterized by surface activity and fluorescence measurements, as shown in Figure 6.3. Figure 6.3a shows the surface tension as a function of time for the three peptides at a peptide concentration of 0.5 mg/mL. For each profile, the surface tension decreases fast initially before slowly approaching equilibrium. This change with time corresponds to the dynamic process of the adsorption of peptide molecules/assemblies at the air-liquid interface, leading to the decrease in surface tension.[248] Comparing the surface tensions of the three profiles at 2 h (near equilibrium), they follow a trend: EAK16-II > EAK16-IV > EFK16-II. In general, the lower the surface tension is, the more hydrophobic is the molecule. Thus, the hydrophobicity of the three peptides and their assemblies (coexisting in solution) has a reversed trend: EFK16-II > EAK16-IV > EAK16-II. This is reasonable that EFK16-II is the most hydrophobic peptide among the three since it contains phenylalanine residues, which are more hydrophobic than alanine residues in EAK16-II and EAK16-IV. The reason why EAK16-IV has a lower equilibrium surface tension than EAK16-II is probably due to the formation of a β-turn structure through the intramolecular ionic interactions in EAK16-IV. This conformational change may cause the exposure of hydrophobic alanine residues toward the aqueous phase, resulting in a slight increase in hydrophobicity of the molecule and lowering the surface tension.[45]

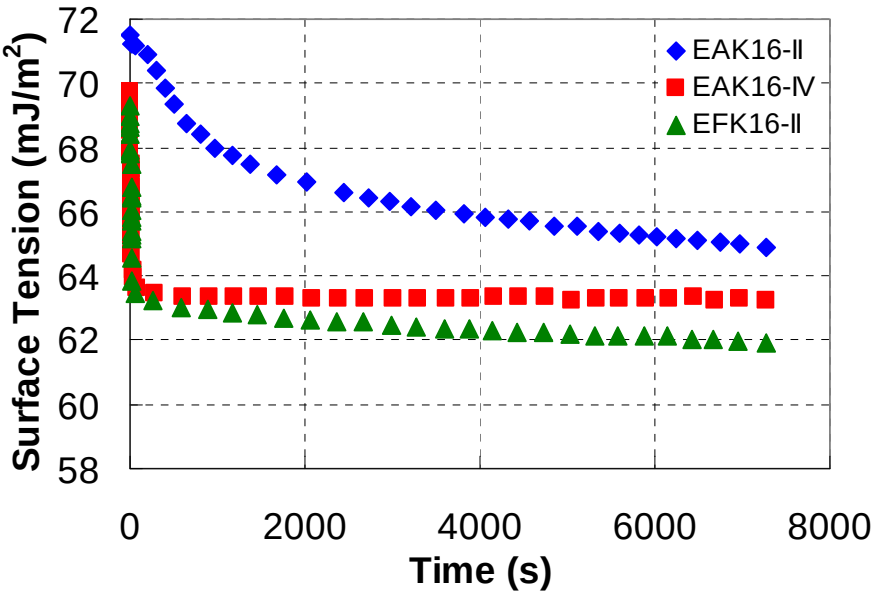

(a)

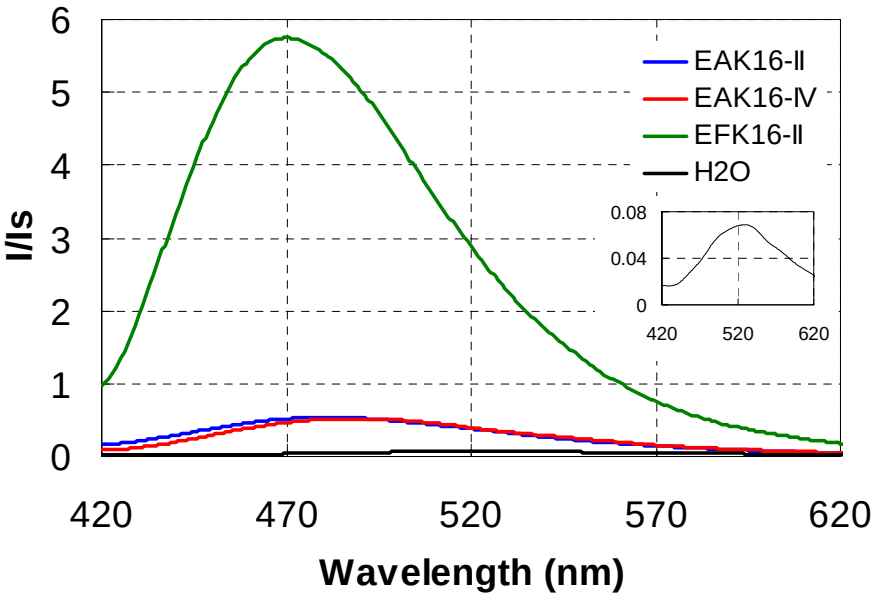

(b)

Figure 6.3 The hydrophobicity of the three peptides and their assemblies by dynamic surface tension (a) and ANS fluorescence (b). The inset is the ANS fluorescence control with the absence of peptides. The peptide concentration is 0.5 mg/mL (0.3 mM).

Figure 6.3b shows the fluorescence spectra of the ANS probe in the three peptide solutions compared to that in pure water (black line and the inset). The normalized fluorescence intensities of ANS in different solutions follow the trend: EFK16-II >> EAK16-II ≈ EAK16-IV > H_2O. Meanwhile, the peak positions of the spectra are different; it locates at ~520 nm in pure water (inset), but shifts to ~485 nm in EAK16-II and EAK16-IV solutions. The ANS fluorescence spectrum has a peak of ~470 nm in the EFK16-II solution. The changes in ANS fluorescence intensity and peak position indicate that the ANS probe is in different environments. ANS is a widely used probe to study protein aggregation as well as cell membrane composition and function due to its extreme sensitivity to the changes in the polarity of the probed environment.[246,249,250] A less polar environment will cause a shift of the fluorescence spectrum of ANS toward lower wavelengths (blue shift) and a significant increase in the fluorescence quantum yield.[246] Thus, the changes in ANS fluorescence in different peptide solutions (Figure 6.3b) can be related to the hydrophobicity of the local environment where ANS resides. This leads to a conclusion that EFK16-II provides a more hydrophobic environment for ANS than the other two peptides. These results also suggest that EFK16-II may have different impacts on the complexation with the hydrophobic anticancer agent ellipticine, compared with EAK16-II and EAK16-IV.

It is worth noting that the hydrophobicity determined by the two methods may correspond to two different situations. Surface tension is a property based on the molecular adsorption at the air-solution interface, affecting the surface free energy. Usually, the adsorption process favors small molecules due to their fast diffusion from bulk to the interface. Thus, in self-assembling peptide systems, the surface tension may reflect predominantly the properties of peptide monomers and small peptide assemblies, rather than those of the large peptide aggregates. On the other hand, ANS fluorescence depends predominantly on the local probe environment. The binding of ANS to peptide monomers may not significantly affect its fluorescence properties as it still “feels” surrounding

solvent molecules (i.e., water in this case). Only when the ANS probe is enclosed in a different environment from the solvent does its fluorescence greatly change. Therefore, the observed changes in ANS fluorescence in Figure 6.3b should result from the properties of peptide assemblies/aggregates. This is probably why the difference in surface tension measurements in EAK16-II and EAK16-IV solutions is not observed in the case of ANS fluorescence measurements.

6.3.2 Sequence Effect on the Complex Formation

Since the different peptide sequences affect the peptide assemblies and their properties, they should further influence the formation of peptide-ellipticine complexes. The results are shown in Figure 6.4. The differences among the complexes made of the three peptides can be directly visualized from the appearance of the suspensions (Figure 6.4a). For EAK16-II, the peptide-ellipticine solutions appear to be slightly turbid at peptide concentrations of 0.2 and 0.04 mg/mL, indicating the formation of large colloidal suspensions. However, at a concentration of 0.5 mg/mL, the solution becomes clearer with a light yellow color (far left vial). Similar appearances of the peptide-ellipticine solutions are found for EAK16-IV (central three vials) except that the solution looks less yellow at a peptide concentration of 0.5 mg/mL. For EFK16-II, all solutions appear cloudy. Compared with the control sample (with the absence of peptides, far right vial) that remains colorless and transparent, the changes in the solution appearance of the peptide-ellipticine samples reveal that ellipticine has been uptaken by the peptides and stabilized in solution.

The different appearances of the solutions may indicate different molecular states of ellipticine in the complexes. Recent studies on the complexation of EAK16-II with ellipticine have demonstrated that two molecular states of ellipticine, either protonated or crystalline, can be obtained in the complexes depending on the peptide and ellipticine concentrations (Chapter 4). The protonation of ellipticine usually occurs at a higher peptide concentration, related to a relatively low solution pH

(< 5, pKa of ellipticine is ~6);[73] protonated ellipticine can be stabilized by ionic interaction with the negatively charged residues (glutamic acid E in this case) of the peptide. The ellipticine microcrystals are stabilized by peptide assemblies coating on the surface (Chapter 4).[56] When ellipticine is protonated, it can dissolve in aqueous solution and cause the solution to have a yellow, transparent appearance. On the other hand, the suspended ellipticine microcrystals make the solution turbid and cloudy. Thus, by looking at the appearance of the samples, one can possibly predict that EAK16-II and EAK16-IV can stabilize protonated or crystalline ellipticine while ellipticine stabilized by EFK16-II may be predominantly in microcrystal form.

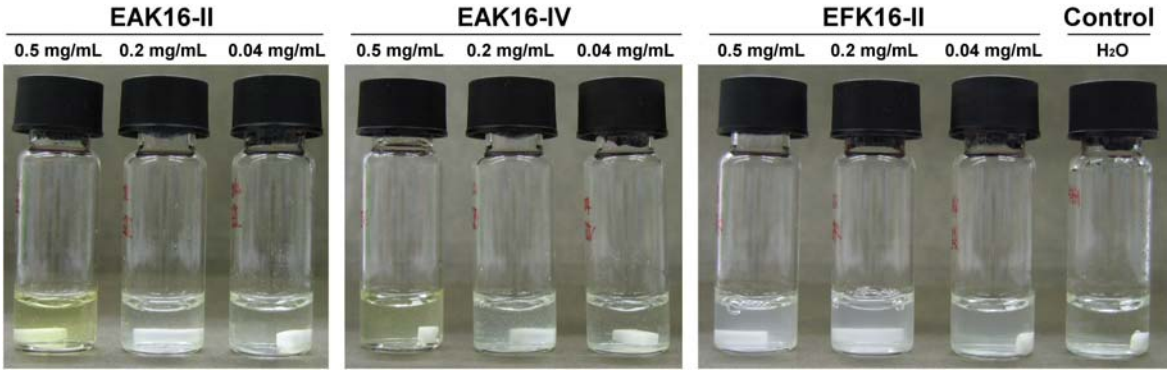

(a)

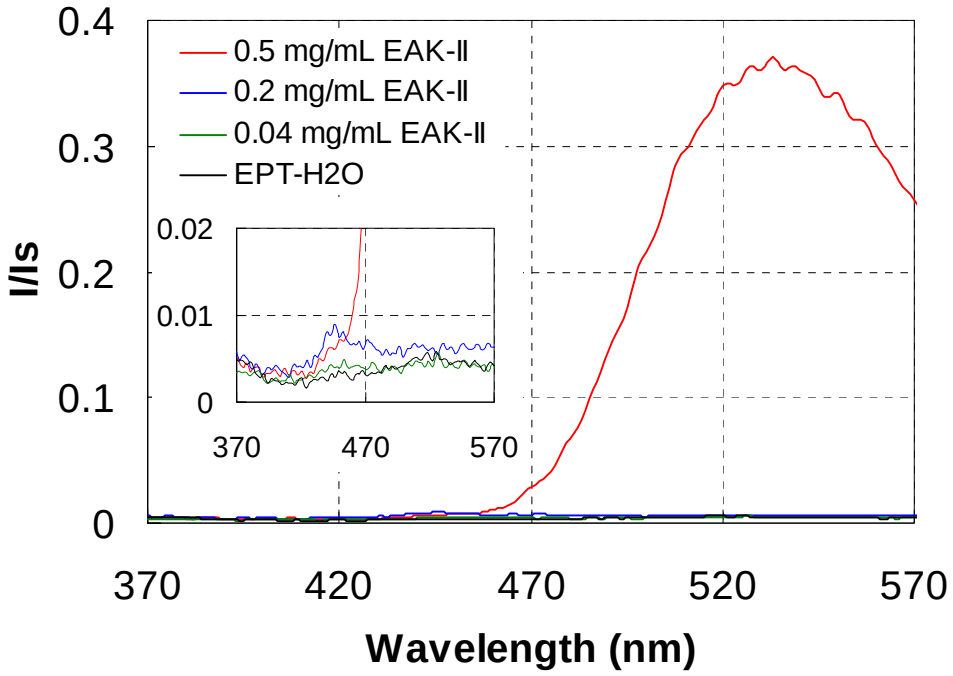
0.5 mg/mL EAK-Ⅱ
0.2 mg/mL EAK-Ⅱ
0.04 mg/mL EAK-Ⅱ
EPT-H2O
I/Is
Wavelength (nm)
0.4
0.3
0.2
0.1
0
370
420
470
520
570
0.02
0.01
0
370
470
570

(b)

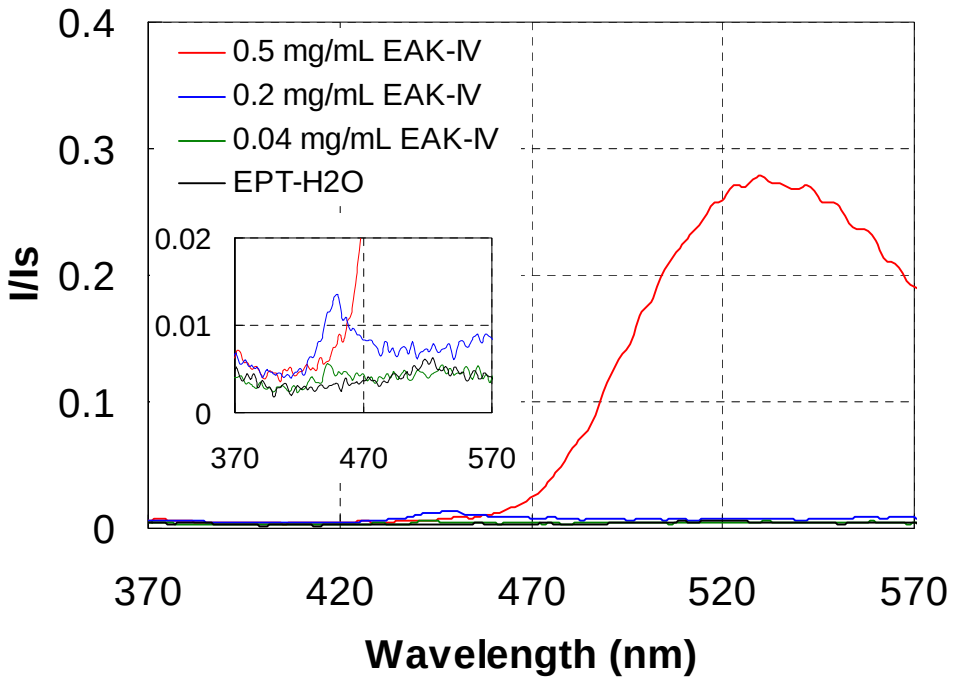
0.5 mg/mL EAK-Ⅳ
0.2 mg/mL EAK-Ⅳ
0.04 mg/mL EAK-Ⅳ
EPT-H2O
I/Is
Wavelength (nm)
0.4
0.3
0.2
0.1
0
370
420
470
520
570
0.02
0.01
0
370
470
570

(c)

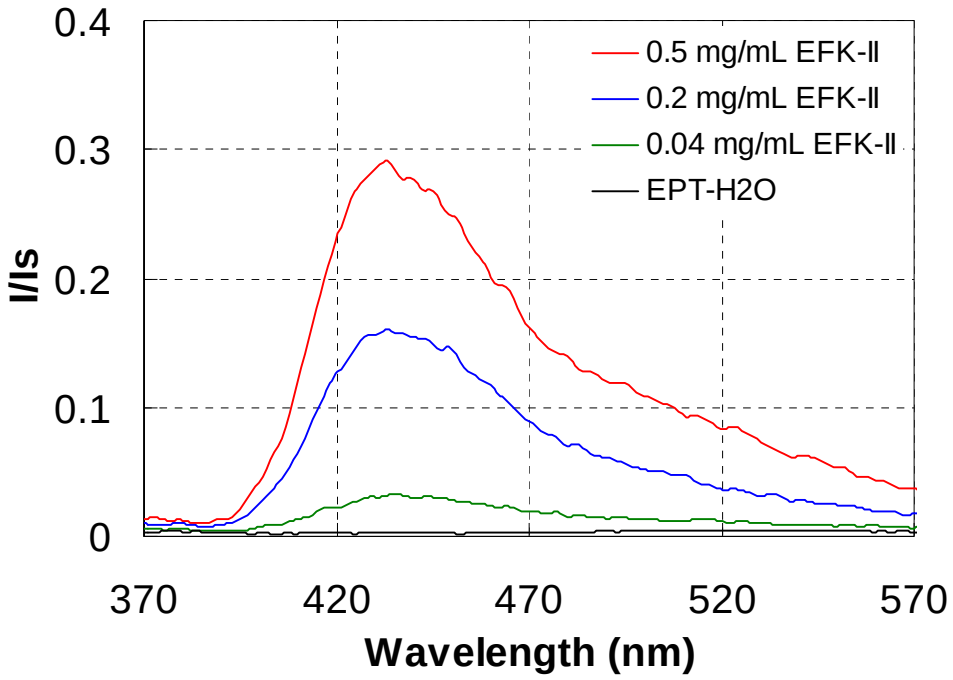

(d)

Figure 6.4 The formation of peptide-ellipticine complexes. (a) Photographs of the complexes with the three peptides at different peptide concentrations and the ellipticine in pure water as a control. The normalized fluorescence spectra of ellipticine in the complexes with EAK16-II (b), EAK16-IV (c) and EFK16-II (d). The insets show the spectra of the complexes with low peptide concentrations. The ellipticine concentration was fixed at 0.04 mg/mL (0.16 mM).

The molecular state of ellipticine can be further elucidated by the ellipticine fluorescence spectra. It has been found that protonated ellipticine molecules have a fluorescence peak at ~520 nm while the fluorescence peak at ~430 nm is attributed to neutral ellipticine molecules (Chapter 3); crystalline ellipticine exhibits a fluorescence peak at ~470 nm with an extremely low intensity.[56] The fluorescence spectra of the complexes with the three peptides, EAK16-II, EAK16-IV and EFK16-II, are shown in Figure 6.4b, c and d, respectively. For EAK16-II and EAK16-IV, the complexes with

0.5 mg/mL peptide have a fluorescence peak located ~520 nm, indicating that ellipticine is protonated. At peptide concentrations below 0.5 mg/mL, the spectra have a peak close to 470 nm with an extremely low intensity (insets in Figure 6.4b and c), representing crystalline ellipticine. Interestingly, the complexes with EFK16-II exhibit a fluorescence spectrum with a major peak located at ~435 nm and a small shoulder covering the wavelengths from 470 to 570 nm (Figure 6.4d), very different from those of protonated and crystalline ellipticine. The peak located at ~435 nm represents neutral (non-charged) ellipticine, present as individual molecules in a much less polar environment (Chapter 3). The peak intensity is proportional to the EFK16-II concentration. These results indicate that EFK16-II can stabilize neutral, molecular ellipticine in aqueous solution; in contrast, the other two molecular states of ellipticine, protonated and crystalline, can be formed in the complexes with EAK16-II and EAK16-IV. EFK16-II assemblies provide a more hydrophobic environment than those of EAK16-II and EAK16-IV as shown in Figure 6.3b, possibly facilitating the stabilization of neutral ellipticine molecules. Note that in addition to neutral ellipticine, crystalline and protonated ellipticine can coexist in the suspensions as indicated by the turbid appearance of the suspensions and a shoulder from the fluorescence spectra. The fluorescence signals from crystalline ellipticine, however, are too small to be seen compared to those of neutral ellipticine. The different quantum yields and overlapping of the fluorescence signals from the three molecular states of ellipticine make it difficult to determine the percentage of each state among the three in the complexes. However, the total amount of stabilized ellipticine can be obtained.

To determine how much ellipticine can be stabilized in solution by the peptides, aliquots of the peptide-ellipticine suspensions were diluted in DMSO, and the UV absorption of ellipticine was collected in the resulting mixture. The ellipticine absorbance was then converted to corresponding ellipticine concentration in the suspensions. This concentration was compared with the given ellipticine concentration (0.04 mg/mL) to obtain the maximum suspension (%) as shown in Figure

6.5. Initially in the preparation, ellipticine is in solid form as a thin film at the bottom of the vial. With the help of the peptides and mechanical stirring over time, ellipticine can be uptaken and stabilized in the solution as protonated, neutral or crystalline ellipticine. Not all given ellipticine can be stabilized and suspended in solution; the deposition of ellipticine thin film can still be observed at the bottom of most sample vials. The amount of stabilized ellipticine varies with peptide type and concentration. The maximum amount of ellipticine in suspension is found to be ~71% (by wt.) at 0.5 mg/mL EAK16-II. At the same peptide concentration, such a value decreases to ~56% for EAK16-IV and to ~46% for EFK16-II. The lowest maximum suspension appears to be ~13% by 0.04 mg/mL EAK16-IV, which is 3 fold higher than the control (~4.5%) with the absence of peptides. The amount of ellipticine suspended by the peptide in water is found to be much higher than the reported solubility in water (~0.6 μM)[71]. With the peptide concentration, the maximum suspension varies largely for EAK16-II and EAK16-IV but less so for EFK16-II. Overall, EAK16-II appears to be the most effective peptide among the three at stabilizing protonated ellipticine (at a high peptide concentration of 0.5 mg/mL); EFK16-II, on the other hand, can stabilize neutral ellipticine (in addition to crystalline and protonated ellipticine), and it has less variation in the maximum suspension with different peptide concentrations.

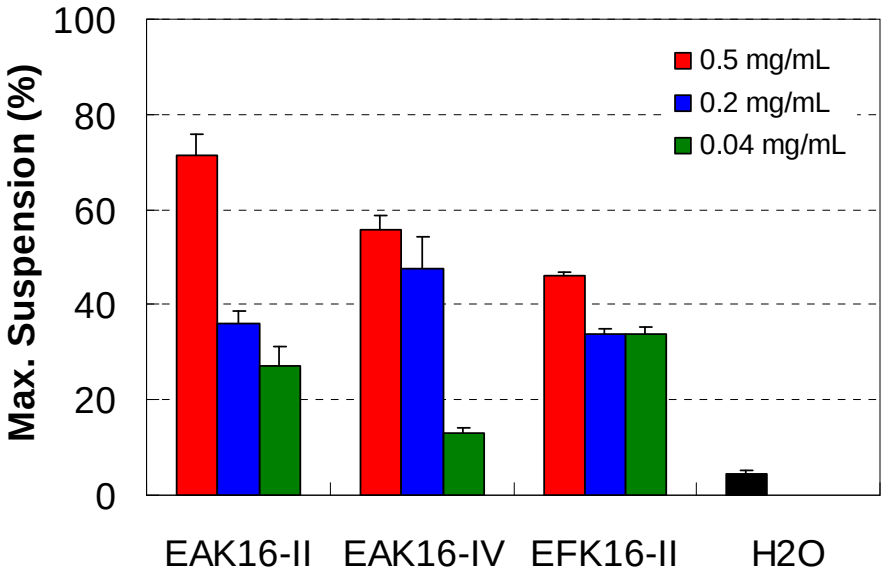

Figure 6.5 The maximum suspension (%) of ellipticine in aqueous solution stabilized by the three peptides and with the absence of peptides. 0.04 mg/mL (0.16 mM) of ellipticine was used in the sample preparation.

6.3.3 Size of the Complexes

The size distribution of the peptide assemblies and complexes at a peptide concentration of 0.5 mg/mL is shown in Figure 6.6. For all three peptides, the peptide assemblies have a broad size distribution from 10 to several hundred nanometers (Figure 6.6a). They all have a major size population around 30 nm and a second one corresponding to a shoulder located at ~300 nm, 100 nm and 200 nm for EAK16-II, EAK16-IV and EFK16-II, respectively. The size distribution of EAK16-II obtained here correlates well with our earlier findings, and the two populations represent short peptide nanofibers and fiber clusters.[68] When the peptides interact with ellipticine to form complexes, the size distributions change significantly as shown in Figure 6.6b. Note that only the size distributions of the complexes with EAK16-II and EAK16-IV are shown in the plot because the size of the complexes

with EFK16-II is very polydispersed, and goes beyond the detection limit of the instrument. The EAK16-II-ellipticine complexes have a relatively wider size distribution than EAK16-IV-ellipticine complexes; two size populations with one centered at about 90 nm and the other at about 500 nm can be found in both distributions.

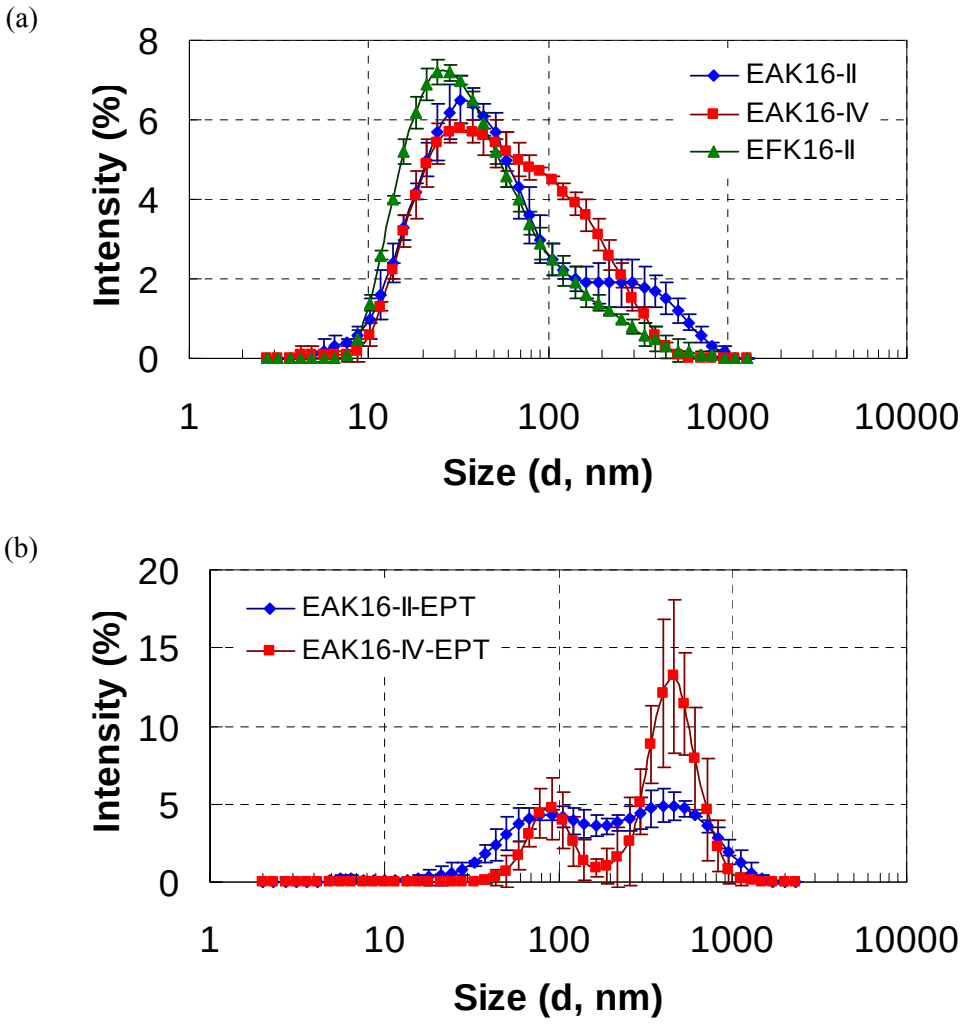

Figure 6.6 The size distribution of the three peptides at 0.5 mg/mL (0.3 mM) in pure water (a) and the complexes with 0.5 mg/mL EAK16-II and EAK16-IV (b) by DLS. EPT: ellipticine (0.04 mg/mL, 0.16 mM).

SEM imaging was applied as a complementary method to examine the size and morphology of the complexes for the three peptides at different peptide concentrations. The representative images are shown in Figure 6.7. It is clearly seen that the dimensions of the complexes with 0.5 mg/mL EAK16-II and EAK16-IV are in the range of ~100-200 nm. For these two peptides, at peptide concentrations below 0.5 mg/mL, the size of the complexes can be as large as several micrometers. These complexes tend to have a rod-like or fiber-like structure, aggregating into bundles or entanglements. Such structures are very different from ellipticine crystals suspended in water (control).

For EFK16-II, the dimensions of the complexes range from hundreds of nanometers to several micrometers regardless of the peptide concentrations. However, the morphology of these complexes looks different according to the peptide concentration. At 0.04 mg/mL, the majority of the complexes are also rod-like although they seem to be shorter and more dispersed than those with EAK16-II and EAK16-IV; at higher peptide concentrations, the complexes appear to have irregular shapes. In addition, more membrane-like structures are observed in the background with the increase in EFK16-II concentration. These membrane-like EFK16-II assemblies could play an important role in stabilizing neutral ellipticine molecules. This may explain the increase in the fluorescence intensity of neutral ellipticine as a function of EFK16-II concentration shown in Figure 6.4d. Meanwhile, the ellipticine microcrystals could be stabilized by the amphiphilic EFK16-II monomers and small assemblies via forming peptide coatings on the surface of the crystals, leading to the formation of cloudy suspensions at all peptide concentrations.

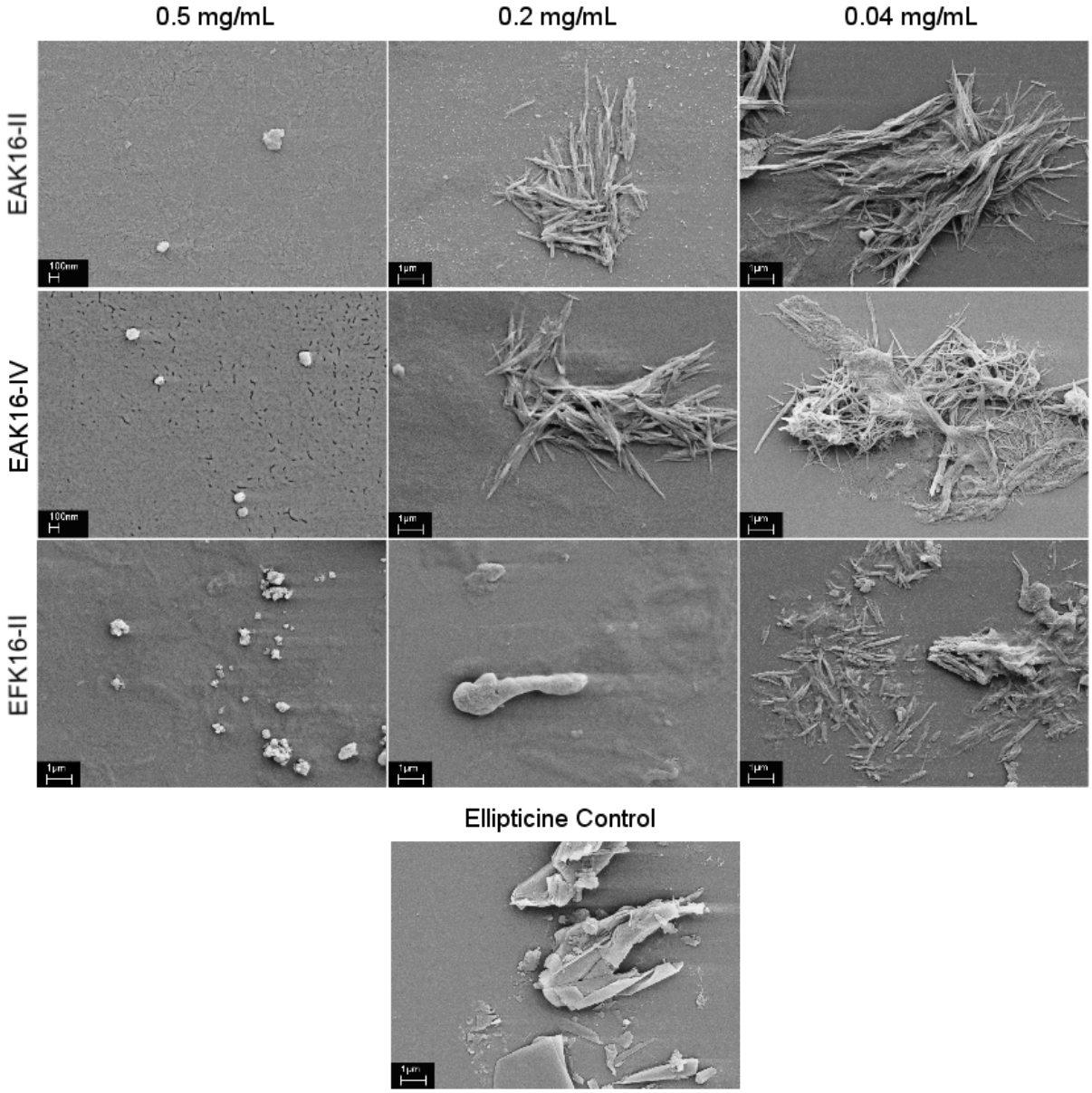

Figure 6.7 SEM images of the complexes with the three peptides at different peptide concentrations and ellipticine crystals in pure water as the control. 0.04 mg/mL (0.16 mM) ellipticine was used for sample preparation.

6.3.4 Cellular Toxicity of the Complexes and Their Dilutions

From the characterization of the complexes above, it can be summarized that peptide sequence will affect the molecular state of ellipticine in the peptide-ellipticine complexes/assemblies. EAK16-II and EAK16-IV can solubilize protonated ellipticine or encapsulate ellipticine microcrystals, depending on the peptide concentration. EFK16-II, on the other hand, can stabilize neutral ellipticine molecules in addition to the other two states in aqueous solution; the amount of neutral ellipticine that can be carried by EFK16-II assemblies is peptide concentration dependent. The size and structure of the complexes also depend on the type of peptide and peptide concentration. To gain more insight concerning these differences in the molecular state of ellipticine as well as the size and structure of the complexes, we investigated their cellular toxicity against two cancer cell lines and the stability of the complexes upon dilution in water. The information regarding the complex stability after dilution would be useful for later animal studies and preclinical experiments.

Figure 6.8 shows the viability of both A549 and MCF-7 cancer cells upon being treated with peptide-ellipticine complexes for 48 h. For A549 cells (Figure 6.8a), all peptide-ellipticine complexes reduce the cell viability to less than 0.3 compared with the viability of non-treated cells (viability is 1). The toxicity of complexes is 2-fold higher than that of the ellipticine control with the absence of peptides (light green bar). The peptide controls exhibit some toxicity to the cells, causing the decrease of viability to the values between 0.6 and 0.8. The much lower cell viability resulted from the peptide-ellipticine complexes compared with that from the ellipticine control is probably due to the fact that the peptides can stabilize large amounts of ellipticine in aqueous solution as shown in Figure 6.5. Interestingly, the cells treated with the complexes formulated with 0.5 mg/mL EAK16-II and EAK16-IV have almost zero viability. This may indicate that protonated ellipticine is more effective at killing A549 cells than other forms of ellipticine in the complexes. Such a result seems to

contradict to the already known fact that neutral ellipticine is the active form to suppress the cancer cell growth.[73]

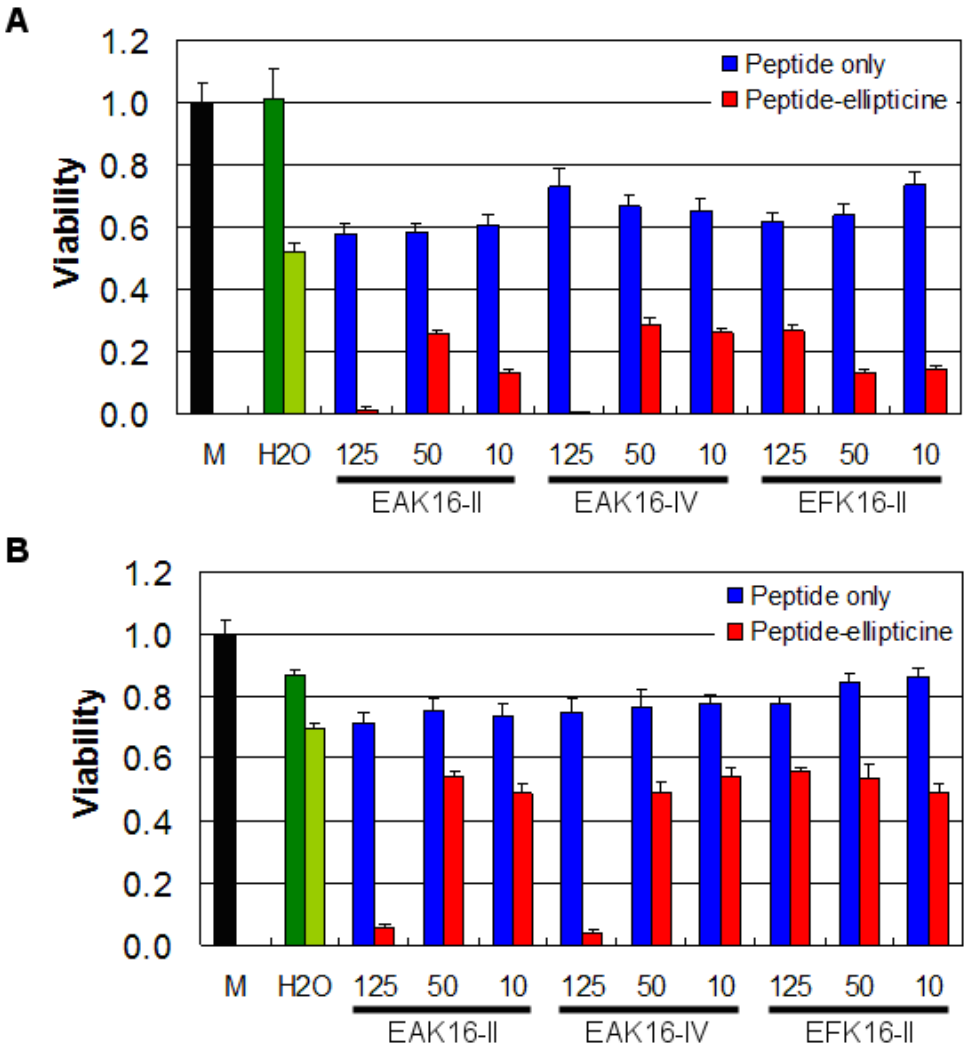

Figure 6.8 Cellular toxicity of the peptides and their complexes with ellipticine for A549 cells (a) and MCF-7 cells (b). The viability of non-treated cells is 1 (M: cells were treated with culture medium). For the solvent control, cells were treated with pure water (dark green bar); for the drug control, cells were treated with ellipticine in pure water (light green bar). The numbers represent different final peptide concentration in μg/mL. The final ellipticine concentration is 10 μg/mL.

The high efficacy of protonated ellipticine against cancer cells may be explained in the following. First, the protonated ellipticine has a positive charge, which can interact with a negatively charged cell membrane surface, leading to accumulation of ellipticine at the cell membrane surface. In addition, such a small hydrophobic molecule is expected to cross the cell membrane easily into the cytoplasm. Second, the protonated ellipticine molecules release much faster from the complexes compared with that from ellipticine microcrystals, due to the differences in complex size and a relatively weak interaction between protonated ellipticine and the peptide in the complexes (Chapter 4). This accelerates the diffusion speed of ellipticine from the complexes to the cells, facilitating a fast cellular uptake of ellipticine. Third, although EFK16-II is capable of stabilizing neutral ellipticine molecules, the amount of stabilized molecules are probably low; the release rate may be slow due to the likely stronger hydrophobic interaction between neutral ellipticine and EFK16-II in the complexes. This is probably why the complex prepared with 0.5 mg/mL EFK16-II has much less effect on the cellular toxicity than protonated ellipticine stabilized by EAK16-II and EAK16-IV at the same peptide concentration.

For MCF-7 cells, the efficacy of protonated ellipticine on anti-proliferation of the cells becomes more significant when compared with the other forms of ellipticine (Figure 6.8b). The lowest cell viability for the complexes with neutral ellipticine and/or ellipticine crystals is around 0.5, which is about 70% of the viability for the ellipticine control (~0.7). This percentage can be as low as ~25% in the case of A549 cells. Such a difference may imply that the peptide-ellipticine suspensions act less effectively on MCF-7 cells than on A549 cells. However, the complexes with protonated ellipticine have similar efficacy at killing both cells, although the reason behind is still unclear. It could be related to the different sensitivity, internalization pathway and/or cell defense mechanism of the two cells in response to ellipticine. Nevertheless, these results provide evidence that the molecular state of ellipticine in the complexes significantly affects their cellular toxicity. Accordingly, one

should be aware that selection of an appropriate formulation method is important in treating different cancer cells.

Figure 6.9 shows the toxicity of the complexes with 0.5 mg/mL EAK16-II, EAK16-IV and EFK16-II upon serial dilution in water against both cell lines. The ellipticine control is diluted the same way for comparison. It is clearly seen that dilution has a significant effect on the toxicity of the complexes with EAK16-II and EAK16-IV, where ellipticine is stabilized in protonated form. For A549 cells (Figure 6.9a), the cell viability is very low and less than 0.05 in the presence of these complexes before dilution; it increases largely to above 0.6 for 16-fold dilution of the complexes. A similar trend is found for MCF-7 cells as the viability increases from less than 0.05 to above 0.7 (Figure 6.9b). Such changes imply that the complexes may not be stable, altering the protonated form of ellipticine after dilution in water. This instability of complexes is probably due to the rise in solution pH, leading to the deprotonation of ellipticine and the formation of ellipticine microcrystals after dilution. This may explain why a sudden increase in cell viability occurs upon 2-time dilution for MCF-7 cells as they seem to be more sensitive to protonated ellipticine than ellipticine microcrystals.

The EFK16-II-ellipticine complexes, on the other hand, exhibit good stability upon dilution in water. The viability increases from ~0.25 to ~0.5 for A549 cells; for MCF-7 cells, it remains unchanged at ~0.57 up to 4-time dilution and then slightly increases to ~0.65 for 16-time dilution. Such a good stability may result from a stronger interaction between EFK16-II and ellipticine in the complexes due to a higher hydrophobicity of the peptide. In addition, a possible increase in solution pH after dilution should not affect the state of the stabilized neutral ellipticine molecules or ellipticine microcrystals. It is worth noting that although these complexes are not as effective as protonated ellipticine at killing cancer cells, their stability is much better, which is especially important for

practical applications in clinics where drug dilution always occurs after administration into the bloodstream.

(a)

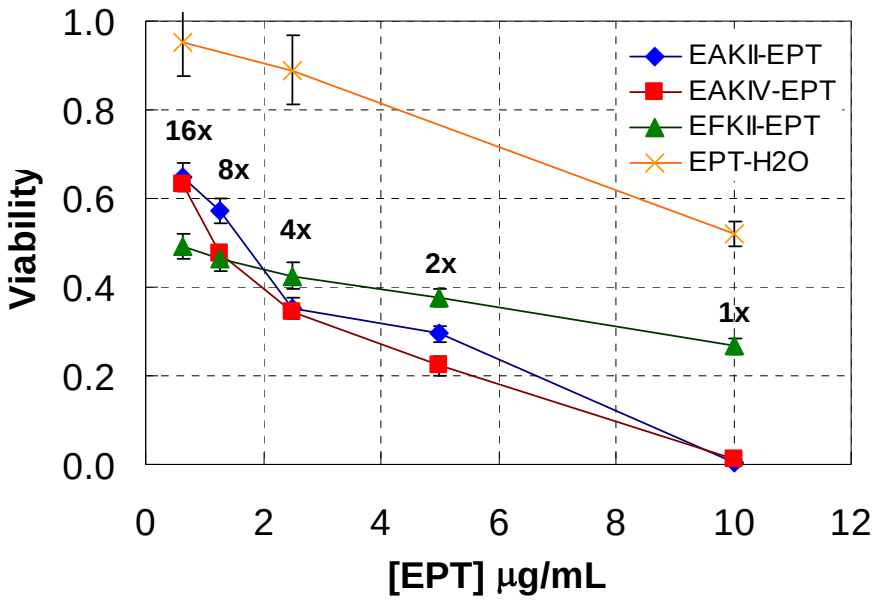

(b)

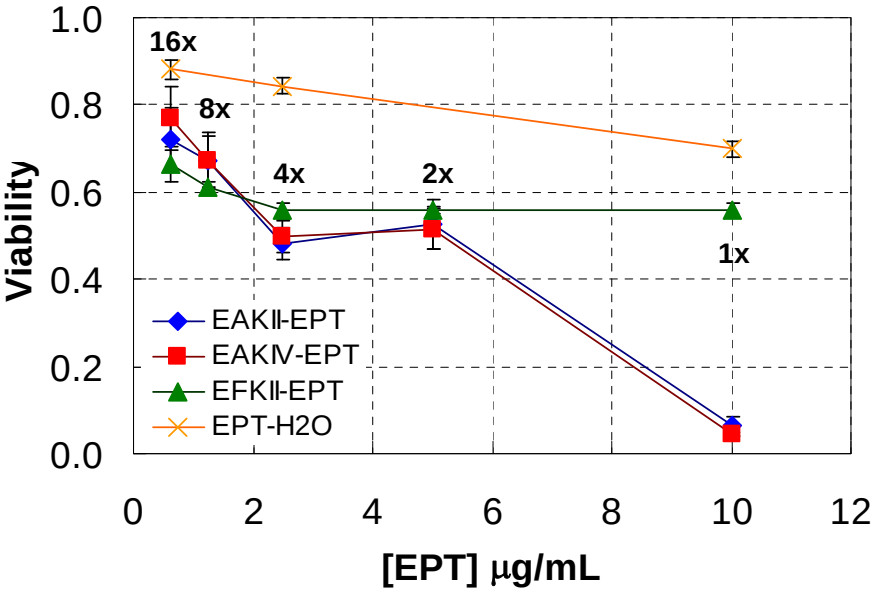

Figure 6.9 Cellular toxicity of the complexes formulated with the three peptides at a peptide concentration of 0.5 mg/mL (0.3 mM) and their serial dilutions in water for A549 cells (a) and MCF-7 cells (b). EPT: ellipticine.

Overall, this study has demonstrated the effect of peptide sequence on its ability to stabilize hydrophobic ellipticine in protonated, neutral as well as crystalline forms in aqueous solution. The difference in charge distribution (type II vs. type IV) on the peptide sequence seems not to have much effect on the complex formation and the molecular state of ellipticine in the complexes. The size, anticancer activity and stability of the complexes are very similar, although the charge distribution does affect, to some degree, the peptide assemblies: nanofibers vs. globular aggregates. It may be because the complexation of ellipticine with EAK16-II and EAK16-IV is mainly based on the peptide monomers but not on the peptide assemblies. The increase in hydrophobicity of the peptide by replacing alanine (A) with phenylalanine (F), however, significantly alters the molecular state of ellipticine in the complexes, the complex stability and its therapeutic effect due to the following reasons: (i) the EFK16-II assemblies provide a more hydrophobic, enclosed environment where neutral ellipticine molecules can be solubilized; (ii) a stronger hydrophobic interaction between ellipticine and EFK16-II may further enhance the stability of the complexes upon dilution.

Different peptide sequences have different advantages in formulating the ellipticine drug. For example, 0.5 mg/mL EAK16-II (or EAK16-IV) can solubilize protonated ellipticine in nanoscale complexes with high anticancer activity against both A549 and MCF-7 cells, but these complexes are pH sensitive and not very stable after dilution. In contrast, the complexes formulated with 0.5 mg/mL EFK16-II are more stable upon dilution, but most of their sizes are in the micrometer range and their anticancer activity is relatively low. Nevertheless, these results provide essential information to design an appropriate peptide sequence that would optimize the delivery of hydrophobic anticancer drugs. One could utilize the advantages of different molecular states of ellipticine to improve the delivery efficacy, through a proper peptide design to form a stable, peptide nanocarriers, which can encapsulate neutral or crystalline ellipticine; if such a carrier enters cells through endocytosis, the

encapsulated ellipticine becomes protonated at low pH in the lysosomes, and the protonated ellipticine can be released and cross the lysosome membrane into cytoplasm.

6.4 Conclusions

Three ionic-complementary self-assembling peptides, EAK16-II, EAK16-IV and EFK16-II, with different charge distributions and hydrophobicities were found to be able to stabilize the hydrophobic anticancer agent ellipticine in aqueous solution. Ellipticine was stabilized in the form of microcrystals, protonated and neutral molecules depending on the peptide sequence and the peptide concentration. 0.5 mg/mL EAK16-II and EAK16-IV stabilized protonated ellipticine to form nano-complexes while crystalline ellipticine was obtained in the complexes with these peptides at lower peptide concentrations. On the other hand, EFK16-II was able to stabilize both neutral and crystalline ellipticine within the range of tested peptide concentrations; the amount of neutral ellipticine that can be stabilized was proportional to the peptide concentration. The different molecular states of stabilized ellipticine in the complexes greatly affected the anticancer activity of the complexes and their stability upon dilution in water. The complexes with protonated ellipticine were found to be very effective at killing both A549 and MCF-7 cells with a cell viability close to zero; however, these complexes were not very stable and their anticancer activity reduced significantly after serial dilution in water. The complexes formulated with EFK16-II (containing neutral ellipticine and ellipticine microcrystals), on the contrary, appeared to be stable after serial dilution, although their original anticancer activity was relatively low. These results showed that the differences in charge distribution of the peptides did not have much effect on the complex formation and their cellular toxicity, whereas the increase in peptide hydrophobicity could strengthen the interaction between the peptide and ellipticine, which gives the stability of their complexes upon dilution. This study provides necessary

information on peptide sequence design to construct functional peptide carriers for hydrophobic anticancer drug delivery.

Chapter 7
Original Contributions and Recommendations

7.1 Original Contributions to Research:

This thesis presented the potential of self-assembling peptides as carriers for hydrophobic drug delivery. We explored a special class of self-assembling, ionic-complementary peptides for the delivery of a hydrophobic anticancer agent, ellipticine. The thesis includes the following parts: (i) systematic study the photophysical properties of ellipticine in different solution environments; (ii) characterization of the complex formation of ellipticine with a self-assembling peptide and the release kinetics of ellipticine from the complexes; (iii) investigation of the therapeutic effect of the complexes *in vitro* and the ellipticine uptake into two cancer cell lines; (iv) study of the peptide sequence effect on the complex formation and the *in vitro* delivery for future design of appropriate self-assembling peptide-based delivery vehicles for hydrophobic anticancer drugs. The original contributions to research of each part are summarized in the following sections.

Solvent Effect on Photophysical Properties of Ellipticine. The photophysical properties of the anticancer agent ellipticine were systematically studied in different solution environments, including 16 organic solvents, some of their mixtures and lipid vesicles. The UV absorption and fluorescence emission of ellipticine were found to be solvent/environment dependent. As the solvent polarity increased, ellipticine exhibited a spectral shift to the red (lower energy) for both absorption and emission. The spectral shifts could be correlated with the solvent dielectric constants and the solvent polarity using the Lippert-Mataga equation. The presence of a non-linear trend in the Lippert-Mataga plot indicated the existence of specific solvent effects. Such effects were related to intramolecular charge transfer (ICT) due to the large dipole moment difference between the ground state and the

excited state as well as the hydrogen bonding between the solvent and ellipticine. The formation of stronger hydrogen bonds in alcohols led to larger extinction coefficients and longer lifetimes, although methanol was an exception. In EPC liposome suspensions, ellipticine exhibited an emission band at 436 nm, indicating that ellipticine was located in a rather polar environment, close to the hydrophilic surface of the liposomes rather than buried in the hydrophobic interior of the lipid bilayers. This study not only provides detailed information on the photophysical properties of ellipticine in various environments, but also suggests that the dependence of the spectral shift of ellipticine with its local environment can be a good indicator of where ellipticine is located in a heterogeneous medium like EPC liposomes or cultured cells.

Complexation and Release of Ellipticine with EAK16-II. A model self-assembling, ionic-complementary peptide, EAK16-II, was found to be able to stabilize the hydrophobic anticancer agent ellipticine in aqueous solution. Both crystalline and protonated forms of ellipticine can be obtained in the EAK16-II-ellipticine complexes. The complex formation in water is peptide concentration-dependent. When the peptide concentration was close to its critical aggregation concentration (~0.1 mg/mL), the equilibration time for complex formation could be as short as 5 h. At higher and lower peptide concentrations, the time required to reach equilibrium became much longer. High peptide concentrations (> 0.1 mg/mL) facilitated the formation of protonated ellipticine during the complexation while low peptide concentrations favored crystalline ellipticine formation. With a combination of 0.1 mg/mL ellipticine and 0.5 mg/mL EAK16-II, protonated ellipticine could be stabilized at equilibrium.

The transfer rate of ellipticine from the complexes into EPC liposomes (cell membrane mimics) was dependent on the peptide concentration used during formulation. A higher peptide concentration resulted in a faster release rate, related to the fact that higher peptide concentrations favor the protonation of ellipticine and the formation of smaller complexes. In addition, the size of the

EAK16-II-ellipticine complexes could be tuned by adjusting the peptide-to-ellipticine ratio (by mass) during formulation. This study demonstrates the capability of self-assembling, ionic-complementary peptides as carriers for hydrophobic anticancer drug delivery.

***In Vitro* Delivery of EAK16-II-Ellipticine Complexes.** EAK16-II was able to stabilize protonated or crystalline ellipticine in aqueous solution depending on the peptide-to-ellipticine ratio (by mass). At an ellipticine concentration of 0.1 mg/mL, the stabilized ellipticine was protonated at and above the ratio of 5:1; below this ratio, ellipticine was mostly in crystalline form in the complexes. These two molecular states of ellipticine in the complexes exhibited different toxicity against two cancer cell lines, A549 and MCF-7, with protonated ellipticine being more toxic. Such an effect became more pronounced for MCF-7 cells than for A549 cells. The time-dependent toxicity showed that the complexes with protonated ellipticine reduced the cell viability of MCF-7 cells to ~50% at 4 h, whereas 12 h treatment was required in order to achieve the same effect for A549 cells. This may be due to that MCF-7 cells were more sensitive to protonated ellipticine. Although the complexes with protonated ellipticine showed high toxicity to both cancer cells, they were not stable upon dilution in water.

The uptake of ellipticine in both cell lines appeared to follow a diffusion mechanism. It was found that both cancer cells exhibited strong ellipticine fluorescence at 4 °C, indicating the uptake is energy-independent (i.e., not through endocytosis). The complexation of ellipticine with EAK16-II seemed not to alter the internalization pathway of ellipticine. However, it significantly enhanced the uptake over a shorter time period (~5 min). These results demonstrate that the EAK16-II-ellipticine complexes with protonated ellipticine are effective at killing cancer cells *in vitro*; the existence of some unfavorable properties of the complexes, such as unspecific cellular uptake, suggests that an appropriate design of peptide sequence is critical for future development of self-assembling peptide carriers.

Peptide Sequence Effect on the Complexation and *In Vitro* Delivery of Ellipticine. Three self-assembling ionic-complementary peptides, EAK16-II, EAK16-IV and EFK16-II (with different charge distributions and hydrophobicities), were found to be able to stabilize ellipticine in aqueous solution in the form of crystalline, protonated and/or neutral molecules, depending on the peptide sequence and the peptide concentration. 0.5 mg/mL EAK16-II and EAK16-IV stabilized protonated ellipticine to form nano-complexes while crystalline ellipticine was stabilized at lower peptide concentrations. On the other hand, EFK16-II was able to stabilize mainly neutral ellipticine molecules and ellipticine microcrystals; the amount of neutral ellipticine that can be stabilized was proportional to the peptide concentration.

The different molecular states of stabilized ellipticine in the complexes greatly affected the anticancer activity of the complexes and their stability upon dilution in water. The complexes with protonated ellipticine were found to be effective at killing both A549 and MCF-7 cells (with a cell viability close to zero); however, these complexes were not very stable and their anticancer activity reduced significantly after serial dilution in water. The complexes formulated with EFK16-II (containing neutral ellipticine and ellipticine microcrystals), on the contrary, appeared to be stable after serial dilution, although their original anticancer activity was relatively low.

These results showed that the differences in charge distribution of the peptides did not have much effect on the complex formation and their cellular toxicity, whereas the increase in peptide hydrophobicity could strengthen the interaction between the peptide and ellipticine, leading to a high stability of their complexes upon dilution. Although the three peptides had different nanostructures owing to the peptide propensity, the difference in nanostructures may not be a necessary factor affecting the complexation and cellular delivery of ellipticine. This study provides useful information on peptide sequence design for constructing peptide-based carriers for hydrophobic anticancer drug delivery.

7.2 Recommendations

Recommended future work to develop self-assembling peptide-based nanocarriers for hydrophobic anticancer drug delivery can be divided into three major parts: (a) optimization of the peptide-drug formulation; (b) enhancement of the delivery efficacy; (c) evaluation of the complexes *in vivo*. The details in each part are listed in the following:

Optimize the peptide-drug formulation:

1. An appropriate peptide design is required to form the complexes with high stability, high loading efficiency, controllable release, desired dimension and good biocompatibility. A peptide library has been constructed with rational design as shown in Table A1. One should find an optimal condition to perform high throughput screening on these peptides; hopefully, several candidate sequences can be identified. New peptide library may be built based on the peptide candidates.

2. Current work has developed a method to approximately estimate the maximum suspension concentration of the drugs. However, this concentration does not represent the drug loading capacity, which is an important factor determining the drug density in delivery systems so that the drug dosage forms and scheduling can be accommodated according to chemotherapy requirements. Quite often, large drug doses are required in cancer treatment in order to reduce the number of drug administrations and suppress the drug resistance. A new method should be developed to quantify the amount of peptides as well as the drugs in the complexes, to determine the amount of the drug loaded (encapsulated) in the peptide carrier and obtain the drug-to-peptide ratio. Ultracentrifugation and filtration may be suitable for this purpose.

3. Complete stability studies should be carried out. Once the peptide-anticancer drug complexes are formed, it is necessary to ascertain that such peptide-drug formulation can tolerate various physiological conditions during delivery. In addition to dilution stability, the complexes

should be tested for their stability for long storage (i.e., shelf-life), and in the presence of serum and degradation enzymes, including pepsin, trypsin, chymotrypsin, elasterase, carboxypeptidase and aminopeptidases.

4. The peptide-drug complexes circulating in the bloodstream must avoid significant complement activation, which is the primary cause of immune response. Thus, the complement-activating properties of the peptide nanocarriers should be examined. This can be done using existing methods.[251] Briefly, antibody-sensitized sheep red blood cells are used to monitor the hemolysis following the addition of serum. Titration of serum and peptide-drug complexes will allow one to determine the amount of serum that causes lysis of 50% of the erythrocytes (CH50). If significant complement activation is observed, the use of D-form amino acids in peptide synthesis or PEG coatings could be considered.

5. Different formulation methods can be explored. The complexes can be prepared in an appropriate buffer solution (should be clinical approved) to achieve physiological pH for administration. Cosolvents or additives can also be introduced to enhance the complex stability and biocompatibility, and to possibly control the complex size.

Enhance the delivery efficacy:

1. An advance in cancer chemotherapy is to achieve active targeted delivery. This can be done by incorporating targeting peptide motifs into self-assembling peptide-based nanocarriers. This project would include the following steps: (i) find appropriate targeting peptide sequences from published literature; (ii) construct self-assembling peptide nanocarriers based on the accumulated knowledge from current work; (iii) incorporate targeting sequences into the nanocarriers; iv) test the targeting principles of the peptide vehicles *in vitro* and *in vivo*; (v) investigate the delivery efficacy of the modified nanocarriers for existing anticancer agents.

2. In addition to active targeting, the passive targeting via EPR could be an alternative to improve the delivery efficacy. This can be achieved by controlling the dimension of the complexes (optimal at ~200 nm) during formulation or through peptide sequence design. Different formulation conditions would help control the complex size. For example, cosolvents or clinically approved additives can be introduced during formulation. In addition, fundamental studies on peptide self-assembly should provide important information for proper peptide design.

3. Detailed cell biology studies on the fate of the complexes should be characterized. For instance, the cellular uptake mechanism is important for the design of effective delivery system. In addition, identify the apoptotic pathway could provide a tool for *in vivo* studies.

Evaluate therapeutic effect of the complex in vivo:

1. Once a promising peptide-drug complex is identified, it should be tested *in vivo* using appropriate cancer animal models. This can be achieved by seeking collaborators at other universities or research institutes. Currently, we have collaborated with Dr. Mingyao Liu (and his group) at the University of Toronto for pilot animal studies on the EAK16-II-ellipticine complexes. Successful animal studies should rely on the formulation. For example, the formulation should have good dilution stability and biocompatibility, and satisfy the conditions for intravenous (i.v.) injection. In general, the animal studies should include the complex efficacy (e.g., animal survival), biodistribution, pharmacokinetics and pharmacodynamics.

Other studies:

1. Ellipticine is selected as a model hydrophobic anticancer drug to test the delivery principles using self-assembling peptide-based nanocarriers. The system can be applied to other hydrophobic anticancer therapeutics, such as paclitaxel, for which its commercial formulation Cremophor® EL has

several undesirable side effects in clinics.[35,94] Another fluorescent, pH sensitive anticancer drug, camptothecin could also be considered.[157,238]

2. Other imaging techniques such as transmission electron microscopy (TEM) can be applied as a complement tool to SEM and DLS to study the complex dimension and structure.

3. In this study, the formation of peptide-ellipticine complexes was confirmed by mainly fluorescence spectra and solution appearances in comparison with the drug control (no peptides). However, these results provide indirect evidence for complex formation, and other approaches should be considered to observe the complexation of ellipticine with the peptide. This may be achieved by labeling the peptide with a fluorophore. The interaction of ellipticine with the peptide can then be monitored by either the fluorescence resonance energy transfer technique or a fluorescence confocal microscopy. These approaches also enable us to investigate the cellular distribution of the peptide vehicles.

4. The "inner filter effect" on the ellipticine fluorescence at higher ellipticine concentrations should be characterized further. One could construct a calibration curve of protonated ellipticine in acidic solution to obtain the concentration threshold for the inner filter effect. This may also help quantify the protonated ellipticine stabilized in the complexes.

5. One should consider the effect of free drug on cell culture experiments and *in vivo* studies in the future. An approach should be developed to remove the free drug from the current formulations.

Appendix

A. Peptide Library for Hydrophobic Anticancer Drug Delivery

The designed peptides for hydrophobic anticancer drug delivery are listed in Table A1.

Table A1 Peptide Library for hydrophobic anticancer drug delivery

Design Category	# of Amino Acids	Sequence (n-c)	Charges at pH 7	Charges at pH~4.5
EAK derivatives	16	n-GEGEGKGKGEGEGKGK-c	4+,4-	4+,4-
	16	n-IEIEIKIKIEIEIKIK-c	4+,4-	4+,4-
	8	n-EEKKEEKK-c	4+,4-	4+,4-
Ionic Complementary	16	n-EEIIIIEERRIIIIRR-c	4+,4-	4+,4-
	16	n-AAEEAAEEAAKKAAKK-c	4+,4-	4+,4-
	16	n-AAAAEEEEAAAAKKKK-c	4+,4-	4+,4-
	8	n-LLEELLRR-c	2+,2-	2+,2-
	8	n-FFEEFFRR-c	2+,2-	2+,2-
	8	n-IIEEIIRR-c	2+,2-	2+,2-
	8	n-EEIIIIRR-c	2+,2-	2+,2-
Short Peptides	2	FF		
	3	n-FFR-c	1+	1+
	4	FFFF		
	2	n-YY-c		
	2	YY		
	4	YYYY		
	4	n-YYYQ-c		

	2	FF		
Hydrogen Bonding Complementary	4	n-NFFR-c	1+	1+
	4	n-NFFQ-c		
	8	n-FNFNFRFR-c	2+	2+
	8	n-LNLNLRLR-c	2+	2+
	8	n-VNVNVRVR-c	2+	2+
	8	n-ININIRIR-c	2+	2+
	16	n-ININIRIRININIRIR-c	4+	4+
	16	n-IINRIINRIINRIINR-c	4+	4+
	20	n-WHIHININININIRIRIRIR-c	4+	6+
	8	n-IINNIIRR-c	2+	2+
	8	n-NNIIIIRR-c	2+	2+
	12	n-WNNNIIIIIRRR-c	3+	3+
	18	n-WHIINNIIHHIINNIIRR-c	5+	6+
	20	n-WHHNNNSINISINISINRRR-c	2+	5+
Hydrogen Bonding Complementary	11	n-WRIRIFININW-c	2+	2+
	13	n-WQQQIIIIIRRRH-c	3+	3+
	17	n-NNNISISIWININIRRR-c	3+	3+
Mixed Design	13	n-NIEIINWRIIRIR-c	3+, 1-	3+, 1-
	17	n-NNNNEIIIWIIIRHHHR-c	2+,1-	5+,1-
	21	n-WHHENNININIFISISISIRRRN-c	3+	5+

Note: n- and -c refer to the end protection by acetylation and amidation, respectively.

References

1. Chu, E. and Satorelli, A. C. "Cancer chemotherapy". *in* Basic & Clinical Pharmacology, Edn. 9th. ed. Katzung, B. G. pp. 898-930 (Lange Medical Books/McGraw-Hill, New York; 2004).

2. Karp, G. Cell and Molecular Biology: Concepts and Experiments. (John Wiley & Sons, Inc., New York; 2002).

3. Pratt, W. B., Ruddon, R. W., Ensminger, W. D., and Maybaum, J. The Anticancer Drugs. (Oxford University Press, Inc., New York; 1994).

4. Lupulescu, A. Cancer Cell Metabolism and Cancer Treatment. (Hardwood Academic Publishers, Amsterdam; 2001).

5. Duda, D. G. Antiangiogenesis and drug delivery to tumors: bench to bedside and back. *Cancer Res.* **66**, 3967-3970 (2006).

6. Eckstein, F. "Antisense methodology: an assessment after 25 years". *in* Nucleic Acid Therapeutics in Cancer. ed. Gewirtz, A. M. pp. 3-13 (Humana Press Inc., Totowa, NJ; 2004).

7. Gewirtz, A. M. "Nucleic acid therapeutics: an introduction". *in* Nucleic Acid Therapeutics in Cancer. ed. Gewirtz, A. M. pp. 15-24 (Humana Press Inc., Totowa, NJ; 2004).

8. Abou-Jawde, R., Choueiri, T., Alemany, C., and Mekhail, T. An overview of targeted treatments in cancer. *Clin. Ther.* **25**, 2121-2137 (2003).

9. Dass, C. R. and Choong, P. F. M. Selective gene delivery for cancer therapy using cationic liposomes: in vivo proof of applicability. *J. Control. Release* **113**, 155-163 (2006).

10. Brannon-Peppas, L., Ghosn, B., Roy, K., and Cornetta, K. Encapsulation of nucleic acids and opportunities for cancer treatment. *Pharm. Res.* **24**, 618-627 (2007).

11. Brandwijk, R. J. M. G. E., Griffioen, A. W., and Thijssen, V. L. J. L. Targeted gene-delivery strategies for angiostatic cancer treatment. *Trends Mol. Med.* **13**, 200-209 (2007).

12. Takeshita, F. and Ochiya, T. Therapeutic potential of RNA interference against cancer. *Cancer Sci.* **97**, 689-696 (2006).

13. Wong, H. L., Bendayan, R., Rauth, A. M., Li, Y., and Wu, X. Y. Chemotherapy with anticancer drugs encapsulated in solid lipid nanoparticles. *Adv. Drug Del. Rev.* **59**, 491-504 (2007).

14. Moses, M. A., Brem, H., and Langer, R. Advancing the field of drug delivery: taking aim at cancer. *Cancer Cell* **4**, 337-341 (2003).

15. Gu, F. X., Karnik, R., Wang, A. Z., Alexis, F., Levy-Nissenbaum, E., Hong, S., Langer, R. S., and Farokhzad, O. C. Targeted nanoparticles for cancer therapy. *Nanotoday* **2**, 14-21 (2007).

16. Langer, R. Drug delivery and targeting. *Nature* **392**, 5-10 (1998).

17. Langer, R. Drugs on targets. *Science* **293**, 58-59 (2001).

18. Moghimi, S. M., Hunter, A. C., and Murray, J. C. Long circulating and target-specific nanoparticles: theory to practice. *Pharmacol. Rev.* **53**, 283-318 (2001).

19. Brannon-Peppas, L. and Blanchette, J. O. Nanoparticle and targeted systems for cancer therapy. *Adv. Drug Del. Rev.* **56**, 1649-1659 (2004).

20. Maeda, H., Sawa, T., and Konno, T. Mechanism of tumor-targeted delivery of macromolecular drugs, including the EPR effect in solid tumor and clinical overview of the prototype polymeric drug SMANCS. *J. Control. Release* **74**, 47-61 (2001).

21. Sapra, P. and Allen, T. M. Ligand-targeted liposomal anticancer drugs. *Prog. Lipid Res.* **42**, 439-462 (2003).

22. Medina, O. P., Zhu, Y., and Kairemo, K. Targeted liposomal drug delivery in cancer. *Curr. Pharm. Design* **10**, 2981-2989 (2004).

23. Huh, K. M., Lee, S. C., Cho, Y. W., Lee, J., Jeong, J. H., and Park, K. Hydrotropic polymer micelle system for delivery of paclitaxel. *J. Control. Release* **101**, 59-68 (2005).

24. Kwon, G. S., Naito, M., Kataoka, K., Yokoyama, M., Sakurai, Y., and Okano, T. Block copolymer micelles as vehicles for hydrophobic drugs. *Colloids Surf. B: Biointerfaces* **2**, 429-434 (1994).

25. Torchilin, V. P. Lipid-core micelles for targeted drug delivery. *Curr. Drug Del.* **2**, 319-327 (2005).

26. Torchilin, V. P. "Polymeric micelles as pharmaceutical carriers". *in* Polymers in Drug Delivery. eds. Uchegbu, I. F. and Schatzlein, A. G. pp. 111-130 (CRC Press, Taylor & Francis Group, Boca Raton; 2006).

27. Xu, Z., Gu, W., Huang, J., Sui, H., Zhou, Z., Yang, Y., Yan, Z., and Li, Y. In vitro and in vivo evaluation of actively targetable nanoparticles for paclitaxel delivery. *Int. J. Pharm.* **288**, 361-368 (2005).

28. Hillaireau, H. and Couvreur, P. "Polymeric nanoparticles as drug carriers". *in* Polymers in Drug Delivery. eds. Uchegbu, I. F. and Schatzlein, A. G. pp. 101-110 (CRC Press, Taylor & Francis Group, Boca Raton, FL; 2006).

29. Feng, S.-S., Mu, L., Win, K. Y., and Huang, G. Nanoparticles of biodegradable polymers for clinical administration of paclitaxel. *Curr. Med. Chem.* **11**, 413-424 (2004).

30. Discher, D. E. and Eisenberg, A. Polymer vesicles. *Science* **297**, 967-973 (2002).

31. Uchegbu, I. F., Anderson, S., and Brownlie, A. "Polymeric vesicles". *in* Polymers in Drug Delivery. eds. Uchegbu, I. F. and Schatzlein, A. G. pp. 131-153 (CRC Press, Taylor & Francis Group, Boca Raton, FL; 2006).

32. Stevens, P. J. and Lee, R. J. A folate receptor-targeted emulsion formulation for paclitaxel. *Anticancer Res.* **23**, 4927-4932 (2003).

33. Savic, R., Luo, L., Eisenberg, A., and Maysinger, D. Micellar nanocontainers distribute to defined cytoplasmic organelles. *Science* **300**, 615-618 (2003).

34. Kan, P., Chen, Z. B., Lee, C. J., and Chu, I. M. Development of nonionic surfactant/phospholipid O/W emulsion as a paclitaxel delivery system. *J. Control. Release* **58**, 271-278 (1999).

35. Singla, A. K., Grag, A., and Aggarwal, D. Paclitaxel and its formulations. *Int. J. Pharm.* **235**, 179-192 (2002).

36. Dufes, C., Uchegbu, I. F., and Schatzlein, A. G. "Dendrimers in drug and gene delivery". *in* Polymers in Drug Delivery. eds. Uchegbu, I. F. and Schatzlein, A. G. pp. 199-235 (CRC Press, Taylor & Francis Group, Boca Raton, FL; 2006).

37. Liu, Z., Sun, X., Nakayama-Ratchford, N., and Dai, H. Supramolecular chemistry on water-soluble carbon nanotubes for drug loading and delivery. *ACS Nano* **1**, 50-56 (2007).

38. Sahoo, S. K. and Labhasetwar, V. Nanotech approaches to drug delivery and imaging. *Drug Discov. Today* **8**, 1112-1120 (2003).

39. Moses, M. A., Brem, H., and Langer, R. Novel delivery systems in cancer chemotherapy. *Sci. & Med.* **9**, 264-273 (2003).

40. Fung, S. Y., Keyes, C., Duhamel, J., and Chen, P. Concentration effect on the aggregation of a self-assembling oligopeptide. *Biophys. J.* **85**, 537-548 (2003).

41. Yang, H., Pritzker, M., Fung, S. Y., Sheng, Y., Wang, W., and Chen, P. Anion effect on the nanostructure of a metal ion binding self-assembling peptide. *Langmuir* **22**, 8553-8562 (2006).

42. Haldar, D., Banerjee, A., Drew, M. G. B., Das, A. K., and Banerjee, A. First crystallographic signature of an acyclic peptide nanorod: molecular mechanism of nanorod formation by a self-assembled tetrapeptide. *Chem. Commun.* 1406-1407 (2003).

43. Matsui, H., Gologan, B., and Douberly Jr, G. E. Controlled immobilization of peptide nanotube-templated metallic wires on Au surfaces. *Eur. Phys. J. D* **16**, 403-406 (2001).

44. Santoso, S., Hwang, W., Hartman, H., and Zhang, S. Self-assembly of surfactant-like peptides with variable glycine tails to form nanotubes and nanovesicles. *Nano Lett.* **2**, 687-691 (2002).

45. Hong, Y., Legge, R. L., Zhang, S., and Chen, P. Effect of amino acid sequence and pH on nanofiber formation with self-assembling peptides EAK16-II and EAK16-IV. *Biomacromolecules* **4**, 1433-1442 (2003).

46. Jun, S., Hong, Y., Imamura, H., Ha, B.-Y., Bechhoefer, J., and Chen, P. Self-assembly of the ionic peptide EAK16: the effect of charge distributions on self-assembly. *Biophys. J.* **87**, 1249-1259 (2004).

47. Djalali, R., Chen, Y., and Matsui, H. Au nanocrystal growth on nanotubes controlled by conformations and charges of sequenced peptide templates. *J. Am. Chem. Soc.* **125**, 5873-5879 (2003).

48. Reches, M. and Gazit, E. Casting metal nanowires within discrete self-assembled peptide. *Science* **300**, 625-627 (2003).

49. Moulton, H. M., Hase, M. C., Smith, K. M., and Iversen, P. L. HIV tat peptide enhances cellular delivery of antisense morpholino oligomers. *Antisense Nucleic Acid Drug Dev.* **13**, 31-43 (2003).

50. Kubo, T. and Fujii, M. Interaction of cationic a-helical peptide with phoshporothioate DNA hybrid. *Nucleic Acid Symposium Series* 167-168 (1999).

51. Keyes-Baig, C., Duhamel, J., Fung, S. Y., Bezaire, J., and Chen, P. Self-assembling peptide as a potential carrier for hydrophobic compounds. *J. Am. Chem. Soc.* **126**, 7522-7532 (2004).

52. Tseng, Y. L., Liu, J.-J., and Hong, R.-L. Translocation of liposomes into cancer cells by cell-penetrating peptides penetratin and TAT: a kinetic and efficacy study. *Mol Pharmacol* **62**, 864-872 (2002).

53. Rasmussen, U. B., Schreiber, V., Schultz, H., Mischler, F., and Schughart, K. Tumor cell-trageting by phage-displayed peptides. *Cancer Gene Therapy* **9**, 606-612 (2002).

54. Gozes, I. Neuroprotective peptide drug delivery and development: potential new therapeutics. *Trends Neurosci.* **24**, 700-705 (2001).

55. Lien, S. and Lowman, H. B. Therapeutic peptides. *Trends Biotechnol.* **21**, 556-562 (2003).

56. Fung, S. Y., Yang, H., and Chen, P. Formation of colloidal suspension of hydrophobic compounds with an amphiphilic self-assembling peptide. *Colloid. Surfaces B: Biointerfaces* **55**, 200-211 (2007).

57. Hsieh, P. C. H., Davis, M. E., Gannon, J., MacGillivray, C., and Lee, R. T. Controlled delivery of PDGF-BB for myocardial protection using injectable self-assembling peptide nanofibers. *J. Clin. Invest.* **116**, 237-248 (2006).

58. Davis, M. E., Hsieh, P. C. H., Takahashi, T., Song, Q., Zhang, S., Kamm, R. D., Grodzinsky, A. J., Anversa, P., and Lee, R. T. Local myocardial insulin-like growth factor 1 (IGF-1)

delivery with biotinlylated peptide nanofibers improves cell therapy for myocardial infarction. *Proc. Natl. Acad. Sci. USA* **103**, 8155-8160 (2006).

59. Fung, S. Y., Hong, Y., Dhadwar, S. S., Zhao, X., and Chen, P. "Self-assembly of ionic-complementary peptides and their applications in nanobiotechnology". *in* Handbook of Nanostructured Biomaterials and Their Applications in Nanobiotechnology, Vol. 2. ed. Nalwa, H. S. pp. 1-66 (American Scientific Publishers, Stevenson Ranch, CA USA; 2005).

60. Zhang, S. Emerging biological materials through molecular self-assembly. *Biotechnol. Adv.* **20**, 321-339 (2002).

61. Zhang, S., Holmes, T., Lockshin, C., and Rich, A. Spontaneous assembly of a self-complementary oligopeptide to form a stable macroscopic membrane. *Proc. Natl. Acad. Sci. USA* **90**, 3334-3338 (1993).

62. Zhang, S., Lockshin, C., Cook, R., and Rich, A. Unusually stable β-sheet formation in an ionic self-complementary oligopeptide. *Biopolymers* **34**, 663-672 (1994).

63. Davis, M. E., Michael Motion, J. P., Narmoneva, D. A., Takahashi, T., Hakuno, D., Kamm, R. D., Zhang, S., and Lee, R. T. Injectable self-assembling peptide nanofibers create intramyocardial microenvironments for endothelial cells. *Circulation* **111**, 442-450 (2005).

64. Zhang, S., Holmes, T., DiPersio, C. M., Hynes, R. O., Su, X., and Rich, A. Self-complementary oligopeptide matrices support mammalian cell attachment. *Biomaterials* **16**, 1385-1393 (1995).

65. Hong, Y., Lau, L. S., Legge, R. L., and Chen, P. Critical self-assembly concentration of an ionic-complementary peptide EAK16-I. *J. Adhesion* **80**, 913-931 (2004).

66. Hong, Y., Pritzker, M. D., Legge, R. L., and Chen, P. Effect of NaCl and peptide concentration on the self-assembly of an ionic-complementary peptide EAK16-II. *Colloids Surf. B: Biointerfaces* **46**, 152-161 (2005).

67. Yang, H., Fung, S. Y., Pritzker, M. D., and Chen, P. Modification of hydrophilic and hydrophobic surfaces using an ionic-complementary peptide. *PLoS One* **2**, e1325-11 (2007).

68. Yang, H., Fung, S. Y., Pritzker, M. D., and Chen, P. Surface-assisted assembly of an ionic-complementary peptide: controllable growth of nanofibers. *J. Am. Chem. Soc.* **129**, 12200-12210 (2007).

69. Yang, Hong, Fung, S Y, Pritzker, Mark, and Chen, P. Mechanical force-induced nucleation and growth of peptide nanofibers at liquid/solid interfaces. *Angew. Chem. Int. Ed.* 2007 Submitted.

70. Fung, S. Y., Duhamel, J., and Chen, P. Solvent effect on the photophysical properties of the anticancer agent ellipticine. *J. Phys. Chem. A* **110**, 11446-11454 (2006).

71. Liu, J., Xiao, Y., and Allen, C. Polymer-drug compatibility: a guide to the development of delivery systems for the anticancer agent, ellipticine. *J. Pharm. Sci.* **93**, 132-144 (2004).

72. Duhamel, J. "Pyrene fluorescence to study polymeric systems". *in* Molecular Interfacial Phenomena of Polymers and Biopolymers. ed. Chen, P. pp. 214-248 (Woodhead Publishing Ltd., Cambridge, England; 2005).

73. Garbett, N. C. and Graves, D. E. Extending nature's leads: the anticancer agent ellipticine. *Curr. Med. Chem.* **4**, 149-172 (2004).

74. Clarysse, A., Brugarolas, A., Siegenthaler, P., Abele, R., Cavalli, F., de Jager, R., Renard, G., Rozencweig, M., and Hansen, H. H. Phase II study of 9-hydroxy-2N-methylellipticinium acetate. *Eur. J. Cancer Clin. Oncol.* **20**, 243-247 (1984).

75. Gupta, U., Agashe, H. B., Asthana, A., and Jain, N. K. Dendrimers: novel polymeric nanoarchitechtures for solubility enhancement. *Biomacromolecules* **7**, 649-658 (2006).

76. Lukyanov, A. N. and Torchilin, V. P. Micelles from lipid derivatives of water-soluble polymers as delivery systems for poorly soluble drugs. *Adv. Drug Del. Rev.* **56**, 1273-1289 (2004).

77. Kwon, G. S. Polymeric micelles for delivery of poorly water-soluble compounds. *Critical Rev. Ther. Drug Carr. Sys.* **20**, 357-403 (2003).

78. Langer, R. Biomaterials: Status, Challenges, and Perspectives. *AIChE J.* **46**, 1286-1289 (2000).

79. Allen, T. M. and Cullis, P. R. Drug delivery systems: entering the mainstream. *Science* **303**, 1818-1822 (2004).

80. Kommareddy, S. and Amiji, M. "Targeted drug delivery to tumor cells using colloidal carriers". *in* Cellular Drug Delivery: Principles and Practice. eds. Lu, D. R. and Oie, S. pp. 181-215 (Humana Press, Totowa, NJ; 2004).

81. Im-Emsap, W., Siepmann, J., and Paeratakul, O. "Disperse systems". *in* Modern Pharmaceutics. eds. Banker, G. S. and Rhodes, C. T. pp. 237-285 (Marcel Dekker Inc., New York; 2002).

82. Malmsten, M. Surfactants and Polymers in Drug Delivery. (Marcel Dekker Inc., New York; 2002).

83. Le Garrec, D., Ranger, M., and Leroux, J.-C. Micelles in anticancer drug delivery. *American J. Drug Del.* **2**, 15-42 (2004).

84. Cuchelkar, V. and Kopecek, J. "Polymer-drug conjugates". *in* Polymers in Drug Delivery. eds. Uchegbu, I. F. and Schatzlein, A. G. pp. 155-182 (CRC Press, Taylor & Francis Group, Boca Raton, FL; 2006).

85. Li, C. Poly(L-glutamic acid)-anticancer drug conjugates. *Adv. Drug Del. Rev.* **54**, 695-713 (2002).

86. Minko, T., Kopeckova, P., and Kopecek, J. Efficacy of the chemotherapeutic action of HPMA copolymer-bound Doxorubicin in a solid tumor model of ovarian carcinoma. *Int. J. Cancer* **86**, 108-117 (2000).

87. Rejmanova, P., Kopeek, J., Duncan, R., and Lloyd, J. B. Stability in rat plasma and serum of lysosomally degradable oligopeptide sequences in N-(2-hydroxypropyl) methacrylamide copolymers. *Biomaterials* **6**, 45-48 (1985).

88. Leamon, C. P. and Reddy, J. A. Folate-targeted chemotherapy. *Adv. Drug Del. Rev.* **56**, 1127-1141 (2004).

89. Chandna, P., Saad, M., Wang, Y., Ber, E., Khandare, J., Vetcher, A. A., Soldatenkov, V. A., and Minko, T. Targeted proapoptotic anticancer drug delivery system. *Mol. Pharmaceut.* **4**, 668-678 (2007).

90. Lawrence, M. J. and Rees, G. D. Microemulsion-based media as novel drug delivery systems. *Adv. Drug Del. Rev.* **45**, 89-121 (2000).

91. Gursoy, R. N. and Benita, S. Self-emulsifying drug delivery systems (SEDDS) for improved oral delivery of lipophilic drugs. *Biomed. Pharmacother.* **58**, 173-182 (2004).

92. Gao, P., Rush, B. D., Pfund, W. P., Huang, T., Mauer, J. M., Morozowich, W., Kuo, M. S., and Hageman, M. J. Development of a supersaturable SEDDS (S-SEDDS) formulation of paclitaxel with improved oral bioavailability. *J. Pharm. Sci.* **92**, 2395-2407 (2003).

93. van Zuylen, L., Verweij, J., and Sparreboom, A. Role of formulation vehicles in taxane pharmacology. *Invest. New Drugs* **19**, 125-141 (2001).

94. Gelderblom, H., Verweij, J., Nooter, K., and Sparreboom, A. Cremophor EL: the drawbacks and advantages of vehicles selection for drug formulation. *Eur. J. Cancer* **37**, 1590-1598 (2001).

95. Torchilin, V. P. Structure and design of polymeric surfactant-based drug delivery systems. *J. Control. Release* **73**, 137-172 (2001).

96. Gaucher, G., Dufresne, M.-H., Sant, V. P., Kang, N., Maysinger, D., and Leroux, J.-C. Block copolymer micelles: preparation, characterization and application in drug delivery. *J. Control. Release* **109**, 169-188 (2005).

97. Kataoka, K., Harada, A., and Nagasaki, Y. Block copolymer micelles for drug delivery: design, characterization and biological significance. *Adv. Drug Del. Rev.* **47**, 113-131 (2001).

98. Huang, C.-K., Lo, C.-L., Chen, H.-H., and Hsiue, G.-H. Multifunctional micelles for cancer cell targeting, distribution imaging, and anticancer drug delivery. *Adv. Funct. Mater.* **17**, 2291-2297 (2007).

99. Sharma, A. and Sharma, U. S. Liposomes in drug delivery: progress and limitations. *Int. J. Pharm.* **154**, 123-140 (1997).

100. Voinea, M. and Simionescu, M. Designing of 'intelligent' liposomes for efficient delivery of drugs. *J. Cell. Mol. Med.* **6**, 465-474 (2002).

101. Nagayasu, A., Uchiyama, K., and Kiwada, H. The size of liposomes: a factor which affects their targeting efficiency to tumors and therapeutic activity of liposomal anticancer drugs. *Adv. Drug Del. Rev.* **40**, 75-87 (1999).

102. Lyass, O., Uziely, B., Ben-Yosef, R., Tzemach, D., Heshing, N. I., Lotem, M., Brufman, G., and Gabizon, A. Correlation of toxicity with pharmacokinetics of pegylated liposomal doxorubicin (Doxil) in metastatic breast carcinoma. *Cancer* **89**, 1037-1047 (2000).

103. Oku, N., Tokudome, Y., Asai, T., and Tsukada, H. Evaluation of drug targeting strategies and liposomal trafficking. *Curr. Pharm. Design* **6**, 1669-1691 (2000).

104. Simoes, S., Moreira, J. N., Fonseca, C., Duzgunes, N., and Pedroso de Lima, M. C. On the formation of pH-sensitive liposomes with long circulation times. *Adv. Drug Del. Rev.* **56**, 947-965 (2004).

105. Mamot, C., Drummond, D. C., Hong, K., Kirpotin, D. B., and Park, J. W. Liposome-based approaches to overcome anticancer drug resistance. *Drug Resist. Updates* **6**, 271-279 (2003).

106. Liu, Y., Miyoshi, H., and Nakamura, M. Nanomedicine for drug delivery and imaging: a promising avenue for cancer therapy and diagnosis using targeted functional nanoparticles. *Int. J. Cancer* **120**, 2527-2537 (2007).

107. Brigger, I., Dubernet, C., and Couvreur, P. Nanoparticles in cancer therapy and diagnosis. *Adv. Drug Del. Rev.* **54**, 631-651 (2002).

108. Gasco, M. R. Lipid nanoparticles: perspectives and challenges. *Adv. Drug Del. Rev.* **59**, 377-378 (2007).

109. Gupta, U., Agashe, H. B., Asthana, A., and Jain, N. K. Dendrimers: novel polymeric nanoarchitectures for solubility enhancement. *Biomacromolecules* **7**, 649-658 (2006).

110. Jain, T. K., Morales, M. A., Sahoo, S. K., Leslie-Pelecky, D. L., and Labhasetwar, V. Iron oxide nanoparticles for sustained delivery of anticancer agents. *Mol. Pharmaceut.* **2**, 194-205 (2005).

111. Greish, K. Enhanced permeability and retention of macromolecular drugs in solid tumors: a royal gate for targeted anticancer nanomedicines. *J. Drug Targeting* **15**, 457-464 (2007).

112. Aina, O. H., Sroka, T. C., Chen, M.-L., and Lam, K. S. Therapeutic cancer targeting peptides. *Biopolymers* **66**, 184-199 (2002).

113. Santoso, S. and Zhang, S. "Self-assembled nanobiomaterials". *in* Encyclopedia of Nanoscience and Nanotechnology. ed. Nalwa, H. S. (American Scientific Publishers, Stevenson Ranch, CA; 2003).

114. Santoso, S. S., Vauthey, S., and Zhang, S. Structures, function and applications of amphiphilic peptides. *Curr. Opin. Coll. Inter. Sci.* **7**, 262-266 (2002).

115. Zhang, S., Marini, D. M., Hwang, W., and Santoso, S. Design of nanostructured biological materials through self-assembly of peptides and proteins. *Curr. Opin. Chem. Biol.* **6**, 865-871 (2002).

116. Zhang, S. Fabrication of novel biomaterials through molecular self-assembly. *Nature Biotech.* **21**, 1171-1178 (2003).

117. Lim, Y.-B., Lee, E., and Lee, M. Cell-penetrating-peptide-coated nanoribbons for intracellular nanocarriers. *Angew. Chem. Int. Ed.* **46**, 3475-3478 (2007).

118. Benzinger, T. L. S., Gregory, D. M., Burkoth, T. S., Miller-Auer, H., Lynn, D. G., Botto, R. E., and Meredith, S. C. Two-dimensional structure of β-amyloid(10-35) fibrils. *Biochemistry* **39**, 3491-3499 (2000).

119. Tcherkasskaya, O., Sanders, W., Chynwat, V., Davidson, E. A., and Orser, C. S. The role of hydrophobic interactions in amyloidogenesis: example of prion-related polypeptides. *J. Biomol. Struct. & Dynamics* **21**, 353-365 (2003).

120. Ray, S., Das, A. K., Drew, M. G., and Banerjee, A. A short water-soluble self-assembling peptide forms amyloid-like fibrils. *Chem. Commun.* **40**, 4230-4232 (2006).

121. Aggeli, A., Nyrkova, I. A., Bell, M., Harding, R., Carrick, L., McLeish, T. C. B., Semenov, A. N., and Boden, N. Hierarchical self-assembly of chiral rod-like molecules as a model for peptide β-sheet tapes, ribbons, fibrils, and fibers. *Proc. Natl. Acad. Sci. USA* **98**, 11857-11862 (2001).

122. Aggeli, A., Bell, M., Carrick, L. M., Fishwick, C. W. G., Harding, R., Mawer, P. J., Radford, S. E., Strong, A. E., and Boden, N. pH as a trigger of peptide β-sheet self-assembly and reversible switching between nematic and isotropic phases. *J. Am. Chem. Soc.* **125**, 9619-9628 (2003).

123. Vauthey, S., Santoso, S., Gong, H., Watson, N., and Zhang, S. Molecular self-assembly of surfactant-like peptides to form nanotubes and nanovesicles. *Proc. Natl. Acad. Sci. USA* **99**, 5355-5360 (2002).

124. Zhang, S., Lockshin, C., Herbert, A., Winter, E., and Rich, A. Zoutin, a putative Z-DNA binding protein in *Saccharomyces cerevisiae*. *EMBO. J.* **11**, 3787-3796 (1992).

125. Gelain, F., Bottai, D., Vescovi, A., and Zhang, S. Designer self-assembling peptide nanofiber scaffolds for adult mouse neural stem cell 3-dimensional cultures. *PLoS One* **1**, e119-11 (2006).

126. Ellis-Behnke, R. G., Liang, Y.-X., Tay, D. K. C., Kau, P. W. F., Schneider, G. E., Zhang, S., Wu, W., and So, K.-F. Nano hemostat solution: immediate hemostasis at the nanoscale. *Nanomedicine: Nanotech. Biol. Med.* **2**, 207-215 (2006).

127. Zhang, S., Gelain, F., and Zhao, X. Designer self-assembling peptide nanofiber scaffolds for 3 D tissue cell cultures. *Seminars in Cancer Biology* **15**, 413-420 (2005).

128. Caplan, M. R., Schwartzfarb, E. M., Zhang, S., Kamm, R. D., and Lauffenburger, D. A. Control of self-assembling oligopeptide matrix formation through systematic variation of amino acid sequence. *Biomaterials* **23**, 219-227 (2002).

129. Chen, P. Self-assembly of ionic-complementary peptide: a physicochemical viewpoint. *Colloids Surf. A* **261**, 3-24 (2005).

130. Goeden-Wood, N. L., Keasling, J. D., and Muller, S. J. Self-assembly of a designed protein polymer into β-sheet fibrils and responsive gels. *Macromolecules* **36**, 2932-2938 (2003).

131. Zhang, S. and Altman, M. Peptide self-assembly in functional polymer science and engineering. *Reactive and Functional Polymers* **41**, 91-102 (1999).

132. Thirumalai, D., Klimov, D. K., and Dima, R. I. Emerging ideas on the molecular basis of protein and peptide aggregation. *Curr. Opin. Struct. Biol.* **13**, 146-159 (2003).

133. Stefani, M. and Dobson, C. M. Protein aggregation and aggregate toxicity: new insights into protein folding, misfolding diseases and biological evolution. *J. Mol. Med.* **81**, 678-699 (2003).

134. Holmes, T. C., de Lacalle, S., Su, X., Liu, G., Rich, A., and Zhang, S. Extensive neurite outgrowth and active synapse formation on self-assembling peptide scaffolds. *Proc. Natl. Acad. Sci. USA* **97**, 6728-6733 (2000).

135. Kisiday, J., Jin, M., Kurz, B., Hung, H., Semino, C., Zhang, S., and Grodzinsky, A. J. Self-assembling peptide hydrogel fosters chondrocyte extracellular matrix production and cell division: implications for cartilage tissue repair. *Proc. Natl. Acad. Sci. USA* **99**, 9996-10001 (2002).

136. Caplan, M. R., Moore, P. N., Zhang, S., Kamm, R. D., and Lauffenburger, D. A. Self-assembly of a β-sheet protein governed by relief of electrostatic repulsion relative to van der Waals attraction. *Biomacromolecules* **1**, 627-631 (2000).

137. Chen, P., Lahooti, S., Policova, Z., Cabrerizo-Vilchez, M. A., and Neumann, A. W. Concentration dependence of the film pressure of human serum albumin at the water/decane interface. *Colloids Surf. B: Biointerfaces* **6**, 279-289 (1996).

138. Makievski, A. V., Fainerman, V. B., Bree, M., Wustneck, R., Kragel, J., and Miller, R. Adsorption of proteins at the liquid/air interface. *J. Phys. Chem. B* **102**, 417-425 (1998).

139. Fainerman, V. B., Lucassen-Reynders, E. H., and Miller, R. Adsorption of sufactants and proteins at fluid interfaces. *Colloids Surf. A: Physicochemical and Engineering Aspects* **143**, 141-165 (1998).

140. Soreghan, B., Kosmoski, J., and Glabe, C. Surfactant properties of Alzheimer's Aβ peptides and the mechanism of amyloid aggregation. *J. Biol. Chem.* **269**, 28551-28554 (1994).

141. Lomakin, A., Chung, D. S., Benedek, G. B., Kirschner, D. A., and Teplow, D. B. On the nucleation and growth of amyloid β-protein fibrils: detection of nuclei and quantitation of rate constants. *Proc. Natl. Acad. Sci. USA* **93**, 1125-1129 (1996).

142. Walsh, D. M., Hartley, D. M., Kusumoto, Y., Fezoui, Y., Condron, M. M., Lomakin, A., Benedek, G. B., Selkoe, D. J., and Teplow, D. B. Amyloid β-protein fibrillogenesis. *J. Biol. Chem.* **274**, 25945-25952 (1999).

143. Scherzinger, E., Sittler, A., Schweiger, K., Heiser, V., Lurz, R., Hasenbank, R., Bates, G. P., Lehrach, H., and Wanker, E. E. Self-assembly of polyglutamine-containing huntingtin fragments into amyloid-like fibrils: implications for Huntington's disease pathology. *Proc. Natl. Acad. Sci. USA* **96**, 4604-4609 (1999).

144. Rhoades, E., Agarwal, J., and Gafni, A. Aggregation of an amyloidogenic fragment of human islet amyloid polypeptide. *Biochim. Biophys. Acta* **1476**, 230-238 (2000).

145. Kayed, R., Bernhagen, J., Greenfield, N., Sweimeh, K., Brunner, H., Voelter, W., and Kapurniotu, A. Conformational transitions of islet amyloid polypeptide (IAPP) in amyloid formation *in vitro*. *J. Mol. Biol.* **287**, 781-796 (1999).

146. Yang, G., Woodhouse, K. A., and Yip, C. M. Substrate-facilitated assembly of elastin-like peptides: studies by variable-temperature in situ atomic force microscopy. *J. Am. Chem. Soc.* **124**, 10648-10649 (2002).

147. Brown, C. L., Aksay, I. A., Saville, D. A., and Hecht, M. H. Templated-directed assembly of a *de novo* designed protein. *J. Am. Chem. Soc.* **124**, 6846-6848 (2002).

148. Kowalewski, T. and Holtzman, D. M. *In situ* atomic force microscopy study of Alzheimer's β-amyloid peptide on different substrates: new insights into mechanism of β-sheet formation. *Proc. Natl. Acad. Sci. USA* **96**, 3688-3693 (1999).

149. Murphy, R. M. Peptide aggregation in neurodegenerative disease. *Annu. Rev. Biomed. Eng.* **4**, 155-174 (2002).

150. Zhang, F., Du, H.-N., Zhang, Z.-X., Ji, L.-N., Li, H.-T., Tang, L., Wang, H.-B., Fan, C.-H., Xu, H.-J., Zhang, Y., Hu, J., Hu, H.-Y., and He, J.-H. Epitaxial growth of peptide nanofilaments on inorganic surfaces: effects of interfacial hydrophobicity/hydrophilicity. *Angew. Chem. Int. Ed.* **45**, 3611-3613 (2006).

151. Kopecek, J. Smart and genetically engineered biomaterials and drug delivery systems. *Eur. J. Pharm. Sci.* **20**, 1-16 (2003).

152. Hubbell, J. A. Enhancing Drug Function. *Science* **300**, 595-596 (2003).

153. Hawiger, J. Noninvasive intracellular delivery of functional peptides and proteins. *Curr. Opin. Chem. Biol.* **3**, 89-94 (1999).

154. Schwartz, J. J. and Zhang, S. Peptide-mediated cellular delivery. *Curr. Opin. Mol. Ther.* **2**, 162-167 (2000).

155. Lim, Y., Lee, E., and Lee, M. Cell-penetrating-peptide-coated nanoribbons for intracellular nanocarriers. *Angew. Chem. Int. Ed.* **46**, 3475-3478 (2007).

156. Accardo, A., Tesauro, D., Mangiapia, G., Pedone, C., and Morelli, G. Nanostructures by self-assembling peptide amphiphile as potential selective drug carriers. *Biopolymers* **88**, 115-121 (2007).

157. Garcia-Carbonero, R. and Supko, J. G. Current perspectives on the clinical experience, pharmacology, and continued development of the camptothecins. *Clin. Cancer Res.* **8**, 641-661 (2002).

158. Srivastava, V., Negi, A. S., Kumar, J. K., Gupta, M. M., and Khanuja, S. P. S. Plant -based anticancer molecules: a chemical and biological profile of some important leads. *Bioorg. Med. Chem.* **13**, 5892-5908 (2005).

159. Dias, N., Vezin, H., Lansiaux, H., Lansiaux, A., and Bailly, C. Topoisomerase inhibitors of marine origin and their potential use as anticancer agents. *Top. Curr. Chem.* **253**, 89-108 (2005).

160. Marks, P. A., Rifkind, R. A., Richon, V. M., Breslow, R., Miller, T., and Kelly, W. K. Histone deacetylase and cancer: causes and therapies. *Nat. Rev. Cancer* **1**, 194-202 (2001).

161. Adjei, A. A. and Rowinsky, E. K. Novel anticancer agents in clinical development. *Cancer Biol. Ther.* **2**, S5-S15 (2003).

162. Saijo, N., Tamura, T., and Nishio, K. Strategy for the development of novel anticancer drugs. *Cancer Chemother. Pharmacol.* **52(suppl 1)**, 97-101 (2003).

163. Goodwin, S., Smith, A. F., and Horning, E. C. Alkaloids of *Ochrosia elliptica* Labill. *J. Am. Chem. Soc.* **81**, 1903-1908 (1959).

164. Paoletti, C., Le Pecq, J. B., Dat-Xuong, N., Juret, P., Garnier, H., Amiel, J.-L., and Rouesse, J. Antitumor activity, pharmacology and toxicity of ellipticines, ellipticinum, and 9-hydroxy derivatives: preliminary clinical trials of 2-methyl-9-hydroxy ellipticinium (NSC-264137). *Recent Results Cancer Res.* **74**, 107-123 (1980).

165. Gouyette, A., Huertas, D., Droz, J.-P., Rouesse, J., and Amiel, J.-L. Pharmacokinetics of 2-methyl-9-hydroxyellipticinium acetate (NSC-264137) in cancer patients (phase I study). *Eur. J. Cancer Clin. Oncol.* **18**, 1285-1292 (1982).

166. Dodion, P., Rozencweig, M., Nicaise, C., Piccart, M., Cumps, E., Crespeigne, N., Kisner, D., and Kenis, Y. Phase I clinical study of 9-hydroxy-2N-methyl-ellipticinium acetate (NSC-264137) administered on a 5-day i.v. schedule. *Eur. J. Cancer Clin. Oncol.* **18**, 519-522 (1982).

167. Sainsbury, M. "Ellipticine". *in* The Chemistry of Antitumour Agents. ed. Wilman, D. E. V. pp. 411-435 (Blackie and Son Ltd., Glasgow, UK; 1990).

168. Sbai, M., Ait Lyazidi, S., Lerner, D. A., del Castillo, B., and Martin, M. A. Use of micellar media for the fluorimetric determination of ellipticine in aqueous solutions. *J. Pharm. Biomed. Anal.* **14**, 959-965 (1996).

169. El Hage Chahine, J. M., Bertigny, J.-P., and Schwaller, M.-A. Kinetics and thermodynamics of the formation of inclusion complexes between cyclodextrins and DNA-intercalating agents. Inclusion of ellipticine in γ-cyclodextrin. *J. Chem. Soc. Perkin Trans. II* 629-633 (1989).

170. Le Pecq, J.-B., Xuong, N.-D., Gosse, C., and Paoletti, C. A new antitumoral agent: 9-hydroxyellipticine. Possibility of a rational design of anticancerous drugs in the series of DNA intercalating drugs. *Proc. Natl. Acad. Sci. USA* **71**, 5078-5082 (1974).

171. Moody, T. W., Czerwinski, G., Tarasova, N. I., Moody, D. L., and Michejda, C. J. The development of VIP-ellipticine conjugates. *Regul. Pept.* **123**, 187-192 (2004).

172. Searle, F., Gac-Breton, S., Keane, R., Dimitrijevic, S., Brocchini, S., Sauville, E. A., and Duncan, R. N-(2-hydroxypropyl)methacrylamide copolymer-6-(3-aminopropyl)-ellipticine conjugates. Synthesis, in vitro, and preliminary in vivo evaluation. *Bioconjugate Chem.* **12**, 711-718 (2001).

173. Terce, F., Tocanne, J.-F., and Laneelle, G. Localization of ellipticine derivatives interacting with membranes. A fluorescence-quenching study. *Eur. J. Biochem.* **133**, 349-354 (1983).

174. Sbai, M., Lyazidi, S. A., Lerner, D. A., del Castillo, B., and Martin, M. A. Modified β-cyclodextrins as enhancers of fluorescence emission of carbazole alkaloid derivatives. *Anal. Chim. Acta* **303**, 47-55 (1995).

175. Stiborova, M., Rupertova, M., Schmeiser, H. H., and Frei, E. Molecular mechanisms of antineoplastic action of an anticancer drug ellipticine. *Biomed. Pap. Med. Fac. Univ. Palacky Olomouc Czech Repub.* **150**, 13-23 (2006).

176. Canals, A., Purciolas, M., Aymami, J., and Coll, M. The anticancer agent ellipticine unwinds DNA by intercalative binding in an orientation parellel to base pairs. *Acta Cryst.* **D61**, 1009-1012 (2005).

177. Muggia, F. M. and Burris, H. A. "Clinical development of topoisomerase-interactive drugs". *in* Advances in Pharmacology. DNA Topoisomerases: Topoisomerase-Targeting Drugs, Vol. 29B. ed. Liu, L. F. pp. 1-31 (Academic Press, Inc., San Diego, CA; 1994).

178. Froelich-Ammon, S. J., Patchan, M. W., Osheroff, N., and Thompson, R. B. Topoisomerase II binds to ellipticine in the absence or presence of DNA. Characterization of enzyme-drug interactions by fluorescence spectroscopy. *J. Biol. Chem.* **270**, 14998-15004 (1995).

179. Kuo, P.-L., Hsu, Y.-L., Kuo, Y.-C., Chang, C.-H., and Lin, C.-C. The anti-proliferative inhibition of ellipticine in human breast mda-mb-231 cancer cells is through cell cycle arrest and apoptosis induction. *Anti-Cancer Drugs* **16**, 789-795 (2005).

180. Kuo, P.-L., Hsu, Y.-L., Chang, C.-H., and Lin, C.-C. The mechanism of ellipticine-induced apoptosis and cell cycle arrest in human breast MCF-7 cancer cells. *Cancer Lett.* **223**, 293-301 (2005).

181. Kuo, Y.-C., Kuo, P.-L., Hsu, Y.-L., Cho, C.-Y., and Lin, C.-C. Ellipticine induces apoptosis through p53-dependent pathway in human hepatocellular carcinoma HepG2 cells. *Life Sci.* **78**, 2550-2557 (2006).

182. Stiborova, M., Sejbal, J., Borek-Dohalska, L., Aimova, D., Poljakova, J., Forsterova, K., Rupertova, M., Wiesner, J., Wiessler, M., and Frei, E. The anticancer drug ellipticine forms covalent DNA adducts, mediated by human cytochromes P450, through metabolism to 13-hydroxyellipticine and ellipticine N^2-Oxide. *Cancer Res.* **64**, 8374-8380 (2004).

183. Stiborova, M., Poljakova, J., Ryslava, H., Dracinsky, M., Eckschlager, T., and Frei, E. Mammalian peroxidases activate anticancer drug ellipticine to intermediates forming deoxyguanosine adducts in DNA identical to those found *in vivo* and generated from 12-hydroxyellipticine and 13-hydroxyellipticine. *Int. J. Cancer* **120**, 243-251 (2006).

184. Poljakova, J., Frei, E., Gomez, J. E., Aimova, D., Eckschlager, T., Hrabeta, J., and Stiborova, M. DNA adduct formation by the anticancer drug ellipticine in human leukemia HL-60 and CCRF-CEM cells. *Cancer Lett.* **252**, 270-279 (2007).

185. Stiborova, M., Rupertova, M., Aimova, D., Ryslava, H., and Frei, E. Formation and persistence of DNA adduct of anticancer drug ellipticine in rats. *Toxicology* **236**, 50-60 (2007).

186. Larue, L., Rivalle, C., Muzard, G., Paoletti, C., Bisagni, E., and Paoletti, J. A new series of ellipticine derivatives (1-(alkylamino)-9-methoxyellipticine). Synthesis, DNA binding, and biological properties. *J. Med. Chem.* **31**, 1951-1956 (1988).

187. Lee, I. P. and Dixon, R. L. A possible mechanism for ellipticine-induced hemolysis for human red blood cells. *Fed. Proc.* **31**, 554 (1972).

188. Somers, R., Rouësse, J., van Oosterom, A., and Thomas, D. Phase II study of elliptinium in metastatic soft tissue sarcoma. *Eur. J. Cancer Clin. Oncol.* **21**, 591-593 (1985).

189. Rouesse, J., Spielmann, M., Turpin, F., Le Chevalier, T., Azab, M., and Mondesir, J. M. Phase II study of elliptinium acetate salvage treatment of advanced breast cancer. *Eur. J. Cancer* **29A**, 856-859 (1993).

190. Trubetskoy, V. S. and Torchilin, V. P. Use of polyoxyethylene-lipid conjugates as long-circulating carriers for delivery of therapeutic and diagnostic agents. *Adv. Drug Del. Rev.* **16**, 311-320 (1995).

191. Liu, J., Zeng, F., and Allen, C. Influence of serum protein on polycarbonate-based copolymer micelles as a delivery system for a hydrophobic anti-cancer agent. *J. Control. Release* **103**, 481-497 (2005).

192. Czerwinski, G., Tarasova, N. I., and Michejda, C. J. Cytotoxic agents directed to peptide hormone receptors: defining the requirements for a successful drug. *Proc. Natl. Acad. Sci. USA* **95**, 11520-11525 (1998).

193. Moody, T. W., Czerwinski, G., Tarasova, N. I., and Michejda, C. J. VIP-ellipticine derivatives inhibit the growth of breast cancer cells. *Life Sci.* **71**, 1005-1014 (2002).

194. Ohashi, M. and Oki, T. Ellipticine and related anticancer agents. *Exp. Opin. Ther. Patents* **6**, 1285-1294 (1996).

195. Arteaga, C. L., Kisner, D. L., Goodman, A., and Von Hoff, D. D. Elliptinium, a DNA intercalating agent with broad antitumor activity in a human tumor cloning system. *Eur. J. Cancer Clin. Oncol.* **23**, 1621-1626 (1987).

196. Juret, P., Tanguy, A., Le Talaer, J. Y., Abatucci, J. S., Dat-Xuong, N., Le Pecq, J. B., and Paoletti, C. Preliminary trial of 9-hydroxy-2-methyl ellipticinium (NSC-264137) in advanced human cancers. *Eur. J. Cancer* **14**, 205-206 (1978).

197. Reha, D., Kabelac, M., Ryjacek, F., Sponer, J., Sponer, J. E., Elstner, M., Suhai, S., and Hobza, P. Intercalators. 1. Nature of stacking interactions between intercalators (ethidium, daunomycin, ellipticine, and 4',6-diaminide-2-phenylindole) and DNA base pairs. *Ab initio* quantum chemical, density functional theory, and empirical potential study. *J. Am. Chem. Soc.* **124**, 3366-3376 (2002).

198. Larsen, A. K., Paoletti, J., Belehradek Jr, J., and Paoletti, C. Uptake, cytofluorescence, and cytotoxicity of oxazolopyridocarbazoles (amino acid-ellipticine conjugates) in murine sarcoma cells. *Cancer Res.* **46**, 5236-5240 (1986).

199. Schwaller, M. A., Sureau, F., Turpin, P. Y., and Aubard, J. Intracellular distribution of ellipticine, an antitumor alkaloid in K562 leukemia cells. *J. Lumin.* **48 & 49**, 419-424 (1991).

200. Sailer, B. L., Valdez, J. G., Steinkamp, J. A., Darzynkiewicz, Z., and Crissman, H. A. Monitoring uptake of ellipticine and its fluorescence lifetime in relation to the cell cycle phase by flow cytometry. *Exp. Cell Res.* **236**, 259-267 (1997).

201. Mataga, N., Kaifu, Y., and Koizumi, M. Solvent effects upon fluorescence spectra and the dipole moments of excited molecules. *Bull. Chem. Soc. Jpn.* **29**, 465-470 (1956).

202. Lakowicz, J. R. Principles of Fluorescence Spectroscopy. (Kluwer Academic/Plenum Publishers, New York; 1999).

203. *CRC Handbook of Chemistry and Physics, Internet Version 2005*. Lide, D R Ed. http://www.hbcpnetbase.com/ . 2005. CRC Press, Boca Raton, FL.

204. Masuhara, H., Hino, T., and Mataga, N. Ionic photodissociation of excited electron donor-acceptor systems. 1. An empirical equation on the relationship between the yield and the solvent dielectric constant. *J. Phys. Chem.* **79**, 994-1000 (1975).

205. Rath, M. C., Pal, H., and Mukherjee, T. Interaction of ground and excited (S1) states of C60 and C70 with aromatic amines: exciplex and charge-transfer emissions. *J. Phys. Chem. A* **103**, 4993-5002 (1999).

206. Ghosh, H. N., Pal, H., Sapre, A. V., and Mittal, J. P. Charge recombination reactions in photoexcited C6o-amine complexes studied by picosecond pump probe spectroscopy. *J. Am. Chem. Soc.* **115**, 11722-11727 (1993).

207. Press, W. H., Flannery, B. P., Teukolsky, S. A., and Vetterling, W. T. Numerical Resceipes. The Art of Scientific Computing (Fortran Version). (Cambridge University Press, Cambridge; 1992).

208. Reichardt, C. Solvents and Solvent Effects in Organic Chemistry. (VCH, New York; 1988).

209. Birks, J. B. Photophysics of Aromatic Molecules. (Wiley-Interscience, New York; 1970).

210. Dey, J. and Warner, I. M. Charge-transfer effects on the fluorescence spectra of 9-aminocamptothecin. Steady-state and time-resolved fluorescence studies. *J. Photochem. Photobiol. A Chem.* **116**, 27-37 (1998).

211. Guzow, K., Milewska, M., and Wiczk, W. Solvatochromism of 3-[2-(4-diphenylaminophenyl) benzoxazol-5-yl]alanine methyl ester. A new fluorescence probe. *Spectrochim. Acta, Part A* **61**, 1133-1140 (2005).

212. Kitamura, N. and Sakuda, E. Spectroscopic and excited-state properties of tri-9-anthrylborane I: solvent polarity effects. *J. Phys. Chem. A* **109**, 7429-7434 (2005).

213. Nagy, K., Gokturk, S., and Biczok, L. Effect of microenvironment on the fluorescence of 2-hydroxy-substituted nile red dye: a new fluorescent probe for the study of micelles. *J. Phys. Chem. A* **107**, 8784-8790 (2003).

214. Werner, T. C. and Hoffman, R. M. Relation between an excited state geometry change and the solvent dependence of 9-methyl anthroate fluorescence. *J. Phys. Chem.* **77**, 1611-1615 (1973).

215. Seliskar, C. J. and Brand, L. Electronic spectra of 2-aminonaphthalene-6-sulfonate and related molecules. II. Effects of solvent medium on the absorption and fluorescence spectra. *J. Am. Chem. Soc.* **93**, 5414-5420 (1971).

216. Bosch, P., Fernandez-Arizpe, A., Mateo, J. L., Lozano, A. E., and Noheda, P. New fluorescence probes for monitoring polymerisation reactions 1. Synthesis, solvatochromism and emission properties. *J. Photochem. Photobiol. A Chem.* **133**, 51-57 (2000).

217. Pang, Y. H., Shuang, S. M., Wong, M. S., Li, Z. H., and Dong, C. Study on photophysical properties of intramolecular charge transfer (ICT) compound: 4-(diphenylamino)biphenyl-4'-boronic acid. *J. Photochem. Photobiol. A Chem.* **170**, 15-19 (2005).

218. Nad, S. and Pal, H. Unusual photophysical properties of coumarin-151. *J. Phys. Chem. A* **105**, 1097-1106 (2001).

219. Nad, S., Kumbhakar, M., and Pal, H. Photophysical properties of coumarin-152 and coumarin-481 dyes: unusual behavior in nonpolar and in higher polarity solvents. *J. Phys. Chem. A* **107**, 4808-4816 (2003).

220. Pal, H., Nad, S., and Kumbhakar, M. Photophysical properties of coumarin-120: unusual behavior in nonpolar solvents. *J. Chem. Phys.* **119**, 443-452 (2003).

221. Wallace, B. A. and Janes, R. W. Tryptophans in membrane proteins: X-ray crystallographic analyses. *Adv. Exp. Med. Biol.* **467**, 789-799 (1999).

222. Carlson, C. B., Mowery, P., Owen, R. M., Dykhuizen, E. C., and Kiessling, L. L. Selective tumor cell targeting using low-affinity, multivalent interactions. *ACS Chem. Biol.* **2**, 119-127 (2007).

223. Derossi, D., Chassaing, G., and Prochiantz, A. Trojan peptides: the penetratin system for intracellular delivery. *Trends Cell Biol.* **8**, 84-87 (1998).

224. Lindgren, M., Hallbrink, M., Prochiantz, A., and Langel, U. Cell-penetrating peptides. *Trends Pharmacol. Sci.* **21**, 99-103 (2000).

225. Lundberg, P. and Langel, U. A brief introduction to cell-penetrating peptides. *J. Mol. Recognit.* **16**, 227-233 (2003).

226. Temsamani, J. and Vidal, P. The use of cell-penetrating peptides for drug delivery. *Drug Discov. Today* **9**, 1012-1019 (2004).

227. Oehlke, J., Wiesner, B., and Bienert, M. Model amphipathic peptides. *Cell-Penetrating Peptides* 71-92 (2002).

228. Fung, S. Y., Hong, Y., Keyes-Baig, C., and Chen, P. "Self-assembly of peptides and its potential applications". *in* Molecular Interfacial Phenomena of Polymers and Biopolymers. ed. Chen, P. pp. 421-474 (Woodhead Publishing Ltd., Cambridge, England; 2005).

229. Provencher, S. W. A constrained regulation method for inverting data represented by linear algebraic or integral equations. *Comput. Phys. Commun.* **27**, 213-227 (1982).

230. Hope, M. J., Bally, M. B., Webb, G., and Cullis, P. R. Production of large unilamellar vesicles by a rapid extrusion procedure. Characterization of size distribution, trapped volume and ability to maintain a membrane potential. *Biochim. Biophys. Acta* **812**, 55-65 (1985).

231. Sabin, J., Ruso, J. M., Gonzalez-Perez, A., Prieto, G., and Sarmiento, F. Characterization of phospholipid + semmifluorinated alkane vesicle system. *Colloid. Surfaces B: Biointerfaces* **47**, 64-70 (2006).

232. Tirosh, O., Barenholz, Y., Katzhendler, J., and Priev, A. Hydration of polyethylene glycol-grafted liposomes. *Biophys. J.* **74**, 1371-1379 (1998).

233. Cortez, C., Tomaskovic-Crook, E., Johnston, A. P. R., Scott, A. M., Nice, E. C., Heath, J. K., and Caruso, F. Influence of size, surface, cell line, and kinetic properties on the specific binding of A33 antigen-targeted multilayered particles and capsules to colorectal cancer cells. *ACS Nano* **1**, 93-102 (2007).

234. Kong, G., Braun, R. D., and Dewhirst, M. W. Hyperthermia enables tumor-specific nanoparticle delivery: effect of particle size. *Cancer Res.* **60**, 4440-4445 (2000).

235. Zauner, W., Farrow, N. A., and Haines, A. M. R. In vitro uptake of polystyrene microspheres: effect of particle size, cell line and cell density. *J. Control. Release* **71**, 39-51 (2001).

236. Win, K. Y. and Feng, S.-S. Effects of particle size and surface coating on cellular uptake of polymeric nanoparticles for oral delivery of anticancer drugs. *Biomaterials* **26**, 2713-2722 (2005).

237. Li, X., Hirsh, D. J., Cabral-Lilly, D., Zirkel, A., Gruner, S. M., Jano, A. S., and Perkins, W. R. Doxorubicin physical state in solution and inside liposomes loaded via a pH gradient. *Biochim. Biophys. Acta* **1415**, 23-40 (1998).

238. Hatefi, A. and Amsden, B. Camptothecin delivery methods. *Pharm. Res.* **19**, 1389-1399 (2002).

239. Derossi, D., Calvet, S., Trembleau, A., Brunissen, A., Chassaing, G., and Prochiantz, A. Cell internalization of the third helix of the antennapedia homeodomain is receptor-independant. *J. Biol. Chem.* **271**, 18188-18193 (1996).

240. Vives, E., Richard, J.-P., Rispal, C., and Lebleu, B. TAT peptide internalization: seeking the mechanism of entry. *Curr. Protein Peptide Sci.* **4**, 125-132 (2003).

241. Au, J. L. S., Jang, S. H., and Wientjes, M. G. Clinical aspects of drug delivery to tumors. *J. Control. Release* **78**, 81-95 (2002).

242. Rejman, J., Oberle, V., Zuhorn, I. S., and Hoekstra, D. Size-dependent internalization of particles via the pathways of clathrinand caveolae-mediated endocytosis. *Biochem. J.* **377**, 159-169 (2004).

243. Aggeli, A., Boden, N., and Zhang, S. Self-assembly of peptides in medicine: two sides of the coin. *Mol. Med. Today* **5**, 512-513 (1999).

244. Ellis-Behnke, R. G., Liang, Y.-X., You, S.-W., Tay, D. K. C., Zhang, S., So, K.-F., and Schneider, G. E. Nano neuro knitting: Peptide nanofiber scaffold for brain repair and axon regeneration with functional return of vision. *Proc. Natl. Acad. Sci. USA* **103**, 5054-5059 (2006).

245. Bokhari, M. A., Akay, G., Zhang, S., and Birch, M. A. The enhancement of osteoblast growth and differentiation in vitro on a peptide hydrogel–polyHIPE polymer hybrid material. *Biomaterials* **26**, 5198-5208 (2005).

246. Slavik, J. Anilinonaphthalene sulfonate as a probe of membrane composition and function. *Biochim. Biophys. Acta* **694**, 1-25 (1982).

247. Cardamone, M. and Puri, N. K. Spectrofluorimetric assessment of the surface hydrophobicity of proteins. *Biochem. J.* **282**, 589-593 (1992).

248. Eastoe, J. and Dalton, J. S. Dynamic surface tension and adsorption mechanisms of surfactants at the air-water interface. *Adv. Colloid Interface Sci.* **85**, 103-144 (2000).

249. Torrent, J., Alvarez-Martinez, M. T., Harricane, M.-C., Heitz, F., Liautard, J.-P., Balny, C., and Lange, R. High pressure induces scrapie-like prion protein misfolding and amyloid fibril formation. *Biochemistry* **43**, 7162-7170 (2004).

250. Lindgren, M., Sorgierd, K., and Hammarstrom, P. Detection and characterization of aggregates, prefibrillar amyloidogenic oligomers, and protofibrils using fluorescence spectroscopy. *Biophys. J.* **88**, 4200-4212 (2005).

251. Plank, C., Mechtler, K., Szoka, F. C. J., and Wagner, E. Activation of the complement system by synthetic DNA complexes: A potential barrier for intravenous gene delivery. *Hum. Gene Ther.* **7**, 1437-1446 (1996).